UNIVERSITÀ DEGLI STUDI DI MILANO
FACOLTÀ DI SCIENZE AGRARIE E ALIMENTARI

Scuola di dottorato di ricerca in Agricoltura, Ambiente e Bioenergia

DiSAA-Dipartimento di Scienze Agrarie e Ambientali - Produzione, Territorio, Agroenergia

CORSO DI DOTTORATO IN AGRICOLTURA, AMBIENTE E BIOENERGIA CICLO: XXIX

Multispectral and hyperspectral sensing for nitrogen management in agriculture

Dottoranda: Martina Corti

Supervisore: Ch.mo Prof. Luca Bechini

Co-supervisori: Dott. Pietro Marino Gallina,
Dott. Giovanni Cabassi

Coordinatore della Scuola: Ch.mo Prof. Daniele Bassi

A.A. 2015-2016

“It is only shallow people who do not judge by appearances. The true mystery of the world is the visible, not the invisible…”

Oscar Wilde, The Picture of Dorian Gray

TABLE OF CONTENTS

SUMMARY

In the recent years, agriculture increasingly searched for new techniques that would allow a more efficient use of the agronomic inputs in order to optimize yields while decreasing environmental impact. Precision farming can play a key role to fulfil these requirements. Precision farming uses the newest technologies to monitor within-field and between-field crop variability to support agronomic decisions. Moreover, precision agriculture adopts machines for site-specific distribution of agronomic inputs in order to optimize their efficiency. Among agronomic inputs, fertilizers represent a great cost for farmers and can be a source of environmental pollution if not properly managed. This is particularly true in Lombardy, a region characterized by a high risk of nitrate leaching into the groundwater. In this context, vegetation monitoring to support fertilization is very interesting. Researchers, in particular, have focused on the application of remote sensing with optical sensors, because they are considered the most suitable for in-field applications.

Thus, this research project began with a literature survey, whose results are presented in Chapter 1. The literature survey focused on the use of optical sensors for the estimation of crop variables related to maize nitrogen status: applied nitrogen rate, chlorophyll concentration, plant nitrogen concentration, LAI (leaf area index), above ground biomass, nitrogen uptake, grain yield, and optimal nitrogen rate. Maize was chosen as the target crop because it is the main crop cultivated in Lombardy. Ninety-one papers, published between 1992 and 2016, were identified. Relevant information describing the performance of various sensors was extracted from the papers. The performances of estimation were highly variable (R^2 = 0.60-0.97). Moreover, each experiment produced specific regression equations for location, year, cultivar and development stage. This empiricism is the stronger limitation to the large-scale application of optical sensors for the estimation of nitrogen demands.

The literature survey of Chapter 1 highlighted the successful local use of optical sensors to estimate crop variables related to nitrogen nutrition. However, it showed some limitations, irrespective of the studied crop. Limitations are in fact connected to the platforms on which the sensors are mounted *i.e.,* the low spatial and temporal resolution of the optical information obtained by satellite sensors or the low temporal and spectral resolution of the tractor-mounted sensors. Another limitation of multispectral sensors is their ability to acquire only a small number of broad spectral bands. At the same time, the literature highlighted possible solutions to these issues: the use of unmanned aerial vehicles (UAV) and the use of hyperspectral imaging sensors. The former could fly over the field at any time of the growing season carrying sensors characterized by very high spatial resolution, while the latter could provide high spectral resolution (hundreds of wavelengths) images, which would allow to investigate the effects of combined stressors. Indeed, nitrogen stress is often combined with water stress in the Italian environment, but their on optical sensor responses were not often studied in the literature.

Chapter 2 reports the results of a greenhouse experiment to estimate nitrogen- and water-related variables of a model crop (*Spinacia oleracea* L.) using multivariate partial least squared regression models (PLS) on hyperspectral data. A completely randomized experimental design was arranged with two water levels x four nitrogen levels in two replicates. The reflectance of the canopy was acquired in 121 wavelengths, between 339 and 1094 nm, using a hyperspectral imaging system. For each pot, the average spectrum and the modified hyperspectrograms (a technique to compress the raw spectra, originally proposed in food science) were calculated and used as predictors of plant water content and plant nitrogen concentration. The best performances in cross-validation were reached in the estimation of the water content, both from the average spectrum and the hyperspectrograms. The hyperspectrograms led to slightly better performance than the average spectra: R^2cv

(cross validation) = 0.82 and RMSECV (Root Mean Square Error in Cross Validation) = 0.86% FM for the estimation of the water content and R^2cv = 0.57 and RMSECV = 0.19% DM for the estimation of the nitrogen concentration. The better performances in the estimation of the water content (compared to nitrogen concentration) can be attributed to a greater influence of water stress on the geometry of the canopy and on its spectral properties. This result emphasizes that the combined effect of multiple stressors on the structure and the reflectance of the canopy should be further studied. In conclusion, hyperspectral imaging proved to be a very interesting technique as well as hyperspectrograms extraction, opening new opportunities for the in-field applications of this technique.

Finally, knowing the great interest of UAV-based remote sensing applications, Chapters 3, 4 and 5 report the results obtained in two case studies in the field. The UAV-based optical monitoring was applied to estimate the in-field variability of maize and winter wheat using two multispectral sensors: a modified commercial camera and a professional one.

The experimental maize field (Chapter 3) was monitored during two years (2014-2015) with a commercial digital camera (Canon® Powershot SX260 HS), modified to acquire reflectance in two visible channels (blue and green) and one near-infrared channel. Crop samples were taken at V6 and V9 (sixth and ninth unfolded leaves) phenological stages. These stages are adequate to carry out an N diagnosis of the field, because these are the stages when normally top dressing fertilization is carried out. The plant above ground biomass was determined analytically, while the vegetation indices BNDVI and GNDVI of the entire plots (soil + vegetation) and of the vegetation alone were calculated from the optical images. The very high spatial resolution of the digital camera allowed to estimate also the vegetation fraction cover. The best predictor of the above ground biomass was found to be the estimated vegetation fraction cover: the regression equation built on the two years of experimentation (V9 only) gained R^2= 0.87 and rRMSE (relative RMSE, i.e. the RMSE

expressed as a percentage of the measured average) of 17%. The low cost digital camera led to very good performances in the estimation of the above ground biomass thanks to its high spatial resolution, which compensated the lack of an adequate spectral resolution, as revealed also by the comparison made with the professional camera (presented in Chapter 4).

The experimental wheat field (Chapter 5) was monitored in the year 2016 on three phenological stages (25, 31 and 45 BBCH) to identify the best time to make the UAV survey and to classify the field in homogeneous areas for nitrogen management. The camera used was a MicaSense RedEdge™, which measures reflectance in five channels: blue, green, red, red-edge and near-infrared. Three vegetation indices were calculated from the aerial images (NDVI, GNDVI and NDRE). The NDRE index was found to be the best estimator of grain yield (R^2= 0.76 to 0.91) and above ground biomass (R^2 from 0.37 to 0.90), in all phenological stages. The most suitable time for crop monitoring was found to be 31 BBCH. At this phenological stage, in fact, the crop monitoring guaranteed a satisfactory estimation of wheat above ground biomass which was also found to be closely related to the grain yield. Moreover, three homogeneous zones have been identified, based on the errors in biomass estimation. Finally, the average above ground biomass and nitrogen uptake were calculated for each homogeneous zone, putting the basis for an accurate prescription map for fertilizer applications.

All the experiments carried out during this PhD project confirmed the reliability of optical sensors (multispectral and hyperspectral) to monitor vegetation for fertilization purposes when nitrogen is the main limiting factor. The UAV was found to be a useful and reliable tool for in-field applications. Finally, it was also found that, due to the non-univocal relationships between canopy optical properties and nitrogen-related crop variables, optical monitoring of within-field variability should be conceived as part of an integrated system that combines additional information related to the variability of soil and weather. Only in

this way it would be possible to build a decision support system able to take into account agroecosystem complexity in order to provide accurate fertilization rate prescriptions.

RIASSUNTO

Negli ultimi anni, l'attenzione dell'agricoltura è stata rivolta alla ricerca di tecniche di coltivazione che permettessero un utilizzo più efficiente degli input ottimizzando così le rese e diminuendo l'impatto ambientale del sistema produttivo. Grazie alle recenti tecnologie, l'agricoltura di precisione costituisce un'interessante risposta al problema. Essa sfrutta le recenti tecnologie per il monitoraggio della variabilità di campo (e tra campi) perché confluiscano in un sistema integrato di supporto alle decisioni agronomiche inoltre, traduce le informazioni raccolte attraverso macchinari adatti alla distribuzione sito-specifica degli input agronomici. La fertilizzazione, tra gli altri, rappresenta un importante costo di produzione per l'agricoltore e, se mal gestita, costituisce una fonte di inquinamento ambientale, soprattutto in un territorio come la Lombardia, a rischio di lisciviazione dei nitrati in falda.

Lo sviluppo delle recenti tecnologie, sia di monitoraggio della vegetazione che di distribuzione degli input, ha aperto la possibilità di studiare la variabilità di campo così da poter essere usata come guida alla distribuzione sito-specifica dei fertilizzanti. Il monitoraggio della vegetazione attraverso sensori ottici tramite telerilevamento, in particolare, ha attratto l'interesse della ricerca perché è il più adatto per le applicazioni in pieno campo.

Il progetto di ricerca presentato ha quindi avuto inizio con uno studio approfondito della letteratura, i cui risultati sono stati presentati nel primo capitolo.

Lo studio si è concentrato sull'utilizzo di sensori ottici per la stima di variabili colturali legate allo stato di nutrizione azotata del mais (dose di azoto applicata, concentrazione di clorofilla, concentrazione di azoto nelle piante, LAI (leaf area index), biomassa aerea, azoto assorbito, resa, dose ottimale di fertilizzante). La ricerca si è concentrata sulle tecniche di

telerilevamento con sensori ottici applicati al mais, principale coltura in Lombardia. Sono stati raccolti 91 articoli pubblicati tra il 1992 e il 2016. I risultati sono stati influenzati dallo stadio di sviluppo della coltura, dal target dello strumento, dalle bande spettrali studiate e dagli indici vegetazionali ricavati. Le stime delle variabili colturali indagate sono molto variabili (R^2 = 0.6-0.97) e che ogni esperimento ha prodotto regressioni specifiche per posizione geografica, anno, cultivar, e fase di sviluppo. Questo empirismo rappresenta una limitazione all'utilizzo su vasta di scala di algoritmi generici per la stima degli apporti azotati.

In conclusione, lo studio della letteratura ha evidenziato la possibilità di utilizzare con successo sensori ottici per la stima delle variabili colturali legate alla nutrizione azotata pur evidenziando alcuni limiti, generalizzabili perché indipendenti dalla coltura oggetto di studio. Tali limiti possono essere connessi sia alle piattaforme su cui sono montati i sensori, ad esempio: la bassa risoluzione spaziale e temporale delle informazioni ottiche ricavate da satellite e la bassa risoluzione temporale e spettrale dei sensori montati su trattore; sia al sensore in sé. I sensori maggiormente utilizzati sono infatti multispettrali, caratterizzati dalla possibilità di acquisire un numero ristretto di larghe bande spettrali. Contemporaneamente, dallo studio della letteratura sono emerse due recenti tecnologie che potrebbero superare i limiti mostrati dalle piattaforme e dai sensori ottici più comuni: il drone (come nuova piattaforma) e i sensori di imaging iperspettrali. Il primo può potenzialmente sorvolare il campo in qualsiasi momento del ciclo colturale ad altezze di volo e velocità tali da poter montare sensori ad altissima risoluzione spaziale, mentre i secondi forniscono un'informazione spazializzata ad alta risoluzione spettrale (centinaia di lunghezze d'onda) che permette di studiare più a fondo gli effetti di più stress combinati sulle proprietà ottiche della coltura. Questo punto è infatti un fronte di ricerca aperto, dal momento che nei nostri

ambienti non è infrequente che lo stress nutrizionale per carenza di azoto si sovrapponga allo stress idrico.

Il capitolo 2 presenta quindi un esperimento in serra per stimare gli stati azotato e idrico di una coltura modello (*Spinacia oleracea*) attraverso modelli di regressione multivariata partial least squared (PLS) su dato iperspettrale, quando i fattori di crescita azoto e acqua sono limitanti (disegno sperimentale a randomizzazione completa: due livelli idrici x quattro livelli azotati x due repliche). La riflettanza della canopy è stata acquisita in 121 lunghezze d'onda, tra 339 e 1094 nm, da un sistema di imaging iperspettrale. Lo spettro medio e l'iperspettrogramma, tecnica sviluppata in ambito delle scienze alimentai, sono stati calcolati per ogni vaso e usati come predittori del contenuto idrico e della concentrazione di azoto. Le performance in cross-validazione sono risultate migliori nella stima del contenuto idrico che della concentrazione di azoto, sia da spettro medio che da iperspettrogramma. L'iperspettrogramma ha portato a performance leggermente migliori: R^2cv=0.82 e RMSECV=0.86 % pf per la stima del contenuto idrico e R^2cv=0.57 e RMSECV=0.19% ps per la stima della concentrazione di azoto. Le migliori performance nella stima del contenuto idrico sono ascrivibili ad una maggior influenza dello stress idrico sia sulla geometria della canopy che sulla sua risposta spettrale. Questo risultato sottolinea come l'effetto combinato di più fattori di stress sulla struttura e sulla riflettanza della canopy debba essere ancora approfondito. Infine l'imaging iperspettrale si è rivelata una tecnica molto interessante così come l'estrazione degli iperspettrogrammi, aprendo prospettive per l'uso della tecnica in pieno campo.

Dando seguito, infine, all'interesse crescente per le tecniche di rilevamento ottico da drone, i Capitoli 3-4-5 contengono due casi studio in cui il monitoraggio da drone, per la stima della variabilità in esperimenti di pieno campo su mais e frumento, è stato applicato con due camere: una fotocamera commerciale modificata ed una ad uso professionale.

Il campo sperimentale di mais è stato monitorato in due annate (2014-2015). Il monitoraggio è avvenuto tramite drone con una fotocamera digitale commerciale (Canon® Powershot SX260 HS) modificata per acquisire la riflettanza nel visibile (canali blu e verde) e nel vicino infrarosso. I campionamenti sono avvenuti su mais a stadio fenologico V6 e V9 (due momenti utili per l'applicazione della concimazione di copertura). La biomassa aerea, la concentrazione di azoto e l'azoto asportato sono stati determinati analiticamente, mentre gli indici vegetazionali BNDVI, GNDVI delle parcelle e della sola vegetazione sono stati calcolati dall'immagine aerea. L'alta risoluzione della camera ha permesso di stimare anche la copertura vegetale. Il miglior predittore della biomassa aerea è risultato essere la copertura vegetale stimata da BNDVI: l'equazione di regressione costruita sui due anni di sperimentazione (solo V9) è risultata avere un $R^2 = 0.87$ e rRMSE del 17%. Il sistema di imaging a basso costo ha portato ad ottime prestazioni nella stima della biomassa grazie all'altissima risoluzione spaziale che compensa la mancanza di un'adeguata risoluzione spettrale, limite emerso da un confronto con la camera multispettrale ad uso professionale presentato nel Capitolo 4.

Il campo sperimentale di frumento è stato monitorato nell'anno 2016 in tre stadi fenologici 25, 31 e 45 BBCH con l'obiettivo di individuare il momento migliore per fare la ricognizione aerea e di classificare il campo in zone omogenee per la gestione dell'azoto (Capitolo 5). Il monitoraggio è avvenuto tramite fotocamera multispettrale per uso professionale (MicaSense RedEdge™) che acquisisce l'informazione spettrale in cinque canali: blu, verde, rosso, red-edge e vicino infrarosso. Tre indici vegetazionali sono stati calcolati dalle immagini aeree (NDVI, GNDVI e NDRE). L'indice NDRE è risultato essere il miglior indice per la stima sia della resa in granella (R^2 da 0.76 a 0.91) che della biomassa aerea (R^2 da 0.37 a 0.9) in tutte le fasi fenologiche. Il momento più adatto per il monitoraggio delle colture è risultato essere a 31 BBCH, compromesso tra la miglior stima della resa e le

necessità della coltura in termini di nutrizione azotata. Infine, sulla base dell'errore di stima, sono state identificate tre zone omogenee di cui è stata stimata la produzione media di biomassa e il suo assorbimento di azoto, mettendo le basi per la creazione di un'accurata mappa di prescrizione per le applicazioni di fertilizzante.

Gli esperimenti condotti, hanno confermato l'applicabilità dei sensori ottici, sia multispettrali che iperspettrali, per il monitoraggio della vegetazione ai fini della concimazione azotata, quando l'azoto è il principale fattore limitante. Il drone si è rivelato uno strumento utile e affidabile per le applicazioni di tali tecniche in pieno campo. È infine emerso che, a causa della mancata univocità della relazione tra le proprietà ottiche della canopy e le variabili colturali inerenti la nutrizione azotata, il monitoraggio ottico della variabilità di campo deve essere visto come parte di un sistema integrato che unisca più informazioni legate alla variabilità del suolo, del meteo ecc. in modo da costruire un sistema di supporto alle decisioni che tenga in considerazione la complessità della coltura, così da dare informazioni accurate riguardo alla sola risposta alla concimazione, purificate da elementi di rumore quali le interazioni con altri stress.

GENERAL INTRODUCTION

Matching nitrogen supply with variations in crop nitrogen demand both spatially and temporally will increase crop production, improve food quality and soil quality and reduce costs and nitrogen losses in the environment (Olfs et al., 2005; Pattey et al., 2001). Lemaire et al. (2008) pointed out that, instead of applying excess nitrogen to be sure to cover crop nitrogen demand, N rate should be determined based on estimated target yields and soil nitrogen supply dynamics. With the new technologies, this task could be carried out also within the same field, by identifying areas with different responses to nitrogen (Rodriguez et al., 2006). Determining crop spatial variability, in this case, would be crucial to provide farmers nitrogen diagnostic tools that enable a correct timing and supply of site-specific nitrogen fertilizer (Lemaire et al., 2008).

Remote sensing techniques are useful to assess plant status rapidly and accurately without the need of destructive samplings and time-consuming analytical measurements. In addition, they can be used during the growing season in order to record the dynamics of plant demands. Optical sensors, in particular, can be useful to assess plant nutritional status because nitrogen availability affects chlorophyll content, and chlorophyll, in turn, affects the greenness of leaves (Schlemmer et al., 2005). In fact, the spectra of canopies are characterized by an increase in reflectance in the near- infrared (~725 to 900 nm), because the internal leaf structure of the plant reflects more energy in this portion of the spectrum compared to a bare soil. Moreover, a green peak (~ 550 nm) and a decrease in red reflectance (~650 to 690 nm) occur, due to chlorophyll reflectance and absorption respectively (Barnes et al., 1996).

Sensors acquiring canopy reflectance can be classified as passive and active, depending on their electromagnetic source. While passive sensors measure sunlight reflected by the canopy, active sensors standardise electromagnetic radiation by their own light source.

Moreover, each optical device can be described by indicating its spectral, radiometric, temporal and spatial resolution, here described with the definitions given by Joseph (2005). The spectral resolution identifies the wavelength interval in which the observation is made; the radiometric resolution is a measure of the capability of the sensors to differentiate the smallest change in the spectral reflectance between various targets. Based on these definitions, optical sensors can be defined multispectral or hyperspectral depending on the number and width of wavebands recorded. Hyperspectral sensors collect a set (tens to hundreds) of narrow (<10 nm) and contiguous spectral bands. Multispectral data involve a set (three or more) of optimally chosen spectral broad bands that can be collected from multiple sensors (Lan et al., 2010). Temporal resolution refers to the temporal frequency of the acquisition of a measure. Finally, imaging sensors have been developed in order to obtain information about the spatial variability of the spectrum, and their spatial resolution is the degree to which an image can differentiate spatial variation of terrain features (Tempfli et al., 2009). Spatial and temporal resolution are not strictly linked to sensor properties but also to the platform on which the sensor is mounted. New opportunities in airborne remote sensing have been opened by the increasing use of unmanned aerial vehicles (UAV) in vegetation monitoring applications. The great interest on these platforms is due to the high spatial and temporal resolution of the spectral data collected.

Multispectral sensors are the most common sensors studied in crop nitrogen management. Some tractor-mounted devices are already used in field applications with implemented algorithms that calculate the nitrogen rate; handheld multispectral sensors can also be used for this purpose. On the one hand, these tractor-mounted sensors are very widespread because they are active sensors, so they can be used independently of daylight conditions. Moreover, by using a N-rich reference strip the problems derived from the dependence of reflectance on environment- and crop-specific factors is avoided. On the other hand,

multispectral cameras mounted on UAV are new, economic and flexible devices that are increasingly studied to monitor within-field crop variability. Their use to support agronomic decisions is studied at the initial step of technology demonstration: they have shown good correlations with vegetation indices derived from the most common optical ground-based measurements.

Tractor-mounted and airborne multispectral sensors might have some practical limitations due to the low spectral and radiometric resolutions. Nowadays, the opportunity to use chemometrics to obtain information about crop nitrogen status from the entire canopy reflectance has given a renovated importance to hyperspectral data. In fact, though vegetation indices are good indicators of the plant status, they are calculated using only a few wavelengths and most of the reflectance information is lost. Another technique that could be currently used in agricultural applications is imaging spectroscopy that combines the potential of digital images and hyperspectral measurements. Imaging spectroscopy is particularly adapted to the aims of precision agriculture thanks to its high spectral resolution joined with spatial information about the distribution of the reflectance. This instrumentation is currently studied to prove its feasibility in agriculture applications. Tables 1 and 2 summarize the use of optical sensors for nitrogen management as found in literature, with the distinction between optical and imaging sensors.

Table 1. – Summary table about the use of optical sensors highlighting the sensor used, its output, the variable assessed depending on the nature of the spectral information and the most common application of the sensor output.

Optical Sensor	Index or Reflectance (Sensor Output)	Variable assessed	Use of the sensor output	Notes
Tractor-mounted or handheld multispectral sensors	NDVI and/or other vegetation indices	✓ Green Canopy Cover ✓ Photochemical status; Structural composition	✓ Regression models to estimate: Leaf nitrogen concentration Plant nitrogen uptake Grain yield Chlorophyll content	
			✓ Use of vegetation indices as input for models that calculate crop nitrogen requirements	✓ Some of these models are currently implemented on tractors for the application of a spatially-variable nitrogen rate. A N-rich strip is needed
Spectro-radiometers	Reflectance spectrum	Representative of the complex physiological and biochemical conditions of the crop	✓ Studies on the effects of nitrogen stress on crop canopy reflectance	
			✓ Construction of narrowband indices for plant nitrogen content estimation	
			✓ Multivariate regression models for the estimation of plant nitrogen content by using information from the entire spectrum	
Hyperspectral Imaging sensors	Map of canopy reflected spectrum	Representative of the complex physiological and biochemical conditions of the crop at high spatial resolution	✓ Wavebands selection to estimate leaf chlorophyll content	Image calibration and processing steps are needed to obtain reliable spectral information
			✓ Construction of narrowband indices for the estimation of plant nitrogen content	
			✓ Estimation of plant nitrogen content by using the entire spectrum	
Digital cameras	✓ NDVI, GNDVI, other vegetation indices	✓ Green Canopy Cover ✓ Photochemical status; Structural composition	✓ Regression models to estimate: Leaf nitrogen concentration Plant nitrogen uptake Grain yield Chlorophyll content	Image calibration and processing steps are needed to obtain reliable spectral information

The summarized scientific background shows that only some tractor-mounted or handheld multispectral sensors have become practical tools to support fertilization. Moreover, most of the calibration works relating crop growth characteristics (*e.g.,* yield, nitrogen concentration)

to spectral measurements acquired from plants characterized by different levels of nitrogen availability were carried in presence of adequate water levels. This is a limitation, because several authors have pointed out that spectral measurements are not useful when yield-limiting factors other than nitrogen exist (Pattey et al., 2001; Schepers et al., 1996; Zillmann et al., 2006). The interaction between more stressors is an unsolved issue, in particular when considering water stress. In fact, an incorrect water management causes not only a low water use efficiency but also a loss of water in the root zone that carries away soluble mineral nutrients such as nitrate. Therefore, water and nitrogen management are strongly linked. Furthermore, some authors (Rodriguez et al. 2006, Wang et al., 2011) suggested that under water-limited conditions confounding effects are possibly caused by changes in canopy architecture, reflectance coming from the bare soil and from changes in properties of leaves surface. For instance, changes in LAI could be driven by soil moisture rather than nitrogen availability (Eitel et al., 2008). Therefore research is required to understand if optical sensors can distinguish simultaneous nitrogen and water stress. Imaging spectroscopy, in particular, could play a role due to its high spectral, radiometric and spatial resolution. In addition, the feasibility of UAV-based mapping of crop variability should be studied: its use would allow crop monitoring along the whole season improving spatiotemporal resolutions if compared to both, tractor-mounted and satellite sensors.

RESEARCH STRUCTURE AND OBJECTIVES

The work carried out during this PhD aimed to address some of the research needs in the context of using optical sensors to support crop N fertilization. These research needs are characterized by different Technology Readiness Levels (TRL):

- At a low TRL, we investigated the possibility to use imaging spectroscopy to detect simultaneous water and nitrogen stress. For this exploratory research, we decided to

work in the greenhouse with spinach (chosen as a fast-growing broadleaf model species).

- At a high TRL, we tested the application of different types of UAV-mounted multispectral sensors (a modified consumer-grade camera, and a professional camera) to estimate the above ground biomass and N status of cereals in the field.

The dissertation is organized in three parts (Figure 1):

1) Firstly, a bibliographic study (Chapter 1) aimed to summarize the performances of proximal and remote sensing to estimate N management variables in maize. This review was carried out because, while many experiments were conducted to test the feasibility of optical sensing for supporting nitrogen management decisions, a lack of a summarized knowledge on this topic was observed in the literature.
2) Secondly, a greenhouse experiment was carried out (Chapter 2) to study the capability of hyperspectral line scan imaging (400-1000 nm) to estimate crop variables under combined water and nitrogen stress using multivariate data analysis and two data compression methods: canopy average spectra and hyperspectrogram extraction. Hyperspectral data contain far more information than do multispectral ones and data compression has to be considered if hyperspectral imaging is to be applied for in-field agricultural management. Thus, hyperspectrogram extraction, a technique originally proposed in food science, was tested for the first time for vegetation monitoring purposes.
3) Two field experiments were carried out (Chapters 3, 4 and 5) to test the ability of two UAV-mounted cameras (a low-cost multispectral camera and a professional multispectral camera) to estimate crop nitrogen-related variables and grain yield in cereals. This field work was carried out because, despite the increasing interest in using

UAV-mounted multispectral cameras for in field nitrogen diagnosis, still few experimental tests were carried out so far worldwide.

Figure 1. – Thesis structure. The white boxes define the issues underlying the research activities carried out during the PhD project.

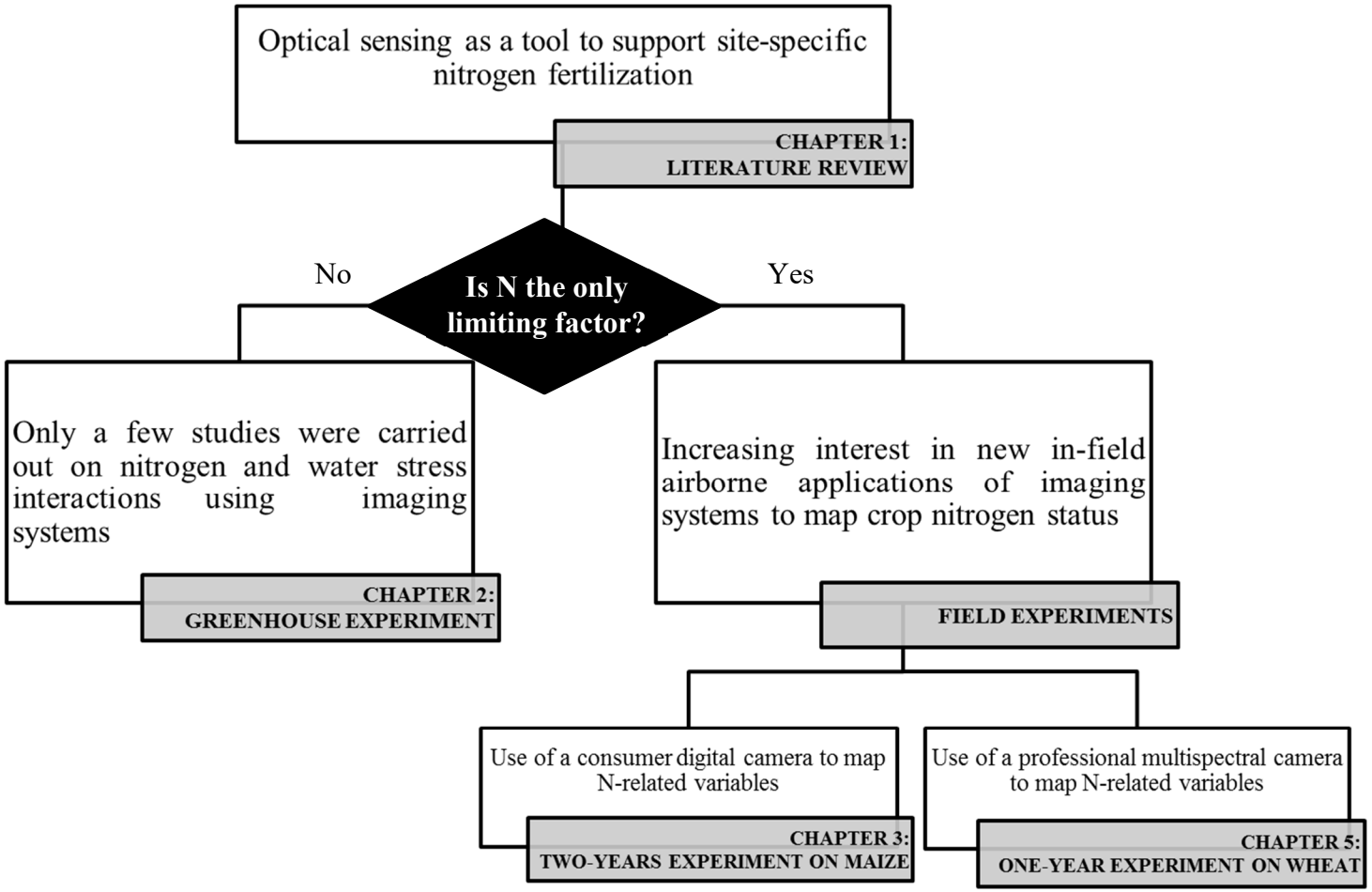

* Chapter 4 contains a short discussion about the differences in signal acquired by the two multispectral cameras used for in-field applications

CHAPTER 1

1. DOES REMOTE AND PROXIMAL OPTICAL SENSING SUCCESSFULLY ESTIMATE MAIZE N VARIABLES? A REVIEW.

(Submitted to the *European Journal of Agronomy*, September 2016)

Martina Corti[1], Giovanni Cabassi[2], Daniele Cavalli[1], Pietro Marino Gallina[1], Luca Bechini[1]

[1]Department of Agricultural and Environmental Sciences - Production, Landscape, Agroenergy, Università degli studi di Milano; via Celoria 2, 20133 Milano (Italy)

[2]Consiglio per la ricerca in agricoltura e l'analisi dell'economia agraria, CREA-FLC; via Antonio Lombardo 11, 26900 Lodi (Italy)

ABSTRACT

Mapping the within-field variability of crop status is of great interest in precision agriculture that seeks to match agronomic inputs to crop demand, both spatially and temporally. In this context, nitrogen (N) management plays a key role that must balance its importance in crop production with its potential to be a source of environmental pollution. Remote and proximal sensing techniques are widely studied to assess the dynamics of plant status during the growing season. While many experiments were conducted to prove the feasibility of optical sensors to estimate N management-linked variables, a summary evaluation of their performance in maize is lacking. This review considers studies of ground-measured maize variables with optical sensor measurements under varying N levels to inform the feasibility of using sensors for N management. We collected and summarised 91 papers published

between 1992 and March 2016 that reported the quantitative performances of remote and proximal sensing techniques used to estimate many variables: applied N rate, chlorophyll content, N concentration, leaf area index, above ground biomass, crop N uptake, crop yield, technically optimum N rate, and economically optimum N rate. Our evaluation highlighted the roles of the most important factors affecting the results (crop development stage, sensed target, spectral bands, and vegetation indices used). Our results indicated that while performance estimates ranged from moderate (R^2 = 0.66-0.81) to excellent (R^2 > 0.97), each experiment produced a unique regression equation that resulted from the specific parameters associated with location, year, cultivar, and development stage. As empiricism severely limits practical application of these highly specific correlations, estimation of optimal N rates for delivery to the soil-crop system will require derivation from compilation of analytical N budgets or more complex mechanistic simulation models with optical data.

1 INTRODUCTION

Optical sensing employs electromagnetic energy to detect and measure characteristics of its target. It is defined as the science of acquiring, processing, and interpreting images and data that record interactions between matter and electromagnetic radiation (Sabins, 2007). Interactions include reflection, absorption, and transmission of solar or artificial radiation by the target matter (crop), in addition to emission of radiation and fluorescence. Sensors in contact with leaves (proximal sensing) measure reflectance or absorbance in the visible and near-infrared regions while sensors that measure reflectance from various distances from the canopy perform remote sensing.

Reflection measured at high resolution allows the reflected radiation to be plotted as a function of wavelength. In turn, a reflectance curve can be constructed for each material, including vegetation (Figure 1).

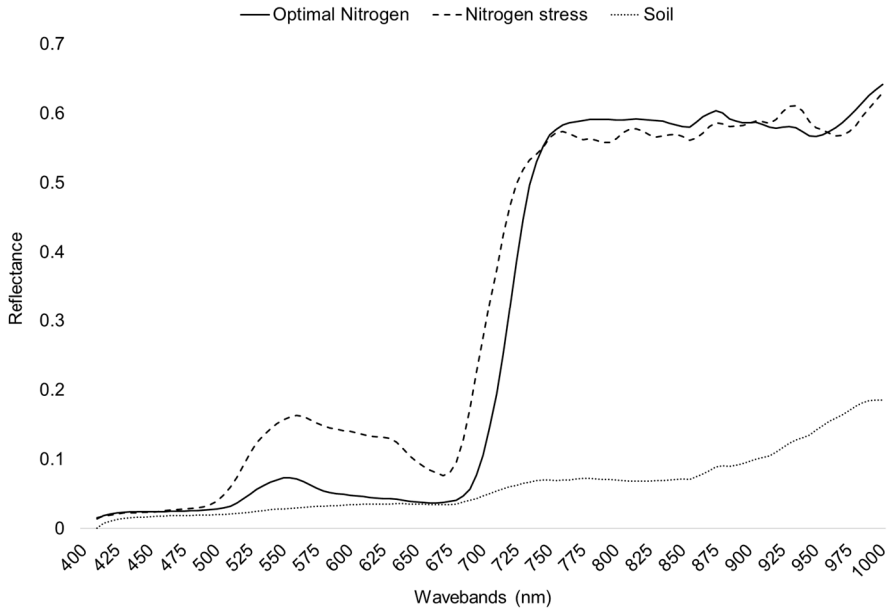

Figure 1. Reflectance curve from 400 to 1000 nm of a crop canopy under optimal (Optimal Nitrogen) and insufficient (Nitrogen stress) nitrogen availability (Corti 2015, unpublished data) and from soil.

Visible range leaf reflectance properties are closely related to leaf pigment contents, and chlorophyll in particular. Chlorophyll causes greater reflectance in the green portion of the electromagnetic radiation spectrum (centered at 550 nm, G) than in the red (650 to 690 nm, R) and blue (430 to 490 nm, B) absorption bands (Barnes et al., 1996). In the 725 - 1000 nm portion of the near-infrared (NIR) region, reflectance is greater than in the visible region, due to light scattering caused by complex interactions between the incident radiation and leaf internal physical structure (cell walls, mesophyll cells, and air cavities) (Bauer, 1985; Peñuelas et al., 1993; Knipling, 1970). The "Red-Edge" (at nearly 700 nm, RE) is the narrow portion of the curve between R and NIR regions where vegetation uniquely causes reflectance to spike because R light is mostly absorbed by chlorophyll and NIR radiation is reflected (Scotford and Miller, 2005), whereas the reflectance increase in the RE region of soils and other terrestrial objects is much smaller. Other plant factors, not strictly dependent on leaf features, also affect the reflectance of canopies: plant species, age, site, leaf orientation, presence of visible background, and presence of biotic and abiotic stress (Tremblay et al. 2009; Shaver et al. 2011). In addition, sensor characteristics (*e.g.,* sensor geometrical and its source of electromagnetic radiation) and weather conditions during data acquisition also affect canopy reflectance measurement (Tremblay et al. 2009; Blackmer et al., 1996a).

Optical sensors that record radiation reflected or absorbed by vegetation in the visible and NIR regions of the electromagnetic spectrum are used to estimate variables associated with N management*,* such as*,* crop N uptake and concentration, final yield, optimum N rate. Indeed, the N contained in chlorophyll of leaves and canopies can be remotely sensed thanks to the high correlation between the compound and element (Samborski et al., 2009), especially if N is limiting (Schut et al., 2003). Leaf N is contained not only in chlorophyll,

but also in proteins where radiation interaction occurs mainly at wavelengths above 1450 nm.

Sensors can be classified as passive or active, depending on their source of electromagnetic radiation. While passive sensors measure sunlight reflected by the canopy, active sensors standardise electromagnetic radiation by their own light source. Passive sensors can be ground-based, such as the FieldSpec spectroradiometer sensor (Analytical Spectral Devices, Inc., Boulder, CO, USA) and Cropscan multispectral radiometer (CROPSCAN, Inc., Rochester, MN) or mainly airborne- and satellite-based, such as the CASI-1500 (ITRES Research Limited, Alberta, Canada), AVIRIS (NASA JPL, Pasadena, CA), and AISA Eagle (Specim, Spectral Imaging Ltd., Oulu, Finland). On the other hand, the most commonly used active sensors for the leaf level is chlorophyll meter Minolta SPAD 502 and for the canopy level is Yara N-Sensor (Yara International ASA, Oslo, Norway). In the case of active tractor-mounted systems, GreenSeeker (NTech Industries, Inc., Ukiah, CA) and CropCircle ACS-470 (Holland Scientific, Lincoln, NE) sensors are employed the most. The GreenSeeker system records two broad-bands (660 and 770 nm), while CropCircle records from two bands (590 and 880 nm) to six bands; the Yara N-Sensor records five bands (450-900 nm).

Optical sensors can be multispectral or hyperspectral, depending on the number and width of wavebands recorded. Hyperspectral sensors have high spectral resolution because they collect sets of 10 to 100 narrow (<10 nm) and contiguous wavebands (Lan et al., 2010). Their make-up makes them powerful and versatile tools, albeit expensive and less suited to routine field applications. Conversely, the less expensive, but lower spectral resolution associated with multispectral sensors that record a maximum of 10 optimally chosen, non-contiguous broad bands (Lan et al., 2010) are potentially better-suited for in-field crop monitoring.

Among the bands available in the visible spectrum, R or G is extremely useful due to its correlation with chlorophyll. NIR (700-1000 nm) sensors are relatively cheap, so they are usually augmented with additional NIR and RE bands to ascertain chlorophyll (RE) and leaf structure (NIR) information. All four bands (R, G, RE, and NIR) are widely reported, and commercial sensors produce reflectance values, analysed alone or combined, for use as vegetation indices (VIs). Most applications focus on a few VIs and typically include NIR and one or two bands from R, G, or RE, as seen with the Normalised Difference Vegetation Index (NDVI) and the Green Normalised Difference Vegetation Index (Gitelson et al., 1996). Appendix 1 lists and defines all VIs used in this work; for a comprehensive VI review, refer to Mulla et al. (2013).

Indices like NDVI are strongly correlated with canopy cover, which makes them good proxies for leaf area index (LAI) from crop emergence until the moment of canopy closure. LAI increases are also indicative of increases in aboveground biomass and crop nitrogen uptake, so an NDVI-like index can be used to estimate both. Moreover, since actual biomass and LAI are among the predictors of future growth, crop yields can be forecasted from VIs measured during stages of early development stages (DVSs), and similarly, fertiliser rates for topdressing can be determined early in the season, if N is the only growth-limiting factor. Hyperspectral sensors detect narrow wavebands to provide information on a select set of vegetation properties (Hansen and Schjoerring, 2003). While these bands are normally used to formulate a new index, potentially useful information contained within the full spectrum is often lost. Multivariate data analysis techniques, however, can resolve this issue as it can consider data from the full spectrum to build prediction models that estimate a single or more crop variables.

Multi- or hyper-spectral “imaging” sensors can register reflectance in tens or hundreds of wavebands for each image pixel, from which descriptive maps of reflectance spatial variability can be derived for the estimated variable. Such capability is highly relevant for field management in which precision agriculture is practised. If spatial resolution differentiates between vegetation and soil, images, it gives rise to the potential to retrieve information on the fraction of canopy cover and to separate the soil signal from that of the canopy. Creation of a pure canopy signal is key to improving the estimation of some crop characteristics as it is more correlated to crop chemical properties than is a canopy + soil signal.

Many experiments have been conducted to evaluate the performances of proximal and remote sensing in estimating variables connected to N management, such as crop N uptake, above ground biomass, grain yield and economically optimum N application rate. For maize, no comprehensive summary exists that describes the performance of multispectral and hyperspectral sensors in relation to factors affecting crop N-status like crop DVS at time of measurement, and in the presence/absence of water stress. This lack of summarised knowledge limits the establishment of generalized rules to translate spectral information acquired with these tools into N management decisions in maize.

This review summarised the state of the art in optical sensors applied to N management in maize cropping-systems to broaden the understanding of sensor feasibility for this use. To this end, we collected and summarised published experiments describing correlations between ground-measured maize variables and optical measurements under varying conditions of N availability. In the cited works, measurements were obtained with imaging or non-imaging multispectral and hyperspectral sensors that were hand-held, tractor-mounted, or airborne and satellite-based.

2 MATERIALS AND METHODS

We identified papers on optical sensing applied to N management in maize in two steps. First, we searched scientific papers in Google Scholar, Scopus, and Web of Science using keywords to describe optical sensing ("leaf optical properties", "leaf reflectance", "remote sensing", "multispectral sensors", "hyperspectral sensors", "satellite sensors", "ground-based sensors", "active sensors", "passive sensors", "tractor-mounted sensors", "airborne sensors", "unmanned aerial vehicle", "UAV", "vegetation indices") in combination with keywords describing nitrogen-related topics ("nitrogen concentration", "nitrogen uptake", "nitrogen stress", "nitrogen and water stress", "nitrogen status", "nitrogen and water status"), and in combination with "maize" or "corn". Second, we collected papers written by authors identified during step one, as well as relevant papers cited selected in step one.

We screened all the papers obtained in the steps described above, and retained only those that reported quantitative results to estimate one of the following variables: applied N rate, chlorophyll content, N concentration, crop N uptake, above ground biomass, leaf area index, crop yield, technically optimum N rate, and economically optimum N rate. While some studies gleaned from the searches were conducted during the 70s and 80s, our review used works from 1992 through March 2016 only. In addition, we excluded studies where chlorophyll meter readings were used as quick, non-destructive chlorophyll content determiners, and which were not regressed against maize crop yield, N uptake, N concentration, or other variables. Indeed, reviews on the use of chlorophyll meter appeared already in the early 90s (Wood et al., 1993).

The papers used for this review are reported in Table S1 provided as supplementary material at the end of the chapter 1. Summary tables, by variable, are contained in Tables 1–8. These summary tables report the metadata (*e.g.*, crop DVS during estimation, sensor used and

target, type of statistical analysis) and estimate performance of crop variables as described by R^2 of the linear or non-linear regression between the crop variable and either vegetation indices or reflectance in single bands. Within each of these tables, records were sorted first by sensed target (leaf level, canopy level without soil signal, canopy level) and then by first author name within the target.

Results are reported first as statistical results for the papers retained. Then, sections are presented in a logical flow from proof of concept (optical measurements distinguish situations varying in N availability) to estimation of crop variables until a formulation of an advised N fertilisation emerges (estimation of the technically and economically optimum N rate). Within each section, we highlight the role of the most important factors affecting results (crop DVS, sensed target, spectral bands and VIs). Crop DVS was codified according to Ritchie et al. (1996).

As regards goodness of regressions, we have classified as "poor" those with an $R^2 < 0.66$, "moderate" as those with an R^2 between 0.66 and 0.81, "good" for 0.82-0.90, "very good" 0.91-0.96, and "excellent" >0.97. Although R^2 is very sensitive to extreme values (a low R^2 over a narrow range can still imply a lower error than a high value obtained from a wider range of variability of the input data), we employed determination coefficients because R^2 is a simple statistic for comparing different regression approaches coming from different experimental works.

3 RESULTS

3.1 Descriptive statistics of the selected papers

We found 91 papers, published between 1992 and 2016 (Figure 2) that considered optical sensing to support maize nitrogen management (Table S1 of the Supplementary material section). Most experiments (78%) took place in the USA, followed by Canada (7%), China and the Middle East (6%), Mexico and South America (5%), and Europe (4%).

Fifty-five percent of experiments employed multispectral sensors, 26% utilised hyperspectral sensors, and 19% used chlorophyll meters. Until 1997, chlorophyll sensors were used most often (Figure 2); thereafter, multispectral sensors became most common (62%). Hyperspectral sensor use adoption increased from 14% before 1997 to 32% after 1997.

The experiments described in the papers estimated the maize variables shown in Figure 3.

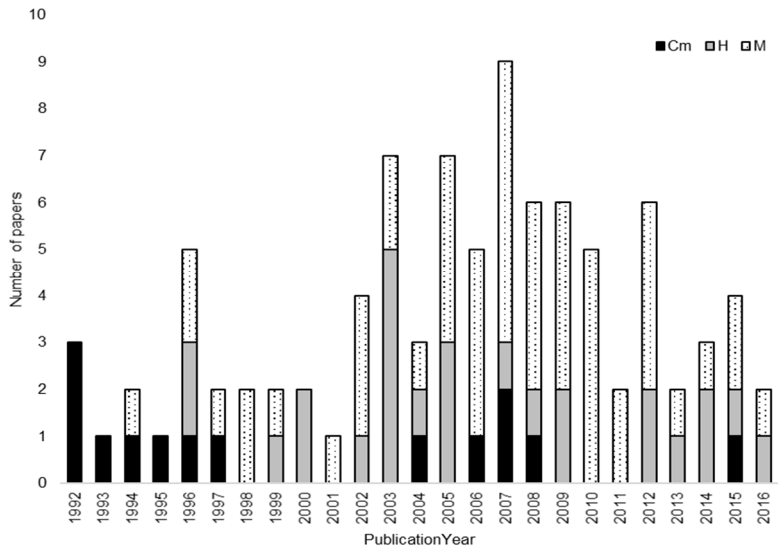

Figure 2. Number of papers reviewed on optical sensing for N management in maize per year (1992-2016) divided into three classes by sensor used: chlorophyll meter (Cm), Hyperspectral optical sensor (H), or Multispectral optical sensor (M).

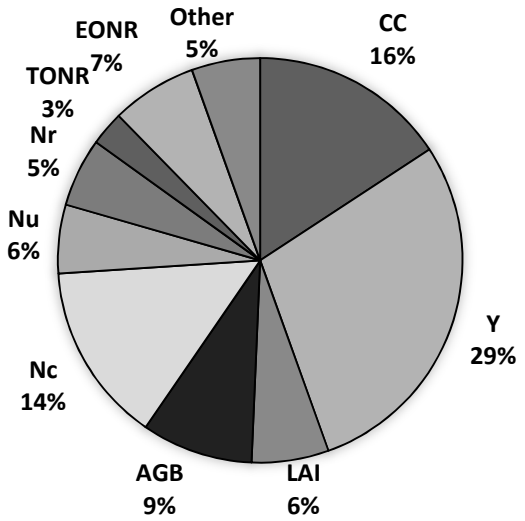

Figure 3. Maize variables estimated in the reviewed papers: chlorophyll content (CC), yield (Y), above ground biomass (AGB) and leaf area index (LAI), nitrogen concentration (Nc), N uptake (Nu), N rate (Nr), Technically Optimum Nitrogen Rate (TONR), Economically Optimum Nitrogen Rate (EONR), and Other (nitrogen nutrition index, responsiveness to fertilisation).

Sensor performances were evaluated under conditions of more than one level of N availability in 73% of the papers. Among these, nitrogen availability was the only factor considered in 64% of the papers, whereas 9% of the papers considered both nitrogen and water availability in an effort to study of the interaction of water stress with nitrogen stress on crop variables. The remaining papers (27%), took place in either field trials or farm fields to exploit spatial variability. Sensors were used at different distances from the target (leaf or canopy), depending on the vector used (Figure 4).

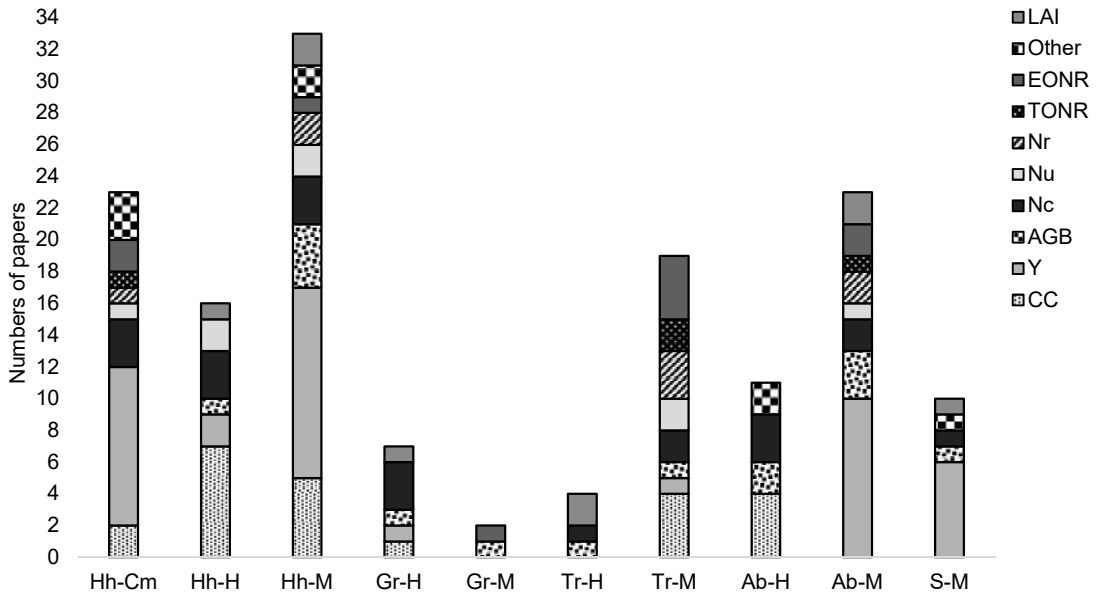

Figure 4. Tools used for the estimation of maize variables (chlorophyll content (CC), yields (Y), biomass and leaf area (B-A), N concentration (Nc), N uptake (Nu), N rate (Nr), technically optimum nitrogen rate (TONR), economically optimum nitrogen rate (EONR), Other) classified in categories combining vector (hand-held (Hh), ground-based (Gr), tractor-mounted (Tr), airborne (Ab) and satellite (S)) and sensor (chlorophyll meter (Cm), hyperspectral sensor (H), multispectral sensor (M)).

Specifically, 23% of experiments evaluated hand-held multispectral sensors, followed by hand-held chlorophyll meters (16%), tractor-mounted multispectral sensors (13%), and airborne multispectral sensors (13%). Hand-held multispectral sensors and chlorophyll meters were used to predict maize grain yields (the most studied variable), while tractor-mounted multispectral sensors were more commonly used when defining optimum nitrogen rates. Among hyperspectral sensors, most were hand-held (44%) or mounted on aircraft (31%), commonly used in maize studies to estimate chlorophyll and nitrogen concentrations. Finally, maize variables were estimated using correlation and simple regression techniques (with linear or non-linear models of fit) in 86% of study papers. Only 14% relied on multivariate data analysis to estimate chlorophyll (23%) and nitrogen concentrations (18%).

3.2 Proof of concept: optical measurements distinguish among N levels

Nine papers described experiments that estimated correlations between N rates and optical crop measures (Table 1). The two that operated at the leaf level (chlorophyll meters) resulted in $R^2 = 0.98$ and the seven at the canopy level (hyperspectral and multispectral sensors) ranged between 0.53 and 0.95. In three additional cases, in which the objective was to discriminate the effects of different N rates on optical properties using ANOVA, neural networks, or decision trees (Goel et al., 2003a and 2003b; Varvel et al., 1997). Of these, only Goel et al. (2003a) quantified estimation performance. In their work to identify nitrogen-stressed plots, they found decision trees and artificial neural network models misclassified rates 22% and 18% of the time, respectively. They obtained their most reliable results at VT, as compared to earlier dates. Thereafter, in a follow-on study, Goel et al. (2003b) identified 498 and 671 nm (G and R) as the best wavelengths at which to detect N stress

Table 1. List of the reviewed papers about the experiments carried out to estimate maize N rate from optical sensors. The papers are sorted first by the sensed target and then by Author within the target.

Authors	DVS[a]	F	Sensor type	Target[b]	Sensor	VIs	Statistical analysis[c]	Performance of estimation	Notes
Bragagnolo et al., 2016	VT	N	Cm	L	SPAD	SPAD units	cR	R^2=0.98	
Varvel et al., 1997	V8, V10, V12, V13, VT, R1	N	Cm	L	SPAD	SI	ANOVA		SI threshold=0.95, was established according to Peterson et al. (1993)
Goel et al., 2003 a	30, 66, 86 DAS	N, We	H	C	CASI	Entire Spectrum	DTree, NN	See notes	Best performances at VT (misclassification at 22% and 15%, for DTree and NN).
Goel et al., 2003 b	30, 66, 86 DAS	N, We	H	C	CASI	Single wavelengths	GLM, ANOVA	See notes	Spectral response changes significantly over time.
Krienke et al., 2015	V11	N	M	C	RapidScan	NDRE	cR	R^2=0.53	
Rambo et al., 2010	V5, V7, V10, R1	N	M	C	GreenSeeker, Cropscan	NDVI	cR	R^2=0.16-0.65	The stage in which differences can be seen depend on soil and hybrid.
Shaver et al., 2011	V8, V10, V12, V14	N	M	C	GreenSeeker	NDVI	cR	R^2=0.62 (V8) R^2=0.89 (V14)	Sensor could reach saturation at high growth stages. At >50 kg N ha^{-1} applied at emergence, NDVI a plateaued.
Shaver et al., 2011	V8, V10, V12, V14	N	M	C	CropCircle	NDVI	cR	R^2=0.62 (V8) R^2=0.95 (V14)	At >50 kg N ha^{-1} applied at emergence, NDVI plateaued.
Tremblay et al.,2009	V3-V5	N	M M	C	Yara-FieldScan, GreenSeeker	NDVI	cR	See notes	NDVI from both instruments increased with N applied up to 60 kg N ha-1

[a] See Table S1 for DVS, F, Type of Sensor, and VI.
[b] Target of optical measurement (L=leaf level, C=canopy level without distinction between canopy and soil)
[c] Statistical analysis technique (cR =correlation and regression with a single explanatory variable; NN = neural networks; Dtree=decision tree; GLM=generalized linear model)

Empty "VI" cells indicate that the whole spectrum or specific wavelengths were used.

3.3 Chlorophyll content

The relationship between spectral crop properties measured by various instruments and chlorophyll content measured or estimated with chlorophyll meters was tested frequently (Table 2). Twelve papers described experiments conducted at the leaf level, using either hyperspectral (9) or multispectral (2) sensing or both (1). Among the experiments (14) conducted at the canopy level, 7 employed multispectral approaches; they could also be differentiated by their soil (10) or vegetation (4) focus. Estimation performance varied highly within each level; specifically R^2 ranged from 0.60 and 0.97 at the leaf level, 0.27-0.95 for canopy + soil, and 0.72-0.89 for pure canopies.

Table 2. Characteristics of papers reviewed from experiments conducted to estimate maize chlorophyll content (CC) or chlorophyll meter readings (Cm readings) from optical sensors. Papers are sorted first by sensed target and then by author within the target.

Authors	Estimated crop variable	DVS[a]	F	Sensor type	Target[b]	Sensor	VIs	Statis-tical analysis[c]	Estimation performance	Notes
Blackmer et al., 1994	Cm readings		N	H	L	Spectroradiometer	Single wavelengths	cR	R^2=0.9	The reported performance was found at 550 nm.
						Spectroradiometer		cR	R^2=0.74	The reported performance was found at 650 nm.
Casa et al., 2015	Cm readings	R3		H	L	Spectroradiometer	Several Entire spectrum	cR PLS	R^2=0.97 (PLS including all the species tested)	Violet, R, and NIR regions were found to be the most informative. VIs performed worse than Cm. PLS performed best.
Ciganda et al., 2009	CC	V3-R		H	L	Spectrradiometer	CI RE	cR	R^2=0.94	RMSE was <38 mg chl m^{-2} for an independent dataset of validation. Using multiple leaf positioned below the ear leaf is recommended to determine canopy Chl with two to four leaves being optimal.
Daughtry et al., 2000	CC	R1	N	H	L and C	Spectroradiometer	Several	cR	R^2=0.77 (at 550 nm) R^2=0.82 (at 715 nm)	VIs based on NIR and R bands minimized background effects, while those based on NIR and G bands were responsive to both CC and background reflectance.
Daughtry et al., 2000	CC	R1	N	H	L and C	Spectroradiometer	Several	cR	R^2=0.95-0.98	Pairs of spectral vegetation indices plotted together produced isolines linearly related to chlorophyll concentration
Gitelson et al., 2005	CC			H	L	Spectroradiometer	CI NIR	cR	R^2=0.93	
							CI RE		R^2=0.93	

Authors	Estimated crop variable	DVS[a]	F	Sensor type	Target[b]	Sensor	VIs	Statis-tical analysis[c]	Estimation performance	Notes
Hunt et al., 2013	Cm readings	V15, VT, R1	N	H, M M	L and C	AVIRIS, Landsat Digital camera	TGI	cR	R=-0.78 to -0.93	The reported correlation coefficients summarized the index performances calculated from all the tested sensors. TGI did not saturated at high values of leaf chlorophyll content. Good relations were found also for RE-based Vis.
Martinez and Ramos, 2015	CC		N	H	L	Spectroradiometer	Several	cR	R^2=0.86 (REIP)	
Rorie et al., 2010	Cm readings (relative)	VT	N	M	L	Digital cameras	relative DGCI	cR	R^2= 0.87	(average R^2)
Rorie et al., 2011	Cm readings	V3-V5	N	M	L	Digital camera	DGCI	cR	R^2=0.85-0.90	Relationship depended on location. Two locations had low R^2 due to poor lighting or to no response to N rates
Schlemmer et al., 2005	CC	V6-V7	N W	H	L	Spectroradiometer	Several	cR	R^2=0.81 (at 525 and 575 nm) R^2=0.80 (in the RE region)	
Zhao et al., 2003	CC		N	H	L	Spectroradiometer	Single wavelengths	cR	r=-0.6	The reported correlation coefficient was found for leaf reflectance at 552 nm
						Spectroradiometer		cR	r=-0.72	The reported correlation coefficient was found for leaf reflectance at 710 nm
Noh and Zhang, 2012	Cm readings	V6-R4	N	M	Cveg	Digital camera	Single wavelengths,s NDVI	cR	R^2 =0.72-0.87 (among tested VIs)See notes	R (R^2 =0.77) and NDVI from a shadow area had a stronger correlation with Cm.
Noh et al., 2005	Cm readings	V6-R2	-	M	Cveg	Digital camera	NDVI, GNDVI, NIR/G	cR	R^2 =0.67 (R) R^2 =0.78 (G) R^2 =0.77 (NDVI)	G, R, NDVI, and GNDVI had good correlations with Cm, not NIR.

Authors	Estimated crop variable	DVS[a]	F	Sensor type	Target[b]	Sensor	VIs	Statis-tical analysis[c]	Estimation performance	Notes
Noh et al., 2006	Cm readings	V6-R4	N	M	Cveg	Digital camera	Entire spectrum	NN	R^2=0.89	Estimated Cm vs measured Cm.
Reum and Zhang, 2007	Cm readings	V8, V9, V10, R1	N	M	Cveg	Digital cameras	Maximum wavelet coefficient	cR	R^2=0.78	
Cilia et al., 2014	CC		N W	H	C	AISA Eagle	Several	cR	R^2=0.69	MCARI/MTVI2 showed the best performances.
Clevers and Gitelson, 2012	CC			H	C	CropScan	Several	cR	R^2=0.91	CIgreen, REP, and MTCI, based on the Sentinel-2 band positions, have a similar performance in terms of R^2 values.
Ma et al., 1996	Cm readings	Pre-anthesis	N	M	C	Radiometer	Single wavelengths	cR	R=-0.52 to -0.95	Correlation coefficient found for leaf reflectance at 600 nm in one year.
						Radiometer		cR		At 450, 500, 700, 750, nm no correlations found.
Miao et a., 2009	Cm readings	V9, R1, R2, R4	N	H	C	Hyperspectral camera	Entire spectrum	Mr	R^2=0.41 (V9) to 0.92 (R4) (simulated M)	The reported performances, from both M and H sensors, were recorded across different maize growth stages and fields.
									R^2=0.61(V9) to 0.94 (R4) (H)	
Miao et al., 2007	Cm readings	V9, R1, R2, R4	N	H	C	AISA Eagle	Entire spectrum	Mr	R^2=0.68 (V9) to 0.94 (R4)	The most consistent bands were 535 and 545 nm. Also, 436, 499, 695, 704, 723, and 943 nm.

Authors	Estimated crop variable	DVS[a]	F	Sensor type	Target[b]	Sensor	VIs	Statis-tical analysis[c]	Estimation performance	Notes
Osborne et al., 2002	Cm readings	V6-V7, V13-V16, V14-R1	N, W	H	C	Spectroradiometer	Entire spectrum	Mr	R^2=0.82 (V6-V7) R^2=0.91 (V13-V16)	G, NIR, and MIDIR were the spectral regions involved in the estimation; the band selection was stable throughout two years.
Solari et al., 2008	Cm readings	V11, V15, R1, R3	N	M	C	Crop Circle	NDVI, CI	cR	Max R^2=0.55 at R-stages Max R^2=0.85 at V-stages	Uniform plant distributions were required for accurate sensor assessment of canopy N status.

[a] See Table S1 for DVS, F, Type of Sensor, and VI.
[b] Target of optical measurement (L=leaf level, C=canopy level without distinction between canopy and soil, Cveg=canopy level, separated soil and vegetation signal)
[c] Statistical analysis technique (cR =correlation and Regression with a single explanatory variable; Mr =Multiple regression; NN = Neural Networks, PLS=Partial Least Square regression)

Empty cells indicate missing data in the original literature source.

3.4 Nitrogen concentration

Nitrogen concentration in maize leaves (Table 3) was studied in 23 papers. Hyperspectral sensors were used to estimate nitrogen concentrations in 7 of 11 leaf and 5 of 12 canopy level papers, while the remaining canopy level papers (7) relied on hand-held spectroradiometers. Again, estimation performances of nitrogen concentrations varied highly, as revealed by R^2 ranging from 0.69-0.90 at the leaf level and 0.57-0.90 at the canopy level. Two papers attempted direct estimation of the nitrogen nutrition index, calculated as the ratio of actual crop nitrogen concentration to critical nitrogen concentration (Lemaire et al., 2008) using multispectral sensors at the canopy level and chlorophyll metres at the leaf level. The experiments led to poor results with R^2 ranging from 0.3 to 0.6.

Table 3. Characteristics of papers reviewed from experiments conducted to estimate maize N concentration (Nc) and Nitrogen Nutrition Index (NNI) with optical sensors. Papers are sorted first by variable, next by sensed target, and finally by author within the target.

Authors	Estimated crop variable	DVS[a]	F	Sensor type	Target[b]	Sensor	VIs	Statis-tical analysis[c]	Estimation performance	Notes
Alchanatis et al., 2005	Nc	V6-VT	N	H	L	Fiber optic reflectance probe	Entire spectrum	PLS	R^2=0.78 (stationary measurement) R^2=0.80 (non-stationary measurement)	Standard error of prediction=2.7 g kg^{-1} for both types of measurement The wavelengths at 530–780 nm and at 1000–1070 nm exhibited the highest correlation to Nc.
Blackmer et al., 1994	Nc		N	Cm	L	SPAD	SPAD units	cR	R^2=0.84	
Blackmer et al., 1994	Nc		N	H	L	Spectroradiometer	Single wavelengths	cR	R^2=0.90 R^2=0.74	The reported performance was found for leaf reflectance at 550 nm The reported performance was found for leaf reflectance at 650 nm.
Lee and Searcy, 2000	Nc		N	H	L	Tractor self-made setup	Entire spectrum	cR, DA, PLS	See notes	In one year, the variation of leaf distance and orientation from the sensor influenced measurements more than N availability.
Lee and Searcy, 2000	Nc		N	H	L	Tractor self-made setup	Entire spectrum	Mr	R^2=0.80 R^2=0.87	Refers to measurements at ear leaf and younger leaf, respectively. The best predictors were wavelengths at 525 and 715 nm. Spectrometer was unable to identify luxury consumption.
Lee et al., 1999	Nc	R3-R5	N	H	L	Laboratory self-made setup	Entire spectrum	cR, Mr, DA, PCA, PCR, PLS	R^2=0.92-0.96	Refers toear leaf measurements.
Lee et al., 1999	Nc	R3-R5	N	H	L	SPAD	SPAD units	cR	R^2=0.94-0.96	Authors found that when using SPAD on the ear leaf, many same plant measurements were required for correct N assessment.

Authors	Estimated crop variable	DVS[a]	F	Sensor type	Target[b]	Sensor	VIs	Statis-tical analysis[c]	Estimation performance	Notes
Rorie et al., 2010	Nc (relative)	VT	N	M	L	Digital cameras	relative DGCI	cR	R^2=0.70	
Rorie et al., 2011	Nc	V3-V5	N	M	L	Digital camera	DGCI	cR	R^2=0.71-0.85	Effects of camera correction and calibration were tested.
Wood et al., 1992	Nc	V10, Midsilk	N	Cm	L	SPAD	SPAD units	cR	R^2=0.88 (V10) R^2=0.91 (midsilk)	Curvature in the relationship between SPAD readings and tissue N concentrations indicates the presence of non-chlorophyll N.
Zhao et al., 2003	Nc		N	H	L	Spectroradiometer	R575/R526	cR	R^2=0.69	
Bausch et al., 2008	Nc	VT	N	M	C	Quick-Bird Satellite	Several	cR	R^2>0.70	Determination coefficient is refers to CI NIR.
Cilia et al., 2014	Nc	V10	N W	H	C	AISA Eagle	Several	cR	R^2 = 0.59	The MCARI/MTVI2 index was the most suitable for the detection of Nc since it was not affected by canopy structure.
Diker and Bausch, 2003	Nc	V6, V9, V12, V15, VT, R1, R2	N	M	C	Radiometer	SI (NIR/G)	cR	R^2=0.77-0.86 (before VT) R^2=0.80-0.84 (after VT)	Determination coefficients refer to two years of experimentation
Li et al., 2014	Nc	V6, V7, V10-V12	N	H	C	Spectroradiometer	Several	cR	R^2=0.65–.68 (V6-V7)	CCCI estimated leaf N concentration better at V6-V7 than at V10-V12.
Oppelt and Mauser, 2003	Nc	12 times during crop growth	N	H	C	AVIS	NDVI OSAVI CAI	cR	R^2=0.90 (CAI)	

Authors	Estimated crop variable	DVS[a]	F	Sensor type	Target[b]	Sensor	VIs	Statis-tical analysis[c]	Estimation performance	Notes
Osborne et al., 2004	Nc	V6-V7, V13-V16, R1-R5	N W	M	C	Multispectral Imagery	NDVI, GNDVI	cR	Max R^2=0.74 (G) Max R^2=0.62 (GNDVI)	The GNDVI performed better than NDVI. The reported determination coefficients were the best during two years of experiment.
Perry and Roberts, 2008	Nc	V14, V15, R1	N W H H	H	C	AVIRIS, Field Spec	Several	cR	See notes	Indices based on RE were more sensitive to differences among nitrogen treatments than those based on VIS-NIR regions only.
Sullivan et al., 2004	Nc	V4-R2	N	H	C	Spectroradiometer	Single wavelengths	cR	r=-0.45 to -0.84 (V8)	Wavelengths 450 and 690 nm performed the same in the two locations at V8. The authors highlighted the dependence of the correlation from DVS and crop conditions.
Sullivan et al., 2004	Nc	V4-R2	N	M	C	ATLAS (Airborne)	NDVI GNDVI	cR	r=0.62-0.81 (V6)	The reported correlation coefficient was found for leaf reflectance at 760-2080 nm at V6.
									r=-0.64 (GNDVI, NDVI)	The GNDVI and NDVI correlated negatively with Nc due to the effects of soil background noise at V6. At one of the two sites studied, no correlations were found.
									R^2=0.23-0.89 (NDVI, GNDVI)	Results were highly variable, depending on year and DVS.
Varco et al., 2013	Nc	V6	N	M	C	Yara-N-Sensor	Several	cR	R^2=0.79	CCCI, among VIs tested, performed best to when estimating Nc because of its indifference to biomass effect.
Varco et al., 2013	Nc	V6	N	M	C	Yara-N-Sensor	Several	cR	R^2=0.83	
Xia et al., 2015	Nc	V5-V10	N	M	C	GreenSeeker	NDVI, RVI	cR	R^2=0.57-0.73	Poor correlation at V5-V6

Authors	Estimated crop variable	DVS[a]	F	Sensor type	Target[b]	Sensor	VIs	Statis-tical analysis[c]	Estimation performance	Notes
Ziadi et al., 2008	NNI		N	Cm	L	SPAD	SPAD units	cR	R^2=0.50 Cm R^2=0.60 RCm	Cm and relative Cm (RCm) readings correlated significantly to NNI, but the intercepts and/or slopes of the response curves varied with site-year.
Xia et al., 2015	NNI	V5-V10	N	M	C	GreenSeeker	NDVI, RVI	cR	R^2=0.26 R^2=0.31	The reported performance is related to NDVI. RVI performance

[a] See Table S1 for DVS, F, Type of Sensor, and VI.
[b] Target of optical measurement (L=leaf level, C=canopy level without distinction between canopy and soil, Cveg=canopy level, separated soil and vegetation signal)
[c] Statistical analysis technique (cR =correlation and Regression with a single explanatory variable; Mr =Multiple regression; DA=Discriminant Analysis, PCA=Principal Component Analysis, PCR=Principal Component Regression, PLS=Partial Least Square regression)

Empty cells indicate missing data in the original literature source.

3.5 Leaf area index (LAI)

LAI were estimated (Table 4) at the canopy level without separating soil from vegetation. Multispectral sensors (hand-held, tractor-mounted, airborne, or satellite-mounted) were most used (5 papers), followed by hyperspectral sensors (4). The highly variable performance estimation produced R^2 values of 0.53-0.98.

Table 4. Characteristics of papers reviewed from experiments conducted to estimate maize leaf area index (LAI) and green area index (GAI) from optical sensors. Papers are sorted first by the sensed target and then by author within the target.

Authors	Estimated crop variable	DVS[a]	F[a]	Sensor type[a]	Target[b]	Sensor	VIs[a]	Statistical analysis[c]	Performance of estimation	Notes
Báez-González et al., 2005	LAI	84,103 DAS		M	C	Landsat-7 ETM	NDVI	cR	R^2=0.53	
Elwaldie et al., 2005	LAI	V6-R	N W	M	C	Cropscan	Several	cR	RSME=0.43	NDVI was the best predictor.
Gilabert et al., 1996	LAI	V4, V6, V8, V14, V16, R5		H	C	Spectroradiometer	NDVI, RE	cR	R^2=0.94-0.98	
Gitelson et al., 2003	LAI			H	C	Spectroradiometer	Several	cR	R^2=0.97 (VARI)	NDVI was sensitive to LAI in early stages of the growing season.VARI followed LAI throughout its whole range of variation, until VT.
Kira et al., 2016	LAI			H	C	Radiometer	NDRE CI RE	cR NN PLS	R^2=0.89 (PLS) R^2=0.90 (NDRE, simple regression)	RE and NIR bands were the most useful. B and R bands were also selected by the PLS method.
Ma et al., 1996	LAI , GAI	Pre-anthesis	N	M	C	Radiometer	Single wavelengths	cR	r=-0.49 to -0.87 r=0.37 to 0.78	The reported correlation coefficient was found for leaf reflectance at 600 nm in one year at different times from pre-anthesis. The reported correlation coefficient was found for leaf reflectance at 800 nm. At 450, 500, 700, and 750 nm, none were found
Nguy-Robertson et al, 2012	GAI	V1-R7		H	C	Spectroradiometer	Several	cR	R^2=0.65 (TGI) to 0.91 (CI RE)	

Authors	Estimated crop variable	DVS[a]	F[a]	Sensor type[a]	Target[b]	Sensor	VIs[a]	Statistical analysis[c]	Performance of estimation	Notes
Sakamoto et al., 2012a	LAI , GAI	V1-R6		M	C	Digital camers, MODIS	Several	cR	R^2=0.99 (CI NIR) R^2=0.98 (VARI)	The reported performance relate to the index CI NIR for the estimation of LAI, and index VARI, for estimating GAI.
Sakamoto et al., 2012b	LAI , GAI	V1-R5		M	C	Digital camers	Several		R^2=0.99 (VARI) R^2=0.98 (2*G-R-B)	The reported performance is related to the index VARI for the estimation of GAI and (2*G-R-B), for the estimation of LAI (where G, R, and B are reflectance in the green, red, and blue regions).

[a] See Table S1 for DVS, F, Type of Sensor, and VI.
[b] Target of optical measurement (C=canopy level without distinction between canopy and soil)
[c] Statistical analysis technique (cR =correlation and Regression with a single explanatory variable; Mr =Multiple regression; NN = Neural networks; PLS=Partial Least Square regression)

Empty cells indicate missing data in the original literature source.

3.6 Above ground biomass (AGB)

Similar to the LAI finding, all experiments that considered AGB (Table 5) occurred at the canopy level, did not separate soil from vegetation, utilised multispectral sensors (hand-held, tractor-mounted, airborne or satellite-mounted) most often (10), and hyperspectral tools less often (5). The performance of estimation also demonstrated high variability as it ranged from R^2 values from 0.31 to 0.99.

Table 5. Characteristics of papers reviewed of experiments conducted to estimate maize aboveground biomass (AGB) from optical sensors. Papers are sorted first by sensed target and then by author within the target.

Authors	DVS[a]	F	Sensor type	Target[b]	Sensor	VIs	Statistical analysis[c]	Estimation performance	Notes
Bragagnolo et al., 2016	V4, V6, V8, V10, V12, VT	N	M	C	Yara sensor	New VI	cR	R^2=0.94	A new index was proposed (VI= (ln R760 - ln R730) x 100)
Cilia et al., 2014		N, W	H	C	AISA Eagle	Several	cR	R^2= 0.21-0.69	The reported performance was found for different vegetation indices
Freeman et al., 2007	V8-VT		M	C	GreenSeeker	NDVI	cR	R^2=0.31	Weak but significant relationship was found at maize growth stages V8 to V10
Gilabert et al., 1996	V4, V6, V8, V14, V16, R5		H	C	Spectroradiometer	NDVI, RE	cR	R^2=0.94-0.98	
Martin et al., 2007	V3-VT		M	C	GreenSeeker	NDVI	cR	Max R^2=0.66	The highest correlation was found between V8-V12. The combined use of CV of NDVI, GNDVI, yield and plant spacing lead to identify the best time for sensing
Osborne et al., 2002	V6-V7, V13-V16, V14-R1	N, W	H	C	Spectroradiometer	Entire spectrum	Mr	R^2=0.45 (V14-R1) to 0.87 (V13-V16)	The equations are different for different years and cannot be transferred to other regions
Osborne et al., 2004	V6-V7, V13-V16, R1-R5	N, W	M	C	Multispectral Imagery	NDVI, GNDVI	cR	R^2=0.52 (G) R^2=0.50 (GNDVI)	GNDVI and the G band performed better than NDVI
Perry and Roberts, 2008	V14, V15, R1	N, W	H H	C	AVIRIS, Field Spec	Several	cR	See notes	The biomass best correlated with the water band indices
Sakamoto et al., 2012a	V1-R6		M	C	Digital cameras	Several	cR	R^2=0.98	NRBI-NIR was taken during night during the entire season

Authors	DVS[a]	F	Sensor type	Target[b]	Sensor	VIs	Statistical analysis[c]	Estimation performance	Notes
Sakamoto et al., 2012b	V1-R5		M	C	Digital cameras	Several		R^2=0.99	NRBI-NIR was taken during night during the entire season
Thenkabail et al., 1994			M	C	Landsat-5 TM	Several	cR	R^2=0.80	
Thenkabail et al., 1994			M	C	Landsat-5 TM	Several	cR	R^2=0.66-0.67	
Thomason et al., 2007	V2-V4, V6-V9, V11-V14, VT		M	C	GreenSeeker	NDVI	cR	R^2=0.81	The reported performance was found at V3-V15
Xia et al., 2015	V5-V10	N	M	C	GreenSeeker	NDVI,RVI	cR	R^2=0.90	NDVI saturated at 3 t ha^{-1}. The best correlation was found at V7-V10

[a] See Table S1 for DVS, F, Type of Sensor, and VI.
[b] Target of optical measurement (C=canopy level without distinction between canopy and soil)
[c] Statistical analysis technique (cR =correlation and Regression with a single explanatory variable; Mr =Multiple regression; NN = Neural networks; PLS=Partial Least Square regression)

Empty cells indicate missing data in the original literature source.

3.7 Nitrogen uptake

The canopy level was studied in six of seven papers that evaluated nitrogen uptake estimation (Table 6), of which only a single paper isolated vegetation from soil (when digital cameras were used). Multispectral sensors were used most (6), while hand-held or tractor-mounted sensors were used less often to estimate N uptake. The performance of estimation varied widely from an R^2 value of 0.92 at the leaf level (1), while it ranged from 0.35 and 0.91 at the pure canopy level, and 0.35-0.74 for vegetation + soil.

Table 6. Characteristics of reviewed papers of experiments conducted to estimate maize N uptake (Nu) from optical sensors. Papers are sorted first by the sensed target and then by author within the target.

Authors	DVS[a]	F[a]	Sensor type[a]	Target[b]	Sensor	VIs[a]	Statistical analysis[c]	Performance of estimation	Notes
Blackmer et al., 1994		N	Cm	L	SPAD	SPAD units	cR	R^2=0.92	
Tomer et al., 1997	Crop maturity	N	M	Cveg	Digital camera	Single bands	Mr PCA	R^2=0.38 to 0.59	The R and NIR reflectance of the crop and NIR reflectance of soil consistently predicted Nu across two years.
Bragagnolo et al., 2016	V4, V6, V8, V10, V12, VT	N	M	C	Yara sensor	New VI	cR	R^2=0.91	A new VI was proposed ((ln R760 - ln R730) x 100).
Freeman et al., 2007	V8-V10	-	M	C	GreenSeeker	NDVI	cR	R^2=0.65	
Freeman et al., 2007	V11-R1	-	M	C	GreenSeeker	New VI	cR	R^2=0.77	A new VI was proposed (NDVI x Plant Height). The best performance was found at high DVSs.
Li et al., 2014	V6, V7, V10-V12	N	H	C	Spectroradiometer	Several	cR		N uptake was better estimated than N concentration across the stages.
Varco et al., 2013	V6	N	M	C	Yara-N-Sensor	Several	cR	R^2=0.96 (CCCI)	All tested indices had a strong relationships ($R^2 \geq 0.93$).
Xia et al., 2015	V5-V10	N	M	C	GreenSeeker	NDVI, RVI	cR	R^2=0.35-0.74	NDVI saturated; no saturation for RVI was observed.

[a] See Table S1 for DVS, F, Type of Sensor, and VI.
[b] Target of optical measurement (L=leaf level, C=canopy level without distinction between canopy and soil, Cveg=canopy level, separated soil and vegetation signal)
[c] Statistical analysis technique (cR =correlation and Regression with a single explanatory variable; Mr =Multiple regression; DA=Discriminant Analysis, PCA=Principal Component Analysis, PCR=Principal Component Regression, PLS=Partial Least Square regression)

Empty cells indicate missing data in the original literature source.

3.8 Crop yield

Forage and grain yield estimation (Table 7) was studied principally at the canopy level (32 of 40 papers). The remaining papers (8) were conducted at the leaf level with the use of chlorophyll meters. Only two papers at the canopy level differentiated vegetation from soil, and thirty-one used multispectral sensors (hand-held, tractor-mounted, airborne, or satellite-mounted). The R^2 values of performance of estimation resulted as highly variable, ranging from 0.05-0.84 (leaf level) and from 0.34 and 0.99 (canopy level).

Table 7. Characteristics of papers reviewed of experiments conducted to estimate maize yield (forage yield, FY and grain yield, GY) from optical sensors. Papers are sorted first by sensed target and then by author within the target.

Authors	Estimated crop variable	DVS[a]	F[a]	Sensor type[a]	Target[b]	Sensor	VIs[a]	Statistical analysis[c]	Estimation performance	Notes
Argenta et al., 2004	GY	V3-V4,V6-V7,V10-V11, R1	N	Cm	L	SPAD	SPAD units	cR	See notes	The regressions between SPAD readings and grain yield were significant for the two hybrids only in the stage of V10-V11 (R^2=0.74), and only for one hybrid at R1 (R^2=0.80).
Blackmer and Schepers, 1995	GY	V6, R4-R5	N	Cm	L	SPAD	SPAD units	cR	R^2=0.25 (V6) R^2=0.84 (R4-R5)	
Blackmer and Schepers, 1996	GY	R3	N	Cm	L	SPAD	SPAD units	cR	R^2=0.05	
Blackmer et al., 1994	GY (relative)		N	Cm	L	SPAD	SPAD units	cR	R^2=0.75	
Rorie et al., 2010	GY (relative)	VT	N	M	L	Digital cameras	relative DGCI	cR	Average R^2= 0.80	
Rorie et al., 2010	GY (relative)	VT	N	Cm	L	SPAD	SPAD units	cR	Average R^2= 0.79	
Wood et al., 1992	GY	V10, Midsilk	N	Cm	L	SPAD	SPAD units	cR	R^2=0.82 (V10) to 0.88 (midsilk)	For both DVSs tested.
Ziadi et al., 2008	GY (relative)		N	Cm	L	SPAD	SPAD units	cR	See notes	The Cm readings were significantly correlated to relative yield, but varied with site-year.

Authors	Estimated crop variable	DVS[a]	F[a]	Sensor type[a]	Target[b]	Sensor	VIs[a]	Statistical analysis[c]	Estimation performance	Notes
Tomer et al., 1997	GY	Crop maturity	N	M	Cveg	Digital camera	Single bands	Mr PCA	R^2=0.47 to 0.64	The R and NIR reflectance of crop and the NIR reflectance of soil consistently predict GY across two years.
Alganci et al., 2014	GY			M M	C Cveg	Satellite sensors Ground digital camera	NDVI, GI	cR Crop growth model (LUE)		Estimation error was 5% in test parcels and 10% in the region-based analysis.
Báez-González et al., 2002	GY	V4-R1		M	C	NOAA-Advanced Very High Resolution Radiometer (AVHRR)	NDVI	cR Crop growth model	See notes	Differences of 0.1 to 0.5 Mg ha^{1} were found between simulated and measured yields.
Báez-González et al., 2005	GY	84,103 DAS		M	C	Landsat EMT+	NDVI	Empirical model based on LAI	See notes	Mean simulation error (mSE) <12%. Using LAI estimated by satellite instead of the ground-measured LAI, the mSE increased of 2-5%.
Bausch et al., 2008	FY (relative)	VT	N	M	C	Quick-Bird Satellite	Several	cR	R^2=0.59	Relative G had the highest correlations of any of the other indices investigated.
Bausch et al., 2008	GY (relative)	VT	N	M	C	Quick-Bird Satellite	Several	cR	R^2=0.81	SI (using the G band) had the highest correlation of any of the other indices investigated.
Blackmer and Schepers, 1996	GY	R3	N	M	C	Camera	R band	cR	R^2=0.42	

Authors	Estimated crop variable	DVS[a]	F[a]	Sensor type[a]	Target[b]	Sensor	VIs[a]	Statistical analysis[c]	Estimation performance	Notes
Blackmer et al., 1996a	GY (relative)	R5	N	H	C	Spectroradiometer	Single wavelengths	cR	R^2=0.78	Best performances using relative reflectance. The wavelengths 550 nm and 710 nm were most correlated with GY. Also ratios using R, G, RE, and NIR showed high correlations
Blackmer et al., 1996b	GY	R5	N	M	C	Digital camera	Single wavelengths	cR	R^2=0.76-0.94	The R and G bands led to better performances than using the B band across four maize hybrids.
Chang et al., 2002	GY	V2, V6-V8, R-R.5		H	C	Digtal camera	NDVI, GNDVI	Mr PCA	Max R^2 =0.80	The PCA, on reflectance taken at different dates, followed by Mr permitted to retrieve information from soil and vegetation.
Clay et al., 2006	GY (losses caused by N stress)	V8–V9, V11–VT, R1–R2	N W	H M	C	Cropscan	Several	Mr	R^2=0.63 to 0.68	Three models to predict N rate were tested based on 1) yield loss caused by nitrogen stress, 2) yield, and 3) yield loss caused by water stress. The best model to drive N requirements was 1.
Doraiswamy et al., 2002	GY			M	C	NOAA-Advanced Very High Resolution Radiometer (AVHRR)	NIR	cR Crop growth model (LUE)	See notes	Model applied to regional scale.
Elwaldie et al., 2005	GY	V6-R	N W	M	C	Cropscan	Several	cR	R^2=0.70 to 0.98	G-based and R-based VIs performed better in the estimation of GY at R5.
Freeman et al., 2007	FY	V8-VT		M	C	GreenSeeker	NDVI	cR	R^2=0.37	

Authors	Estimated crop variable	DVS[a]	F[a]	Sensor type[a]	Target[b]	Sensor	VIs[a]	Statistical analysis[c]	Estimation performance	Notes
GopalaPillai et al., 1998	GY	55, 75, 99, 125, 141, 147DAS	N	M	C	Digital Camera	R, G, R/G	cR Mr	R^2=0.89	Best performance at 125 DAS.
GopalaPillai et al., 1999	GY	125 DAS	N	M	C	Digital camera	Several Single wavelengths	cR Mr	r=-0.84 to -0.99 R^2=0.60-0.99	G and R bands showed higher correlations than NIR. The NIR band was inconsistent between sites (weed presence invalidated the correlation). Better performances were found after pollination. The equations were specific for field and time of acquisition.
Inman et al., 2007	GY	V6-V8		M	C	GreenSeeker	NDVI/ratio	cR	R^2=0.65 for all site-years combined	The index NDVI/GDD from planting to sensing led to a better performance (R^2=0.58) than NDVI alone.
Krienke et al., 2015	GY	V11	N	M	C	RapidScan sensor	NDRE	cR	R^2=0.90	
Ma et al., 1996	GY	V6	N	M	C	Radiometer	Single wavelengths	cR	r=-0.54 to -0.97	Correlation coefficients found were found for leaf reflectance at 600 nm in different years.
Ma et al., 1996	GY	V6	N	M	C	Radiometer	NDVI	cR	r=0.50 to 0.80	The relation changed during years (in particular at anthesis and post-anthesis).
Martin et al., 2007	GY	V3-VT		M	C	GreenSeeker	NDVI	cR	R^2 max=0.66	The highest correlation was found between V8 and V12.

Authors	Estimated crop variable	DVS[a]	F[a]	Sensor type[a]	Target[b]	Sensor	VIs[a]	Statistical analysis[c]	Estimation performance	Notes
Osborne et al., 2002	GY	V6-V7, V13-V16, V14-R1	N W	H	C	Spectroradiometer	Entire spectrum	Mr	R^2=0.88-0.95 (V13-R4, in two years)	The model selected different wavelengths for different growing seasons and DVSs Poor relationship was found at V6-V7.
Osborne et al., 2004	GY	V6-V7, V13-V16, R1-R5	N W	M	C	Multispectral Imagery	NDVI, GNDVI	cR	R^2=0.74-0.78 (GNDVI and G, in two years at R-stages)	GNDVI and G band performed better than NDVI.
Rambo et al., 2010	GY	V5, V7, V10, R1	N	M	C	GreenSeeker, Crop scan	NDVI	cR	R=0.46 (V10) to 0.64 (R1)	NDVI correlated with grain yield only in V10 and R1 stages.
Senay et al., 1998	GY			M	C	Multispectral sensor	Several	cR	R^2=0.99	Best performance using NIR band.
Shanahan et al., 2001	GY	V6-R3	N	M	C	Multispectral Imagery		cR	R=0.70-0.92 (in two years)	The GNDVI was the index most correlated to the GY during the two studied seasons.
Shaver et al., 2011	GY	V8, V10, V12, V14	N	M	C	GreenSeeker, CropCircle	NDVI	cR Mr	R^2=0.66-0.75	Authors highlighted difficulties to direct N recommendations using only linear relationships between grain yield and VIs.
Solari et al., 2008	GY	V11, V15, R1, R3		M	C	Crop Circle	NDVI, CI	cR	R^2=0.75	NDVI and CI performed in a similar way.
Solari et al., 2010	GY (relative)	V11, V15	N	M	C	CropCircle	NDVI, CI	cR	R^2=0.61 (V11) R^2=0.81 (V15)	Algorithm needs to be tested in different conditions.

Authors	Estimated crop variable	DVS[a]	F[a]	Sensor type[a]	Target[b]	Sensor	VIs[a]	Statistical analysis[c]	Estimation performance	Notes
Sullivan et al., 2004	GY	V4-R2	N	M	C	ATLAS (Airborne)	NDVI GNDVI	cR	R^2=0.34-0.81	High variability was recorded among years, DVSs, and sites. Good prediction peaked at V8.
Teal et al., 2006	GY	V7-V9		M	C	GreenSeeker	NDVI	cR	R^2=0.77 at V8	The DVS was the main influence on the prediction of yield.. Categorizing sensor data by GDD extended the sensing window from V7 to V9.
Thenkabail et al., 1994	GY			M	C	Landsat-5 TM	Several	cR	R^2=0.52	
Thomason et al., 2007	GY	V2-V4, V6-V9, V11-V14, VT		M	C	GreenSeeker	NDVI	cR	R^2=0.65 (V6-V9)	The highest correlation was found at V6-V9.

[a] See Table S1 for DVS, F, Type of Sensor, and VI.
[b] Target of optical measurement (L=leaf level, C=canopy level without distinction between canopy and soil, Cveg=canopy level, separated soil and vegetation signal)
[c] Statistical analysis technique (cR =correlation and Regression with a single explanatory variable; Mr =Multiple regression; NN=Neural networks, PCA=Principal Component Analysis)

Empty cells indicate missing data in the original literature source.

3.9 Estimating technically optimum and economically optimum nitrogen rates

Ten and four authors derived empirical regressions between sensor readings and technically optimum (TONR) or economically optimum nitrogen rates (EONR), respectively (Table 8). Both of these estimated variables were studied at the leaf and at canopy levels using multispectral and chlorophyll meters. The optimum N rate was estimated at the leaf level in five papers using chlorophyll meters, in nine papers at the canopy level (vegetation + soil), and in two papers using a pure canopy signal after it was separated from that of the soil. Hand-held, tractor-mounted, and airborne multispectral sensors were all used in the estimations, resulting in highly variable EONR estimations (R^2 ranged from 0.53 and 0.84) and poor to moderate TONR performance estimations with R^2 values ranging between 0.30 and 0.70.

Table 8. Characteristics of papers reviewed papers from experiments conducted to estimate maize economically optimum nitrogen rate (EONR) and technically optimum nitrogen rate (TONR) from optical sensors. Papers are sorted first by sensed target and then by Author within the target.

Authors	Variable estimated	DVS[a]	F	Sensor type	Target[b]	Sensor	VIs	Statistical analysis[c]	Estimation performance	Notes
Hawkins et al., 2006	EONR	V8, V15, R1, R3	N	Cm	L	SPAD	Relative Cm readings	cR	R^2=0.73-0.76	The Cm readings differentiated N levels well both at the two early vegetative stages (V8 and V15) and at the two reproductive stages (R1 and R3).
Scharf and Lory, 2009	EONR	V6	N	M	L and C	CropScan	VIS/NIR ratios	cR	R^2=0.56-0.76	The highest R^2 were observed for relative reflectance at 510, 560, and 710 nm. A better prediction occurred when the sensor was oriented straight down.
Scharf et al., 2006	EONR	V5-R5	N	Cm	L	SPAD	Relative Cm readings	cR	R^2=0.53-0.76	R^2 were lower from V5 to V9 stage than at later stages (V10-R5).
Varvel et al., 2007	TONR	V8, V10, V12	N	Cm	L	SPAD	SPAD units	cR	R^2=0.70	
Kim et al., 2006	TONR		N	M	Cveg	MSIS	NDVI	cR Model for N recommendation	See notes	NDVI was used to estimate SPAD units, which were model inputs.
Scharf and Lory, 2002	EONR	V6-V7	N	M	Cveg	Multispectral Camera	Several	cR	R^2=0.60-0.79	Good predictions if: no N applied at planting, only vegetation pixels are used and colours are expressed in reference to an N-rich strip.
Barker and Sawyer, 2010	EONR	V9-V14	N	M	C	GreenSeeker, CropCircle	Several	cR	R^2=0.64-0.75	Several indices related to canopy biomass or canopy chlorophyll can be used in an N rate algorithm for applying N fertilizer in-season.

Authors	Variable estimated	DVS[a]	F	Sensor type	Target[b]	Sensor	VIs	Statistical analysis[c]	Estimation performance	Notes
Dellinger et al., 2008	EONR	V6-V7	N	M	C	CropCircle	rGNDVI	cR	R^2 = 0.84	EONR was strongly related to relative GNDVI for the control and manure pre-plant treatments, but unrelated when NH_4NO_3 was applied at planting (R^2 = 0.20).
Kitchen et al., 2010	EONR	V4-V15	N	M, Cm	C L	CropCircle, SPAD	SI	cR	Max R^2=0.70	SI correlated with EONR only in 50% of fields.
Kitchen et al., 2010	TONR	V4-V15	N	M Cm	C	CropCircle, SPAD	SI	cR	Max R^2=0.71	
Schmidt et al., 2009	EONR	V6-V7	N	M	C	CropCircle	rGNDVI	cR	R^2 = 0.76	
Sripada et al., 2005	EONR	VT	N	M	C	Multispectral Camera	Several	cR	R^2=0.67	The best model was a linear-plateau model based on GNDVI and rGNDVI (using a N-rich strip).
Sripada et al., 2006	TONR	V7	N	M	C	Digital camera	Several	cR	Max R^2=0.33 (V7)	Indices based on G reflectance had the best performances. Soil pixels should be eliminated for improved relationships between maize colour and optimum N rates at V7.
Sripada et al., 2008	EONR	V6-V7	N	M	C	CropCircle	Several	cR	Max R^2=0.79 (GNDVI at V6)	A better prediction of EONR was obtained by VIs calculated relative to a high N plot rather than absolute indices

[a] See Table S1 for DVS, F, Type of Sensor, and VI.
[b] Target of optical measurement (L=leaf level, C=canopy level without distinction between canopy and soil, Cveg=canopy level, separated soil and vegetation signal)
[c] Statistical analysis technique (cR =correlation and Regression with a single explanatory variable).

Empty cells indicate missing data in the original literature source.

4 DISCUSSION

4.1 Distinguishing situations with different N availability

For the simple objective of estimating applied N (Table 1), NDVI performed best at crop development stages V14 to VT. These results suggest that, in these experiments, the effects of different N application rates prior to DVS V14 did not appear until the crop began to take up high amounts of N during rapid stalk elongation. This phenomenon was also particularly evident in experiments where pre-planting and emergence nitrogen rates (50-60 kg N applied ha^{-1}) were among the highest applied (Shaver et al., 2011; Tremblay et al., 2009). On a broader scale, this underscores the importance of undertaking optical sensing with an N budget approach. It must be recognized that at high N availability—be it from natural sources of native organic matter mineralisation, or precipitation, or from accumulated residual fertility (leguminous crop), or from pre-planting mineral N application—canopy optical properties that occur from N fertilisation treatment differences do not appear or appear after sensing. Consequently, when N is not a limiting factor, proximal or remote sensing may fail to differentiate among plots treated with differing N rates.

Estimation variability reported in Table 1 also related to field geographic location, which meant it was influenced by weather (temperature and precipitations), growing season length, soil variability, and a myriad of management practices not limited to irrigation, planting dates, and maize varieties (Rambo et al., 2010; Shaver et al., 2011). Therefore, results from different experiments produced location-specific regression equations, not generalizable for widespread use (Bragagnolo et al., 2016; Kitchen et al., 2010; Krienke et al., 2015; Rambo et al., 2010; Shaver et al., 2011; Tremblay et al., 2009; Varvel et al., 2007).

4.2 Chlorophyll content

In general, the best performing estimates ($R^2 \geq 0.87$) of chlorophyll content at the leaf level were obtained using the RE, NIR, R, and G bands (Table 2) (Blackmer et al., 1994; Casa et al., 2015; Ciganda et al., 2009; Daughtry et al., 2000; Gitelson et al., 2005; Rorie et al., 2010 and 2011). However, these bands were not always successful, as the lower R^2 values of Blackmer et al. (1994) (R^2=0.74) and Zhao et al. (2003) (R^2=0.36-0.52) demonstrate.

The canopy signal was separated from that of soil in only four papers (Noh et al., 2005 and 2006; Noh and Zhang, 2012; Reum and Zhang, 2007), all of which were carried out with tractor-mounted or hand-held digital cameras. The bands (R, G, and NIR) identified in all studies at the leaf level were the same for those at the canopy level; however, only the lowest R^2 value (0.72)—not the highest R^2 value (0.89)—obtained at the canopy level was comparable to those obtained at the leaf level. Note that the RE band was not identified because it was not measureable with the digital cameras used in these four experiments. The best performance (R^2 = 0.89) obtained used a neural network approach (Noh et al., 2006) to the information coming from all available bands. In general, the enhanced spatial resolution in digital cameras that permits soil and vegetation pixel separation is valuable, but that few broad bands can limit their performance.

At the canopy level, the non-separation of soil spectrum from vegetation spectrum approach was most common. Both simple and multivariate regression confirmed large variability of performance estimation. The highest R^2 was found using indices based on G, NIR, and RE by Clevers and Gitelson (2012), however, we were unable to discern the reasons why in some cases the performance was better than in others.

At both leaf and canopy levels, factor DVS seemed unable to explain result variability. This means, together with the moderate to very good performance, that sensing can be carried out

in the most appropriate moment (determined by farm organisation and sensing objectives), without worrying about performance.

4.3 Nitrogen concentration

Most of the observations identified for chlorophyll are valid also for nitrogen concentrations (Table 3). Chlorophyll content information, gleaned most from the VIS and NIR ranges of the spectrum, is highly correlated to nitrogen content and therefore, can be used to assess nitrogen concentration.

At the leaf level, predictions were moderate to excellent. In some cases, single bands were tested to estimate leaf nitrogen concentration; the G and R bands were found to be most successful (R^2 0.74-0.90) (Blackmer et al., 1994 and 1995). Leaf N concentration was also estimated with vegetation indices or chlorophyll meter readings (R^2 0.70-0.90) (Rorie et al., 2010 and 2011; Zhao et al., 2003). Finally, multivariate data analysis estimated nitrogen concentration using the entire spectrum from 400-1100 nm as set of predictors with an R^2 of 0.96 based on leaf discs in the laboratory (Lee et al., 1999), and in general, to obtain an average R^2 of 0.92 (Alchanatis et al., 2005; Lee et al., 1999; Lee and Searcy, 2000). The work of authors considered for this review identified the same regions (G and R), in addition to NIR, as the most informative. Finally, as noted by Lee and Searcy (2000), the orientation and distance of the leaf from the sensor is of high import. In one experimental year, canopy architecture affected sensor measurement results more than N did.

Results at the canopy level were less satisfactory with R^2 as low as 0.20 (Sullivan et al., 2004). The fact that signal was unaffected by canopy geometry accounts for the better performances at leaf level. Nevertheless, moderate to good performances at the canopy level were obtained with R^2 values as high as 0.90 (Oppelt and Mauser, 2003; Sullivan et al., 2004). In the case of the most informative wavebands, the findings were very similar to those

of chlorophyll. We did not identify a clear effect of sensor type on prediction quality, which suggests that adequate predictions are possible with sensors at distances far from the canopy (satellite, Bausch et al., 2008). The exemptions to this rule are hand-held instruments (Sullivan et al., 2004), which are insufficient to ensure good predictions at large distances. In addition, we found that both at the leaf and canopy levels, successful predictions were obtained for a wide range of DVSs (from V3 to R5) with no trends observed over time. In conclusion, we found no evidence to support that nitrogen concentration be estimated at specific DVSs or with specific sensors. Thus we submit no recommendations for the variable.

Authors who focused on NNI obtained rather low R^2 values. Chlorophyll meter readings were positively, but weakly correlated with NNI (R^2=0.26-0.60) during the growing season. The relationships were site-specific (Xia et al., 2015; Ziadi et al., 2008), but other selected authors showed that chlorophyll meter readings from an over-fertilised strip corrects for cultivar and site effects (Blackmer and Schepers, 1995; Schepers et al., 1992).

4.4 Leaf area Index

Experiments aimed at LAI estimation found moderate to very good relationships (R^2=0.50-0.90) between LAI and VIs (Table 4) (Báez-González et al., 2005; Elwadie et al., 2003; Gilabert et al., 1996; Gitelson et al., 2003; Kira et al., 2016; Ma et al., 1996; Nguy-Robertson et al, 2012; Sakamoto et al., 2012a, 2012b; Thenkabail et al., 1994). The experiments agree that G, R, RE and NIR regions are the most suitable for LAI estimation (Bragagnolo et al., 2016, Cilia et al., 2014; Kira et al., 2016; Nguy-Robertson et al, 2012). The most reliable DVS range from which to estimate LAI using NDVI or similar VIs resulted as V7-V12 (Freeman et al., 2007; Martin et al., 2007; Xia et al., 2015). Furthermore, LAI is best estimated early in the season because after full canopy cover (V9-V12), any increase in LAI

is not accompanied by a corresponding increase of fraction cover, and thus, not of VIs, which proceed to lose correlation with LAI.

4.5 Above ground biomass

The fact that all studies that estimated AGB were carried out at the canopy level is obvious. Indeed, leaf-level measurements do not detect increases in leaf proportion, for which AGB is a proxy, relative to soil that occurs over time. Canopy level measurements do. Despite the fact that canopy level measurements do perform in this way, we found results that contrasted with this approach as an adequate solution. For example, using R-based VIs like NDVI, Freeman et al. (2007) found a weak relationship (R^2=0.37) with maize AGB at V8-V10, while Xia et al. (2015) reported better performances (R^2=0.90) at V5-V10. Martin et al. (2007) and Thomason et al. (2007) found intermediate NDVI performances (R^2=0.66-0.80) at V3-VT. Moreover, NIR and RE bands and related VIs (NDRE) that were reported from different optical sensors resulted in very good to excellent estimations (R^2=0.91-0.98) with AGB (Bragagnolo et al., 2016; Sakamoto et al., 2012a and 2012b). As was the case of N concentration, AGB did not clearly indicate which of the various factors (DVS, VI, type of sensor) best estimated the variable. The absence of a DVS trend surprised us, as we expected that VIs describing fraction cover would perform well at early DVSs, and poorly after full cover. This is not demonstrated in the experiments reviewed.

4.6 Nitrogen uptake

Prediction of N uptake by maize, mainly undertaken at the canopy scale, produced seemingly contrasting results (Table 6). Some selected studies found N uptake could be successfully estimated using VIs based on RE bands (Bragagnolo et al., 2016; Li et al., 2014; Xia et al., 2015). However, estimations were not consistently good across DVSs. For example, Xia et

al. (2015) found an R^2 of 0.36 at V5 and 0.75 at V8. RE-based indices were successful because the bands are good predictors of N concentration, as shown by work of Perry and Roberts (2008). Conversely, other researchers found N uptake could be estimated using NDVI and GNDVI (Varco et al., 2013); in these cases, these indices achieved success because they were strongly correlated to AGB (Freeman et al., 2007; Teal et al., 2006). On the other hand, these results seem to be in contrast to each other because the same variable (N uptake) was estimated with different. The contrast is explained by recalling that N uptake is calculated as the product of N concentration and AGB. Freeman et al. (2007) proposed an index (NDVI multiplied by crop height) to improve N uptake estimation, designed to overcome NDVI saturation-related problems after canopy. The key contribution of AGB to N uptake explains why it was studied most at canopy scale.

Relationships between VIs and N uptake were speci c to sensor, location, and DVS. Osborne et al. (2002) analysed hyperspectral data and outlined the issue of N uptake estimation as a function of crop development. Despite the good predictions they achieved with multivariate regression models, they found wavelengths selected by statistical models were inconsistent across phenological stages. Moreover, their results depended strictly on location and were not transferrable to other areas.

The best results for both N uptake and concentration were found across a range of development stages (from V4 to R5) far larger than the one identified (see above) to estimate N rate (Table 1). This result contrasts starkly with canopy changes not revealed at varying N rates until V14. One possible explanation is that for N concentration and uptake estimation (Table 4), several experiments utilised VIs or statistical procedures that were either more complex or based on different bands, thereby capturing canopy differences beyond NDVI measurability, and in contrast to instances of N rate estimation (Table 1) in which NDVI or

chlorophyll meters were generally used. It is also possible that experimental conditions (Table 4) were such that canopy differentiation occurred much earlier (at V4) than it did in Table 1 experiments (at V14).

4.7 Crop Yield

At the leaf level, most attempts were carried out with SPAD. Blackmer and Schepers (1995) found a poor correlation between SPAD units at V6 and final grain yield (Table 7) (R^2 = 0.25). Moderate to good correlations were found at V10 or later (R^2=0.74-0.88 in most cases and R^2=0.05 in a single case) in their later study (Blackmer and Schepers, 1996). Using SPAD as a predictor of final yield requires nitrogen to be the only limiting factor. Absent this condition (Blackmer and Schepers, 1996), no correlation is found.

At the canopy level, some studies found moderate relationships (R^2=0.60-0.70) between NDVI measured during early development stages (V5-V9) and final grain yield (Teal et al., 2006; Martin et al., 2006; Thomason et al., 2007), although different relationships were obtained in different growing seasons. At later development stages (V12 and later) poor to excellent estimations of grain yields (R^2 = 0.21-0.99) were produced using single wavebands, NDVI and GNDVI obtained by hand-held multispectral instruments (Rambo et al., 2010; Shaver et al., 2011; Solari et al., 2008) and aerial images (GopalaPillai et al., 1999; Osborne et al., 2004 and Shanahan et al., 2001). Using satellite-mounted sensors, Bausch et al. (2008) and Rorie et al. (2010) found moderate relationships between VIs (measured at VT) and relative grain yield (R^2 =0.81). Nearly all authors working at the canopy level agreed that G band was best to assess grain yield. Alternatively, Krienke et al. (2015) predicted maize grain yield (R^2=0.90) at V11 using a RE-based index. Tomer et al. (1997) used the signals emitted by a digital camera of crop R and NIR reflectance and soil NIR reflectance with multivariate data analysis (PCA and MLR) to predict yield consistently over

two years (R^2=0.47 to 0.64). Yet, as this case highlights, the potential of multivariate data analysis is not enough to overcome these not particularly encouraging results.

Reviewed studies showed wide variability in the relationship between VIs and grain yields across sites (soil and weather) and years. In addition, such relationships were often location- and/or hybrid-speci c, making it essentially impossible to make efficacious, yet generalizable, VI-based nitrogen recommendations (Shaver et al., 2011). Osborne et al. (2002) noticed this same variability, and consequently selected different wavelengths for different DVSs and growing seasons using step-wise multivariate regressions. To reduce the effect of DVS on prediction quality, Raun et al. (2001) used growing-degree day (GDD) counts (day of planting to day of optical measurement) to standardize NDVI values (INSEY=NDVI/GDD), from which they obtained regression models to predict winter wheat grain yields applicable to many site × year combinations. Inman et al. (2007) and Teal et al. (2006) turned to the INSEY approach on maize. Teal et al. (2006) noticed good grain yield predictions were possible earlier in the season with INSEY compared to the timing of simple NDVI, but Inman et al. (2007) noted that the NDVI ratio in the field portion to-be-managed and the NDVI in an N-rich strip in the same field (used to inform effect of variety × environment on canopy optical properties) correlated better and significantly with observed maize grain yields than with INSEY.

Site differences of soil and weather mainly affected VIs and yield relationships, but factors such as crop hybrid and plant physiological status also played a role (Inman et al., 2007). Considering the interactions between site and other factors is necessary to develop widely-applicable models to estimate grain yields from optical sensors. One method to improve crop yield estimates is to combine satellite optical data and crop growth models. In fact, Báez-González et al. (2002) developed a methodology to estimate maize yield under irrigated (R^2

= 0.89) and non-irrigated (R^2 = 0.76) conditions. It combined satellite-NDVI and ground-based data (Photosynthetic Active Radiation, LAI, crop development stage, and planting dates) and a dynamic mechanistic crop growth model. In another example, Alganci et al. (2014) and Doraiswamy et al. (2002) used satellite sensor data to estimate maize grain yield at the regional scale with a Light Use Efficiency model.

4.8 Estimating technically optimum and economically optimum nitrogen rates

At the leaf level, some authors used standardised chlorophyll meter readings to predict EONR (or TONR), while at the canopy level, most studies (Table 8) used VIs instead of chlorophyll meter readings. Performances at the canopy level were affected by crop development stage and generally moderate, and nearly all reported the most informative regions of the spectrum were G, R, and NIR.

Among tested VIs, GNDVI and standardised GNDVI calculated in early growth (V6-V7) from both ground and airborne sensor data resulted in the best EONR estimates (R^2=0.67-0.74) (Barker and Sawyer, 2010; Dellinger et al., 2008; Scharf and Lory, 2002; Schmidt et al., 2009; Sripada et al., 2005; Sripada et al., 2008). Goel et al. (2003) identified 478 (G) and 671 nm (R) regions as the most useful to detect N stress effects, irrespective of DVS. Scharf and Lory (2009) confirmed that the same spectral regions (510, 560, and 710 nm) correlate much stronger with EONR. Among the authors who used digital cameras, they also stressed the need to separate the canopy from the soil signal when the relationship between VIs and N rate is established early in the season (Scharf and Lory, 2002; Sripada et al., 2006). Moreover, even if part of the inter-site variability is eliminated using the N-rich strip, these relationships remain site-specific because they depend on other not sensed N budget components (*e.g.,* final crop yield, potential N mineralisation).

To account for these components, other works took a more analytical approach and developed complex models to calculate TONR and EONR. Holland and Schepers (2010) and Solie et al. (2012) epitomize these advanced approaches because their algorithms were developed into commercial products CropCircle and GreenSeeker, respectively. These models are characterised by two approaches to estimate optimum N rates: "nitrogen mass-balance" concept-based models (Holland and Schepers, 2010) and yield prediction-based models (generalized algorithm for variable-rate nitrogen application in cereal grains by Solie et al., 2012).

Holland and Schepers' model relies on a Sufficiency Index (SI), calculated as the ratio of optical sensor vegetation readings to a reference N-rich strip. The researchers developed a generalised exponential function model that relates the measured SI to an estimate of infield N rate. Finally, the estimated N rate is used to determine a simplified N budget from local conditions (local maximum N rate and nitrogen credit from applied manure and previous crop). Solari et al. (2010) and Varvel et al. (2007) also proposed an algorithm to translate SI into recommended N rates. As opposed to Holland and Schepers (2010), these authors established an empirical SI and N rate relationship, from which they could estimate optimum N rate via measurements taken at V7-V1 with a chlorophyll meter and multispectral sensor ($R^2 \approx 0.70$). Kim et al. (2007) successfully employed the algorithm proposed by Francis and Piekielek (1999) to estimate optimum N rates from SI, using target yield, applied manure, and crop development stage as inputs. On the contrary, Kitchen et al. (2010) had a less satisfactory experience with SI, which empirically correlated with optimal N rates in only 50% of managed fields.

The generalised algorithm for variable rate nitrogen application to cereal grains by Solie et al. (2012) came from algorithms of Lukina et al. (2001) and Raun et al. (2005). The model

relies on three assumptions: 1) there is a maximum potential yield for any field, or zone within it, for any year; 2) SI can determine any yield obtainable with sufficient nitrogen fertiliser because of the VI and yield relationship; 3) nitrogen rate is determined by dividing N removal estimated from the predicted yield by the projected use efficiency. Inputs to this algorithm are growing-degree days from planting to sensing, SI based on NDVI (in their case), and maximum within-field yield. Coefficients are determined empirically for VI-based yield estimates.

Optimum nitrogen rate estimation results were best when an N-rich strip was used as a reference to calculate a relative index like SI (Dellinger et al., 2008; Hawkins et al., 2006; Kitchen et al., 2010; Sripada et al., 2005; Sripada et al., 2008). N-rich strips were used because optical measurements are strongly affected by local conditions other than N, such as weather, soil fertility, hybrid, and crop management. These factors and their interactions lead to site- and year-specific regression coefficients. To overcome this problem, an N-rich strip was frequently used to obtain a reference measurement describing the effects on the crop of other environmental and management factors under non-N-limiting conditions. This reference allowed standardised measurements to be carried out in the rest of the field, leading to relative indices like SI. The evidence amassed in this work indicates that an N-rich strip is practically unavoidable, and should be combined with a dedicated algorithm (*e.g.,* Holland and Schepers, 2010; Solie et al., 2012) to formulate a practical indication of the side-dressing rate. Even if attempts were made to estimate optimum N rate at later development stages, most experiments were already able to predict—with poor to good performance (R^2 = 0.33-0.84)—the optimum N rate by V6-V7, when fertiliser can still be side-dressed with a tractor. The G and NIR bands were deemed most informative (Dellinger et al., 2008; Scharf and Lory, 2009; Sripada et al., 2005). Some authors indicated that N fertilisation at planting

results in an underestimation of the required N rate, and can may cause the field to be very similar to the N-rich strip

4.9 Research needs

4.9.1 Interactions between nitrogen and water availability

Most of the works presented so far were conducted with N as the single limiting factor, making it impossible to verify the effects of other factors on sensor response to nitrogen. Water is one of the most important of these other factors. Of note is that spectral effects of water are superimposed onto those of nitrogen, which makes their separation very important. The rare study attempted to verify simultaneous effects of nitrogen and water stress on leaf or canopy reflectance (Clay et al., 2006; Osborne et al., 2002; Schlemmer et al., 2005); others tried to associate VI sensitivity with one stressor or the other (Schlemmer et al., 2005; Perry and Roberts, 2008). These works were limited by the few crop variables predicted in the presence of both stressors: maize chlorophyll content (Schlemmer et al., 2005), yield (Osborne et al., 2002; Elwadie et al., 2005; Clay et al., 2006) and leaf nitrogen concentration (Perry and Roberts, 2008; Cilia et al., 2014). The research was also limited by the absence of water stress in all experimental years (Osborne et al., 2002; Perry and Roberts, 2008) or separation of the effects of the two stressors during the data analysis (Osborne et al., 2002; Cilia et al., 2014). Moreover, results contrasted across the studies. For example, Schlemmer et al. (2005) and Perry and Roberts (2008) identified the RE region as sensitive to N stress, but not to water stress, as opposed to Clay et al. (2006), who found the RE region was indicative for the interaction between nitrogen and water stress. The uncertain suitability of using optical sensing techniques to drive maize nitrogen fertilisation during times of water stress requires more research.

More practical attempts to manage the simultaneous presence of the two stressors are available for crops other than maize. One approach taken by Fitzgerald et al. (2006) on wheat combined indices measured by identical sensors of different water and nitrogen stress sensitivities. The work used the CCCI (canopy chlorophyll content index), calculated as a two-dimensional index based on NDVI and NDRE (Clarke et al., 2001), relative to nitrogen concentration and expressed as a function of dry biomass, to avoid a water stress effect on tissue N dilution. They reported an R^2 of 0.68, and then described two limitations of the work: CCCI calculation requires seasonal data and its unknown stability across the years. The second approach combined indices from different sensors, typically using optical sensors to identify N stress and thermal infrared sensors for water stress. Cohen et al. (2013) tested the technique by fusing hyperspectral and thermal data on potato that resulted in 83% and 65% classification accuracy on two potato varieties. A third approach utilised multivariate analysis of hyperspectral data on maize (Strachan et al., 2001). Discriminant analysis performed by the authors produced accurate N rate sample classifications during early, mid, and late season with overall success rates of 70%, 88%, and 93%, respectively.

4.9.2 Role of soil

An important issue in the use of optical sensing is the spatial resolution of the sensors. If the vegetation fraction cover is small and the sensor spatial resolution is too low, then the signal receives data from both the soil and from the vegetation. Typically, in the early stages of development, an averaged signal of soil and vegetation is produced, rather than a pure vegetation signal. An increase in spatial resolution, as provided by a multispectral camera, makes it possible to separate the soil signal from the vegetation signal by assigning them to different pixels. The process can enhance the correlation between spectral data and crop variables, which are linked more strictly to leaf chemical constituents than to fraction cover

(*e.g.,* Scharf and Lory, 2002). The separation of soil from vegetation is a time-consuming operation and requires additional skills.

The fact that we propose, in some cases, to separate soil from vegetation does not imply that soil is unimportant. Indeed, soil regulates the availability of nitrogen for the crop through many properties: soil organic matter content, soil structure, microorganism activity, and water movement. While more mechanistic approaches that explicitly use soil information to estimate optimum nitrogen rates were developed recently, although maize examples are unavailable. Other crop examples include sensor fusions that interpret VIs using measurements from soil geophysical instruments (Li et al., 2008). Mechanistic models can also be used to simulate the fate of N in the soil-crop system to support N management decisions (Baret et al., 2007).

4.9.3 Exploration of new bands

Relatively few works addressed the question remains of whether or not bands not yet used would improve predictions. New bands can be explored with hyperspectral sensors; however, some of the experiments that exploited hyperspectral sensors failed to conduct full multivariate analyses; instead, a simplified approach was taken and only some of the available bands were used to calculate indices. This limited the ability to determine if a few or many other wavelengths would improve crop property estimation, a result that could be achieved by conducting a complete multivariate analysis of hyperspectral data.

5 CONCLUSIONS

The studies surveyed show that by using various vectors and tools, remote and proximal sensing of crop canopy has good potential to estimate maize N management-related variables (applied N rate, chlorophyll content, aboveground biomass, LAI, N uptake, N concentration, final yield, and optimum N rate).

Results obtained in different experiments produced different location-specific regression equations. The fact that these relationships are empirical is a major drawback that limits their widespread practical application. N-rich (over-fertilised) plots or strips are a good solution to circumvent at least some of the empiricism, as they help to standardise sensor readings.

Another drawback of simple vegetation indices is that once canopy closure occurs, LAI and biomass growth can no longer be estimated.

The estimation of technically or economically optimum N rates normally requires N-rich strips, used in combination either with vegetation indices or with budget methods. Most experiments successfully predicted optimum N rate at V6-V7, an early stage that still allows application of subsequent tractor side-dressing.

Future research should be aimed at the use of additional wavelengths in the NIR region. Hyperspectral sensors have shown promise for estimating maize N uptake and crop N concentration. Moreover, further research to define better how sensors should guide N management when the crop is stressed by a lack of water. Finally, more mechanistic solutions to estimate optimum N rate should be developed to take into account the role of soil, either by compiling relatively simple analytical budgets or by using more complex dynamic simulation models of the soil-crop system.

6 REFERENCES

Alchanatis, V., Schmilovitch, Z., Meron, M., 2005. In-field assessment of single leaf nitrogen status by spectral reflectance measurements. Precision Agriculture 6, 25–39.

Alganci, U., Ozdogan, M., Sertel, E., Ormeci, C., 2014. Estimating maize and cotton yield in southeastern Turkey with integrated use of satellite images, meteorological data and digital photographs. Field Crops Research 157, 8–19.

Argenta, G., Silva, P.R.F. da, Sangoi, L., 2004. Leaf relative chlorophyll content as an indicator parameter to predict nitrogen fertilization in maize. Ciência Rural 34, 1379–1387.

Báez-González, A.D., Chen, P., Tiscareño-López, M., Srinivasan, R., 2002. Using Satellite and Field Data with Crop Growth Modeling to Monitor and Estimate Corn Yield in Mexico. Crop Science 42, 1943–1949. doi:10.2135/cropsci2002.1943

Baez-Gonzalez, A.D., Kiniry, J.R., Maas, S.J., Tiscareno, M.L., Macias, C., Mendoza, J.L., Richardson, C.W., Salinas, G., Manjarrez, J.R., others, 2005. Large-area maize yield forecasting using leaf area index based yield model. Agronomy Journal 97, 418–425.

Baret, F., Houlès, V., Guérif, M., 2007. Quantification of plant stress using remote sensing observations and crop models: the case of nitrogen management. J. Exp. Bot. 58, 869–880. doi:10.1093/jxb/erl231

Barker, D.W., Sawyer, J.E., 2010. Using Active Canopy Sensors to Quantify Corn Nitrogen Stress and Nitrogen Application Rate. Agronomy Journal 102, 964–971. doi:10.2134/agronj2010.0004

Bauer, M.E., 1985. Spectral inputs to crop identification and condition assessment. Proceedings of the IEEE 73, 1071–1085.

Bausch, W.C., Halvorson, A.D., Cipra, J., 2008. Quickbird satellite and ground-based multispectral data correlations with agronomic parameters of irrigated maize grown in small plots. Biosyst. Eng. 101, 306–315. doi:10.1016/j.biosystemseng.2008.09.011

B. Krienke, R. Ferguson, B. Maharjan, 2015. Using an unmanned aerial vehicle to evaluate nitrogen variability and distance effect with an active crop canopy sensor, in: Precision Agriculture ’15. Wageningen Academic Publishers, pp. 143–150.

Blackmer, T.M., Schepers, J.S., 1996. Aerial photography to detect nitrogen stress in corn. Journal of Plant Physiology 148, 440–444.

Blackmer, T.M., Schepers, J.S., 1995. Use of a chlorophyll meter to monitor nitrogen status and schedule fertigation for corn. Journal of production agriculture 8, 56–60.

Blackmer, T.M., Schepers, J.S., Varvel, G.E., 1994. Light reflectance compared with other nitrogen stress measurements in corn leaves. Agronomy Journal 86, 934–938.

Blackmer, T.M., Schepers, J.S., Varvel, G.E., Meyer, G.E., 1996b. Analysis of aerial photography for nitrogen stress within corn fields. Agronomy Journal 88, 729–733.

Blackmer, T.M., Schepers, J.S., Varvel, G.E., Walter-Shea, E.A., 1996a. Nitrogen deficiency detection using reflected shortwave radiation from irrigated corn canopies. Agronomy journal 88, 1–5.

Bragagnolo, J., Amado, T.J.C., Bortolotto, R.P., 2016. Use efficiency of variable rate of nitrogen prescribed by optical sensor in corn. Revista Ceres 63, 103–111.

Casa, R., Castaldi, F., Pascucci, S., Pignatti, S., 2015. Chlorophyll estimation in field crops: an assessment of handheld leaf meters and spectral reflectance measurements. The Journal of Agricultural Science 153, 876–890. doi:10.1017/S0021859614000483

Chang, J., Clay, D.E., Dalsted, K., Clay, S., O’Neill, M., 2003. Corn (L.) yield prediction using multispectral and multidate reflectance. Agronomy journal 95, 1447–1453.

Ciganda, V., Gitelson, A., Schepers, J., 2009. Non-destructive determination of maize leaf and canopy chlorophyll content. Journal of plant physiology 166, 157–167.

Cilia, C., Panigada, C., Rossini, M., Meroni, M., Busetto, L., Amaducci, S., Boschetti, M., Picchi, V., Colombo, R., 2014. Nitrogen Status Assessment for Variable Rate Fertilization in Maize through Hyperspectral Imagery. Remote Sensing 6, 6549–6565. doi:10.3390/rs6076549

Clarke, T.R., Moran, M.S., Barnes, E.M., Pinter Jr, P.J., Qi, J., 2001. Planar domain indices: A method for measuring a quality of a single component in two-component pixels, in: Geoscience and Remote Sensing Symposium, 2001. IGARSS'01. IEEE 2001 International. IEEE, pp. 1279–1281.

Clay, D.E., Kim, K.-I., Chang, J., Clay, S.A., Dalsted, K., 2006. Characterizing water and nitrogen stress in corn using remote sensing. Agronomy Journal 98, 579–587.

Clevers, J., Gitelson, A.A., 2012. Using the red-edge bands on Sentinel-2 for retrieving canopy chlorophyll and nitrogen content, in: Sentinel-2 Preparatory Symposium, Frascati, Italy. pp. 23–27.

Cohen, Y., Alchanatis, V., Meron, M., Saranga, Y., Tsipris, J., 2005. Estimation of leaf water potential by thermal imagery and spatial analysis. Journal of experimental botany 56, 1843–1852.

Cohen Yafit, Rosen Carl, Alchanatis V., Mulla D., Heuer Bruria, Dar Zion, Ronit Rud, and Tyler Nigon: "Fusion of Hyperspectral and Thermal Images for Evaluating Nitrogen and Water Status in Potato Fields for Variable Rate Application." Final Scientific Report of BARD Project, Number: IS-4255-09.

Daughtry, C.S.T., Walthall, C.L., Kim, M.S., De Colstoun, E.B., McMurtrey, J.E., 2000. Estimating corn leaf chlorophyll concentration from leaf and canopy reflectance. Remote sensing of Environment 74, 229–239.

Dellinger, A.E., Schmidt, J.P., Beegle, D.B., 2008. Developing Nitrogen Fertilizer Recommendations for Corn Using an Active Sensor. Agron J 100, 1546–1552. doi:10.2134/agronj2007.0386

Diker, K., Bausch, W.C., 2003. Radiometric Field Measurements of Maize for estimating Soil and Plant Nitrogen. Biosystems Engineering 86, 411–420. doi:10.1016/j.biosystemseng.2003.08.016

Doraiswamy, P.C., Hatfield, J.L., Jackson, T.J., Akhmedov, B., Prueger, J., Stern, A., 2004. Crop condition and yield simulations using Landsat and MODIS. Remote Sensing of Environment, 2002 Soil Moisture Experiment (SMEX02) 92, 548–559. doi:10.1016/j.rse.2004.05.017

Elwadie, M.E., Pierce, F.J., Qi, J., 2005. Remote sensing of canopy dynamics and biophysical variables estimation of corn in Michigan. Agronomy Journal 97, 99–105.

Fitzgerald, G.J., Rodriguez, D., Christensen, L.K., Belford, R., Sadras, V.O., Clarke, T.R., 2006. Spectral and thermal sensing for nitrogen and water status in rainfed and irrigated wheat environments. Precision agriculture 7, 233–248.

Freeman, K.W., Girma, K., Arnall, D.B., Mullen, R.W., Martin, K.L., Teal, R.K., Raun, W.R., 2007. By-Plant Prediction of Corn Forage Biomass and Nitrogen Uptake at Various Growth Stages Using Remote Sensing and Plant Height. Agronomy Journal 99, 530–536. doi:10.2134/agronj2006.0135

Gilabert, M.A., Gandía, S., Melia, J., 1996. Analyses of spectral-biophysical relationships for a corn canopy. Remote Sensing of Environment 55, 11–20.

Gitelson, A.A., Peng, Y., Masek, J.G., Rundquist, D.C., Verma, S., Suyker, A., Baker, J.M., Hatfield, J.L., Meyers, T., 2012. Remote estimation of crop gross primary production with Landsat data. Remote Sensing of Environment 121, 404–414.

Gitelson, A.A., Viña, A., Arkebauer, T.J., Rundquist, D.C., Keydan, G., Leavitt, B., 2003. Remote estimation of leaf area index and green leaf biomass in maize canopies. Geophysical Research Letters 30.

Gitelson, A.A., Vina, A., Ciganda, V., Rundquist, D.C., Arkebauer, T.J., 2005. Remote estimation of canopy chlorophyll content in crops. Geophysical Research Letters 32.

Goel, P.K., Prasher, S.O., Landry, J.A., Patel, R.M., Bonnell, R.B., Viau, A.A., Miller, J.R., 2003. Potential of airborne hyperspectral remote sensing to detect nitrogen deficiency and weed infestation in corn. Computers and electronics in agriculture 38, 99–124.

Goel, P.K., Prasher, S.O., Patel, R.M., Landry, J.A., Bonnell, R.B., Viau, A.A., 2003. Classification of hyperspectral data by decision trees and artificial neural networks to identify weed stress and nitrogen status of corn. Computers and Electronics in Agriculture 39, 67–93. doi:10.1016/S0168-1699(03)00020-6

GopalaPillai, S., Tian, L., Beal, J., 1998. Detection of nitrogen stress in corn using digital aerial imaging. Urbana 51, 61801.

GopalaPillai, Sreekala, and Lei Tian, 1999. In-field variability detection and spatial yield modeling for corn using digital aerial imaging. Transactions of the ASAE 42.6: 1911.

Hansen, P.M., Schjoerring, J.K., 2003. Reflectance measurement of canopy biomass and nitrogen status in wheat crops using normalized difference vegetation indices and partial least squares regression. Remote Sensing of Environment 86, 542–553. doi:10.1016/S0034-4257(03)00131-7

Hawkins, J.A., Sawyer, J.E., Barker, D.W., Lundvall, J.P., 2007. Using Relative Chlorophyll Meter Values to Determine Nitrogen Application Rates for Corn. Agronomy Journal 99, 1034. doi:10.2134/agronj2006.0309

Holland, K.H., Schepers, J.S., 2010. Derivation of a variable rate nitrogen application model for in-season fertilization of corn. Agronomy journal 102, 1415–1424.

Hunt, E.R., Doraiswamy, P.C., McMurtrey, J.E., Daughtry, C.S.T., Perry, E.M., Akhmedov, B., 2013. A visible band index for remote sensing leaf chlorophyll content at the canopy scale. Int. J. Appl. Earth Obs. Geoinf. 21, 103–112. doi:10.1016/j.jag.2012.07.020

Inman, D., Khosla, R., Reich, R.M., Westfall, D.G., 2007. Active remote sensing and grain yield in irrigated maize. Precision Agriculture 8, 241–252.

Jordan, C.F., 1969. Derivation of leaf-area index from quality of light on the forest floor. Ecology 663–666.

Kim, Y., Reid, J.F., Han, S., 2007. On-the-go nitrogen sensing and fertilizer control for site-specific crop management. Intl. J. Agric. Biosystems Engr 7, 18–26.

Kira, O., Nguy-Robertson, A.L., Arkebauer, T.J., Linker, R., Gitelson, A.A., 2016. Informative spectral bands for remote green LAI estimation in C3 and C4 crops. Agricultural and Forest Meteorology 218, 243–249.

Kitchen, N.R., Sudduth, K.A., Drummond, S.T., Scharf, P.C., Palm, H.L., Roberts, D.F., Vories, E.D., 2010. Ground-Based Canopy Reflectance Sensing for Variable-Rate Nitrogen Corn Fertilization. Agronomy Journal 102, 71. doi:10.2134/agronj2009.0114

Knipling, E.B., 1970. Physical and physiological basis for the reflectance of visible and near-infrared radiation from vegetation. Remote Sensing of Environment 1, 155–159.

Lan, Y., Thomson, S.J., Huang, Y., Hoffmann, W.C., Zhang, H., 2010. Current status and future directions of precision aerial application for site-specific crop management in the USA. Computers and electronics in agriculture 74, 34–38.

Lee, W., Searcy, S.W., 2000. Multispectral sensor for detecting nitrogen in corn plants, in: ASAE Annual International Meeting, Midwest Express Center, Milwaukee, Wisconsin. pp. 9–12.

Lee, W., Searcy, S.W., Kataoka, T., 1999. Assessing nitrogen stress in corn varieties of varying color. Citeseer.

Li, F., Miao, Y., Feng, G., Yuan, F., Yue, S., Gao, X., Liu, Y., Liu, B., Ustin, S.L., Chen, X., 2014. Improving estimation of summer maize nitrogen status with red edge-based spectral vegetation indices. Field Crops Research 157, 111–123.

Li, Y., Shi, Z., Wu, C., Li, H., Li, F., 2008. Determination of potential management zones from soil electrical conductivity, yield and crop data. J. Zhejiang Univ. Sci. B 9, 68–76. doi:10.1631/jzus.B071379

Lukina, E.V., Freeman, K.W., Wynn, K.J., Thomason, W.E., Mullen, R.W., Stone, M.L., Solie, J.B., Klatt, A.R., Johnson, G.V., Elliott, R.L., Raun, W.R., 2001. Nitrogen Fertilization Optimization Algorithm Based on in-Season Estimates of Yield and Plant Nitrogen Uptake. Journal of Plant Nutrition 24, 885–898. doi:10.1081/PLN-100103780

Ma, B.L., Morrison, M.J., Dwyer, L.M., 1996. Canopy light reflectance and field greenness to assess nitrogen fertilization and yield of maize. Agronomy Journal 88, 915–920.

Martinez, L.J., Ramos, A., 2015. Estimation of chlorophyll concentration in maize using spectral reflectance. The International Archives of Photogrammetry, Remote Sensing and Spatial Information Sciences 40, 65.

Martin, K.L., Girma, K., Freeman, K.W., Teal, R.K., Tubańa, B., Arnall, D.B., Chung, B., Walsh, O., Solie, J.B., Stone, M.L., Raun, W.R., 2007. Expression of Variability in Corn as Influenced by Growth Stage Using Optical Sensor Measurements. Agronomy Journal 99, 384. doi:10.2134/agronj2005.0268

Miao, Y., Mulla, D.J., Randall, G.W., Vetsch, J.A., Vintila, R., 2009. Combining chlorophyll meter readings and high spatial resolution remote sensing images for in-season site-specific nitrogen management of corn. Precision agriculture 10, 45–62.

Miao, Y., Mulla, D.J., Randall, G.W., Vetsch, J.A., Vintila, R., Stafford, J.V., others, 2007. Predicting chlorophyll meter readings with aerial hyperspectral remote sensing for in-season site-specific nitrogen management of corn., in: Precision agriculture'07. Papers Presented at the 6th European Conference on Precision Agriculture, Skiathos, Greece, 3-6 June, 2007. Wageningen Academic Publishers, pp. 635–641.

Mulla, D.J., 2013. Twenty five years of remote sensing in precision agriculture: Key advances and remaining knowledge gaps. Biosystems Engineering 114, 358–371.

Muñoz-Huerta, R., Guevara-Gonzalez, R., Contreras-Medina, L., Torres-Pacheco, I., Prado-Olivarez, J., Ocampo-Velazquez, R., 2013. A Review of Methods for Sensing the Nitrogen Status in Plants: Advantages, Disadvantages and Recent Advances. Sensors 13, 10823–10843. doi:10.3390/s130810823

Nguy-Robertson, A., Gitelson, A., Peng, Y., Viña, A., Arkebauer, T., Rundquist, D., 2012. Green leaf area index estimation in maize and soybean: combining vegetation indices to achieve maximal sensitivity. Agronomy journal 104, 1336–1347.

Noh, H., Zhang, Q., 2012. Shadow effect on multi-spectral image for detection of nitrogen deficiency in corn. Computers and Electronics in Agriculture 83, 52–57.

Noh, H., Zhang, Q., Han, S., Shin, B., Reum, D., 2005. Dynamic calibration and image segmentation methods for multispectral imaging crop nitrogen deficiency sensors. TRANSACTIONS-AMERICAN SOCIETY OF AGRICULTURAL ENGINEERS 48, 393–401.

Noh, H., Zhang, Q., Shin, B., Han, S., Feng, L., 2006. A neural network model of maize crop nitrogen stress assessment for a multi-spectral imaging sensor. Biosystems Engineering 94, 477–485.

Oppelt, N., Mauser, W., 2003. Hyperspectral remote sensing - A tool for the derivation of plant nitrogen and its spatial variability within maize and wheat canopies. Wageningen Academic Publishers, Wageningen.

Osborne, S.L., Schepers, J.S., Francis, D.D., Schlemmer, M.R., 2002. Use of spectral radiance to estimate in-season biomass and grain yield in nitrogen-and water-stressed corn. Crop Science 42, 165–171.

Osborne, S.L., Schepers, J.S., Schlemmer, M.R., 2004. Using multi-spectral imagery to evaluate corn grown under nitrogen and drought stressed conditions. Journal of Plant Nutrition 27, 1917–1929. doi:10.1081/LPLA-200030042

Panda, S.S., Ames, D.P., Panigrahi, S., 2010. Application of vegetation indices for agricultural crop yield prediction using neural network techniques. Remote Sensing 2, 673–696.

Peñuelas, J., Filella, I., Biel, C., Serrano, L., Save, R., 1993. The reflectance at the 950–970 nm region as an indicator of plant water status. International journal of remote sensing 14, 1887–1905.

Peñuelas, J., Gamon, J.A., Fredeen, A.L., Merino, J., Field, C.B., 1994. Reflectance indices associated with physiological changes in nitrogen-and water-limited sunflower leaves. Remote Sensing of Environment 48, 135–146.

Perry, E.M., Roberts, D.A., 2008. Sensitivity of narrow-band and broad-band indices for assessing nitrogen availability and water stress in an annual crop. Agronomy journal 100, 1211–1219.

Peterson, T.A., Blackmer, T.M., Francis, D.D., Schepers, J.S., 1993. G93-1171 Using a Chlorophyll Meter to Improve N Management. Historical Materials from University of Nebraska-Lincoln Extension 1353.

Piekkielek, W.P., Fox, R.H., 1992. Use of a Chlorophyll Meter to Predict Sidedress Nitrogen. Agron J 84, 59–65.

Rambo, L., Ma, B.-L., Xiong, Y., Regis Ferreira da Silvia, P., 2010. Leaf and canopy optical characteristics as crop-N-status indicators for field nitrogen management in corn. Journal of Plant Nutrition and Soil Science 173, 434–443.

Raun, W.R., Solie, J.B., Stone, M.L., Martin, K.L., Freeman, K.W., Mullen, R.W., Zhang, H., Schepers, J.S., Johnson, G.V., 2005. Optical Sensor-Based Algorithm for Crop Nitrogen Fertilization. Communications in Soil Science and Plant Analysis 36, 2759–2781.

Reum, D., Zhang, Q., 2007. Wavelet based multi-spectral image analysis of maize leaf chlorophyll content. Comput. Electron. Agric. 56, 60–71. doi:10.1016/j.compag.2007.01.004

Ritchie, S.W., J.J. Hanway, and G.O. Benson., 1996. How a corn plant develops. Rev. ed. Spec. Rep. 48. Iowa State Univ. Coop. Ext. Serv., Ames.

Rorie, R.L., Purcell, L.C., Karcher, D.E., King, C.A., 2011a. The Assessment of Leaf Nitrogen in Corn from Digital Images. Crop Sci. 51, 2174–2180. doi:10.2135/cropsci2010.12.0699

Rorie, R.L., Purcell, L.C., Mozaffari, M., Karcher, D.E., King, C.A., Marsh, M.C., Longer, D.E., 2011b. Association of "Greenness" in Corn with Yield and Leaf Nitrogen Concentration. Agronomy Journal 103, 529. doi:10.2134/agronj2010.0296

Rouse Jr, J., Haas, R.H., Schell, J.A., Deering, D.W., 1974. Monitoring vegetation systems in the Great Plains with ERTS. NASA special publication 351, 309.

Sakamoto, T., Gitelson, A.A., Nguy-Robertson, A.L., Arkebauer, T.J., Wardlow, B.D., Suyker, A.E., Verma, S.B., Shibayama, M., 2012. An alternative method using digital cameras for continuous monitoring of crop status. Agricultural and Forest Meteorology 154, 113–126.

Sakamoto, T., Gitelson, A.A., Wardlow, B.D., Arkebauer, T.J., Verma, S.B., Suyker, A.E., Shibayama, M., 2011. Application of day and night digital photographs for estimating maize biophysical characteristics. Precision Agric 13, 285–301. doi:10.1007/s11119-011-9246-1

Scharf, P.C., Brouder, S.M., Hoeft, R.G., 2006. Chlorophyll Meter Readings Can Predict Nitrogen Need and Yield Response of Corn in the North-Central USA. Agronomy Journal 98, 655. doi:10.2134/agronj2005.0070

Scharf, P.C., Lory, J.A., 2009. Calibrating reflectance measurements to predict optimal sidedress nitrogen rate for corn. Agronomy journal 101, 615–625.

Scharf, P.C., Lory, J.A., 2002. Calibrating Corn Color from Aerial Photographs to Predict Sidedress Nitrogen Need. Agronomy Journal 94, 397. doi:10.2134/agronj2002.3970

Schlemmer, M.R., Francis, D.D., Shanahan, J.F., Schepers, J.S., 2005. Remotely measuring chlorophyll content in corn leaves with differing nitrogen levels and relative water content. Agronomy Journal 97, 106–112.

Schmidt, J.P., Dellinger, A.E., Beegle, D.B., 2009. Nitrogen recommendations for corn: An on-the-go sensor compared with current recommendation methods. Agronomy Journal 101, 916–924.

Scotford, I.M., Miller, P.C.H., 2005. Applications of Spectral Reflectance Techniques in Northern European Cereal Production: A Review. Biosystems Engineering 90, 235–250. doi:doi: DOI: 10.1016/j.biosystemseng.2004.11.010

Senay, G.B., Ward, A.D., Lyon, J.G., Fausey, N.R., Nokes, S.E., 1998. Manipulation of high spatial resolution aircraft remote sensing data for use in site-specific farming. Transactions of the ASAE 41, 489.

Shanahan, J.F., Schepers, J.S., Francis, D.D., Varvel, G.E., Wilhelm, W.W., Tringe, J.M., Schlemmer, M.R., Major, D.J., 2001. Use of Remote-Sensing Imagery to Estimate Corn Grain Yield. Agronomy Journal 93, 583–589. doi:10.2134/agronj2001.933583x

Shaver, T.M., Khosla, R., Westfall, D.G., 2011. Evaluation of two crop canopy sensors for nitrogen variability determination in irrigated maize. Precision Agriculture 12, 892–904.

Solari, F., Shanahan, J., Ferguson, R., Schepers, J., Gitelson, A., 2008. Active Sensor Reflectance Measurements of Corn Nitrogen Status and Yield Potential. Agronomy Journal 100, 571. doi:10.2134/agronj2007.0244

Solari, F., Shanahan, J.F., Ferguson, R.B., Adamchuk, V.I., 2010. An active sensor algorithm for corn nitrogen recommendations based on a chlorophyll meter algorithm. Agronomy Journal 102, 1090–1098.

Solie, J.B., Monroe, A.D., Raun, W.R., Stone, M.L., 2012. Generalized algorithm for variable-rate nitrogen application in cereal grains. Agronomy journal 104, 378–387.

Sripada, R.P., Heiniger, R.W., White, J.G., Meijer, A.D., 2006. Aerial color infrared photography for determining early in-season nitrogen requirements in corn. Agron. J. 98, 968–977. doi:10.2134/agronj2005.0200

Sripada, R.P., Heiniger, R.W., White, J.G., Weisz, R., 2005. Aerial color infrared photography for determining late-season nitrogen requirements in corn. Agronomy Journal 97, 1443–1451.

Sripada, R.P., Schmidt, J.P., Dellinger, A.E., Beegle, D.B., 2008. Evaluating multiple indices from a canopy reflectance sensor to estimate corn N requirements. Agronomy journal 100, 1553–1561.

Strachan, I.B., Pattey, E., Boisvert, J.B., 2002. Impact of nitrogen and environmental conditions on corn as detected by hyperspectral reflectance. Remote Sensing of Environment 80, 213–224.

Sullivan, D.G., Fulton, J.P., Shaw, J.N., Bland, G., 2007. Evaluating the sensitivity of an unmanned thermal infrared aerial system to detect water stress in a cotton canopy. Transactions of the ASABE 50, 1955–1962.

Swain, K.C., Jayasuriya, H.P.W., Salokhe, V.M., 2007. Low-altitude remote sensing with unmanned radio-controlled helicopter platforms: A potential substitution to satellite-based systems for precision agriculture adoption under farming conditions in developing countries.

Teal, R.K., Tubana, B., Girma, K., Freeman, K.W., Arnall, D.B., Walsh, O., Raun, W.R., 2006. In-Season Prediction of Corn Grain Yield Potential Using Normalized

Difference Vegetation Index. Agronomy Journal 98, 1488–1494. doi:10.2134/agronj2006.0103

Thenkabail, P.S., Ward, A.D., Lyon, J.G., 1994. Landsat-5 Thematic Mapper models of soybean and corn crop characteristics. Remote sensing 15, 49–61.

Thomason, W.E., Phillips, S.B., Raymond, F.D., 2007. Defining Useful Limits for Spectral Reflectance Measures in Corn. Journal of Plant Nutrition 30, 1263–1277. doi:10.1080/01904160701555176

Tomer, M.D., Anderson, J.L., Lamb, J.A., 1997. Assessing corn yield and nitrogen uptake variability with digitized aerial infrared photographs. Photogrammetric engineering and remote sensing 63, 299–307.

Tremblay, N., Wang, Z., Ma, B.-L., Belec, C., Vigneault, P., 2009. A comparison of crop data measured by two commercial sensors for variable-rate nitrogen application. Precision agriculture 10, 145–161.

Varco, J.J., Fox, A.A., Raper, T.B., Hubbard, K.J., 2013. Development of sensor based detection of crop nitrogen status for utilization in variable rate nitrogen fertilization, in: Precision agriculture'13. Springer, pp. 145–150.

Varvel, G.E., Schepers, J.S., Francis, D.D., 1997. Ability for in-season correction of nitrogen deficiency in corn using chlorophyll meters. Soil Science Society of America Journal 61, 1233–1239.

Varvel, G.E., Wilhelm, W.W., Shanahan, J.F., Schepers, J.S., 2007. An Algorithm for Corn Nitrogen Recommendations Using a Chlorophyll Meter Based Sufficiency Index. Agronomy Journal 99, 701. doi:10.2134/agronj2006.0190

Wood, C.W., Reeves, D.W., Duffield, R.R., Edmisten, K.L., 1992. Field chlorophyll measurements for evaluation of corn nitrogen status. Journal of Plant Nutrition 15, 487–500. doi:10.1080/01904169209364335

Wood, C.W., Reeves, D.W., Himelrick, D.G., 1993. Relationships between chlorophyll meter readings and leaf chlorophyll concentration, N status, and crop yield: a review, in: Proc. Agron. Soc. NZ. pp. 1–9.

Xia, T., Miao, Y., Mi, G., Khosla, R., Wu, D., Shao, H., Xu, X., 2015. In-season estimation of spring maize nitrogen status with GreenSeeker active canopy sensor, in: 2015 Fourth International Conference on Agro-Geoinformatics (Agro-Geoinformatics). Presented at the 2015 Fourth International Conference on Agro-Geoinformatics (Agro-geoinformatics), pp. 390–395. doi:10.1109/Agro-Geoinformatics.2015.7248155

Zhao, D., Reddy, K.R., Kakani, V.G., Read, J.J., Carter, G.A., 2003. Corn (Zea mays L.) growth, leaf pigment concentration, photosynthesis and leaf hyperspectral reflectance properties as affected by nitrogen supply. Plant and soil 257, 205–218.

Ziadi, N., Brassard, M., Bélanger, G., Claessens, A., Tremblay, N., Cambouris, A.N., Nolin, M.C., Parent, L.-É., 2008. Chlorophyll Measurements and Nitrogen Nutrition Index for the Evaluation of Corn Nitrogen Status. Agronomy Journal 100, 1264–1273. doi:10.2134/agronj2008.0016

SUPPLEMENTARY MATERIAL

Table S1. List of the reviewed papers about the use of optical sensing for nitrogen management in maize.

Authors	DVS[a]	Location	F[b]	Sensor Type[c]	Vector[d]	Bands (nm)	VI[e]	CC[f]	Nc[f]	LAI[f]	AGB[f]	Nu[f]	Y[f]	TONR[f]	EONR[f]	Others[f]
Alchanatis et al., 2005	V6-VT	Israel	N	H	Gr	530-1100			X							
Alganci et al., 2014		Turkey		M M	S Gr	VIS-NIR VIS-NIR	NDVI GI						X			
Argenta et al., 2004	V3-V4, V6-V7, V10-V11, R1	Brazil	N	CM	Hh	650, 940	SPAD units						X			
Báez-González et al., 2002	V4-R1	Mexico		M	S	VIS-NIR	NDVI						X			
Báez-González et al., 2005	84,103 DAS	Mexico		M	S	450-2350	NDVI			X	X		X			
Barker and Sawyer, 2010	V9-V14	IA, USA	N	M	Hh	400–680 and 800–1100	Several								X	
Bausch et al., 2008	VT	CO, USA	N	M	S	RGB-NIR	Several		X				X			
Blackmer et al., 1994		NE, USA	N	Cm H	Hh Hh	650, 940 400-700		X	X			X	X			

Authors	DVS[a]	Location	F[b]	Sensor Type[c]	Vector[d]	Bands (nm)	VI[e]	CC[f]	Nc[f]	LAI[f]	AGB[f]	Nu[f]	Y[f]	TONR[f]	EONR[f]	Others[f]
Blackmer and Schepers, 1995	V6, R4-R5	NE, USA	N	Cm	Hh	650, 940	SPAD units						X			
Blackmer and Schepers, 1996	R3	NE, USA	N	Cm M	Hh Ab	650, 940 RGB	SPAD units R						X			
Blackmer et al., 1996 a	R5	NE, USA	N	H	Hh	400-1100 350-1050							X			
Blackmer et al., 1996 b	R5	NE, USA	N	M	Ab	RGB							X			
Bragagnolo et al., 2016	V4, V6, V8, V10, V12, VT	Brazil	N	M Cm	Tr Hh	730, 760 650, 940	Index= (ln R760 - ln R730) x 100				X	X		X		
Casa et al., 2015	R3	Italy		Cm H	Hh Hh	650, 940 350-2500	Several	X								
Ciganda et al., 2009	V3-R	NE, USA		H	Hh	400-900	CI RE	X								
Cilia et al., 2014	V10	Italy	N W	H	Ab	394-968	Several	X	X		X					
Chang et al., 2003	V2, V6-V8, R2-R.5	SD, USA		M	Ab	RG-NIR	NDVI, GNDVI						X			

Authors	DVS[a]	Location	F[b]	Sensor Type[c]	Vector[d]	Bands (nm)	VI[e]	CC[f]	Nc[f]	LAI[f]	AGB[f]	Nu[f]	Y[f]	TONR[f]	EONR[f]	Others[f]
Clay et al., 2006	V8–V9, V11–VT, R1–R2	SD, USA	N W	M	Hh	RGB-NIR-MIR 400-1800	Several						X			Yield losses caused by N stress and W stress
Clevers and Gitelson, 2012		NE, USA		H	Gr	400-900	CI Others	X								
Daughtry et al., 2000	R1	MD, USA	N	H	Hh	400-1000	Several	X								
Dellinger et al., 2008	V6-V7	PA, USA	N	M	Tr	590, 880	rGNDVI								X	
Diker and Bausch, 2003	V6, V9, V12, V15, VT, R1, R2	CO, USA	N	M	Tr	RG-NIR	SI (NIR/G)		X							
Doraiswamy et al., 2002		IA, USA		M	S	VIS-NIR	NIR						X			
Elwadie et al., 2005	V6-R	MI, USA	N W	M	Hh	460-810	Several			X	X		X			
Freeman et al., 2007	V8-VT	OK, USA	-	M	Hh	650, 770	NDVI				X	X	X			
Gilabert et al., 1996	V4, V6, V8, V14, V16, R5	Spain		H	Gr	400-2500	Several			X	X					

Authors	DVS[a]	Location	F[b]	Sensor Type[c]	Vector[d]	Bands (nm)	VI[e]	CC[f]	Nc[f]	LAI[f]	AGB[f]	Nu[f]	Y[f]	TONR[f]	EONR[f]	Others[f]
Gitelson et al., 2003		NE, USA		H	Tr	400-900	Several			X	X					
Gitelson et al., 2005		NE, USA		H	Hh	400-900	CI RE	X								
Gitelson et al., 2012		MN, NE, IA, IL, USA		M	S	VIS-NIR	Several									GPP
Goel et al., 2003 a	30, 66, 86 DAS	Canada	N We	H	Ab	408.73-947.07										Classification by treatments
Goel et al., 2003 b	30, 66, 86 DAS	Canada	N We	H	Ab	408.73-947.07										Classification by treatments
GopalaPillai et al., 1998	55, 75, 99, 125, 141, 147 DAS	IL, USA	N	M	Ab	VIS-NIR	R,G, R/G						X			
GopalaPillai et al., 1999		IL, USA	N	M	Ab	RG-NIR	Several		X				X	X		
Hawkins et al., 2007	V8, V15, R1, R3	IA, USA	N	Cm	Hh	650, 940							X		X	N rate difference from EONR
Hunt et al., 2013	V15, VT, R1	NE, USA	N	H M	Ab Ab	360 – 2500 350 - 2500	TGI	X								

Authors	DVS[a]	Location	F[b]	Sensor Type[c]	Vector[d]	Bands (nm)	VI[e]	CC[f]	Nc[f]	LAI[f]	AGB[f]	Nu[f]	Y[f]	TONR[f]	EONR[f]	Others[f]
Inman et al., 2007	V6-V8	CO, USA		M	Hh	650, 770	NDVI						X			
Kim et al., 2007	60-90 DAS	USA	N	M	Tr	RG-NIR	NDVI	X						X		
Kira et al., 2016	Each 14 days	NE, USA		H	Tr	400-1100	ND and CI			X	X					
Kitchen et al., 2009	V4-V15	MO, USA	N	M Cm	Tr Hh	590, 880	SI (NDVI); SPAD units							X	X	
Krienke et al., 2015	V11	NE, USA	N	M M	Ab Hh	VIS-NIR	NDRE						X	X		
Lee et al., 1999	R3-R5	TX, USA	N	H	Gr	400-1100			X							
Lee and Searcy, 2000		TX, USA	N	H	Tr	400-1100			X							
Li et al., 2014	V6, V7 V10-V12	China	N	H	Hh	350-2500	Several		X			X				
Ma et al., 1996	Pre- and post-anthesis	Canada	N	M Cm	Hh Hh	450-800	NDVI	X		X	X		X			
Martin et al., 2007	V3-VT	OK, USA		M	Hh	650, 770	NDVI				X		X			

Authors	DVS[a]	Location	F[b]	Sensor Type[c]	Vector[d]	Bands (nm)	VI[e]	CC[f]	Nc[f]	LAI[f]	AGB[f]	Nu[f]	Y[f]	TONR[f]	EONR[f]	Others[f]
Martinez and Ramos, 2015	36,56,108 DAS	Colombia	N	H	Hh	350-2500	Several	X								
Miao et al., 2007	V9, R1, R2, R4	MN, USA	N	H	Ab	392-982		X								
Miao et al., 2009	V9, R1, R2, R4	MN, USA	N	H	Ab	392-982	Several	X								
Nguy-Robertson et al, 2012	V1-R7	NE, USA		H H	Hh Ab	400-1100 380-1000	Several			X	X					
Noh and Zhang, 2012	V6-R4	IL, USA	N	M	Tr	GR-NIR	G, R, NIR and indices	X								
Noh et al., 2005	V6-R[2]	IL, USA	-	M	Tr	GR-NIR	NDVI GNDVI NIR/G	X								
Noh et al., 2006	V6-R4	IL, USA	N	M	Tr	GR-NIR	G, R, NIR	X								
Osborne et al., 2002	V6-V7, V13-V16, V14-R1	NE, USA	N W	H	Hh	350-2500		X	X		X	X	X			
Osborne et al., 2004	V13-V16, R2, R4, V14-R1	NE, USA	N W	M	Ab	RGB-NIR	NDVI GNDVI		X		X		X			
Oppelt and Mauser, 2003	12 times during growth	Germany		H	Ab	550-1000	CAI NDVI OSAVI		X							

Authors	DVS[a]	Location	F[b]	Sensor Type[c]	Vector[d]	Bands (nm)	VI[e]	CC[f]	Nc[f]	LAI[f]	AGB[f]	Nu[f]	Y[f]	TONR[f]	EONR[f]	Others[f]
Panda et al., 2010		ND, USA	N	M	Ab	VIS-NIR	Several						X			
Perry and Roberts, 2008	V14, V15, R1	NE, USA	N W	H H	Ab Hh	400-2500 400-2500	Several		X		X					
Piekielek and Fox, 1992	V6	PA, USA	N	Cm	Hh	650, 940	SPAD units									Identification of N-responsive sites
Rambo et al., 2010	V5, V7, V10, R1	Canada	N	M H	Hh Hh	650, 770 460 - 950	NDVI						X	X		
Reum and Zhang, 2007	V8, V9, V10, R1	IL, USA	N	M M	Hh Hh	RGB RGB-NIR	Max Wavelet coeff	X								
Rorie et al., 2010	VT	AR, USA	N	M	Hh	RGB	DGCI	X	X				X			
Rorie et al., 2011	V3-V5	AR, USA	N	M	Hh	RGB	DGCI	X	X							
Sakamoto et al., 2012 a	V1-R6	NE, USA		M M	Gr S	VIS-NIR	Several			X	X					GAI
Sakamoto et al., 2012 b	V1-R5	NE, USA		M	Gr	VIS-NIR	Several			X	X					GAI

Authors	DVS[a]	Location	F[b]	Sensor Type[c]	Vector[d]	Bands (nm)	VI[e]	CC[f]	Nc[f]	LAI[f]	AGB[f]	Nu[f]	Y[f]	TONR[f]	EONR[f]	Others[f]
Scharf et al., 2006	V5-R5	NE, KS, MO, IL, WI, MI, MN, USA	N	Cm	Hh	650, 940							X		X	
Scharf and Lory, 2002	V6-V7	MO, USA	N	M Cm	Ab Hh	RGB-NIR	Several								X	
Scharf and Lory, 2009	V6	MO, USA	N	M	Gr	510, 560, 610, 660, 710, 760, 810, 760-900	Several								X	
Schepers et al., 1992	V8-R3, R1	IL, NE, USA	N	Cm	Hh	650, 940			X				X			
Schlemmer et al., 2005	V6-V7	NE, USA	N W	H	Hh	350-2500		X								
Schmidt et al., 2009	V6-V7	PA, USA	N	M	Tr	590, 880	GNDVI SI (GNDVI)								X	
Senay e al., 1998	End of growing season	OH, USA		M	Ab	550-1750	Several						X			
Shanahan et al., 2001	V6-R3	NE, USA	N	M	Ab	RGB-NIR	Several						X			
Shaver et al., 2011	V8, V10, V12, V14	CO, USA	N	M	Hh	650, 770 590, 880	NDVI						X	X		

Authors	DVS[a]	Location	F[b]	Sensor Type[c]	Vector[d]	Bands (nm)	VI[e]	CC[f]	Nc[f]	LAI[f]	AGB[f]	Nu[f]	Y[f]	TONR[f]	EONR[f]	Others[f]
Solari et al., 2008	V11, V15, R1, R3	NE, USA	N	M Cm	Hh Hh	590, 880	NDVI CI	X					X			
Solari et al., 2010	V11, V15	NE, USA	N	M	Tr	590, 880	SI (NDVI and CI)						X	X		
Sripada et al., 2005	VT	NC, USA	N	M	Ab	VIS-NIR	Several								X	
Sripada et al., 2006	V7	NC, USA	N	M	Ab	RGB-NIR	Several							X		
Sripada et al., 2008	V6-V7	PA, USA	N	M	Tr	590, 880	Several								X	
Sullivan et al., 2004	V4-R2	AL, USA	N	H M M Cm	Gr Ab S Hh	350-1050 400-12500 450-900 650, 940	NDVI GNDVI NIR/G		X				X			
Teal et al., 2006	V7-V9	OK, USA		M	Hh	650, 770	NDVI						X			
Thenkabail et al., 1994		OH, USA		M	S	VIS-NIR-IR	Several			X	X		X			Plant height
Thomason et al., 2007	V2-V4, V6-V9, V11-V14, VT	VA, USA		M	Hh	650, 770	NDVI				X		X			
Tomer et al., 1997	Crop maturity	MN, USA	N	M	Ab	RG-NIR						X	X			

Authors	DVS[a]	Location	F[b]	Sensor Type[c]	Vector[d]	Bands (nm)	VI[e]	CC[f]	Nc[f]	LAI[f]	AGB[f]	Nu[f]	Y[f]	TONR[f]	EONR[f]	Others[f]
Tremblay et al., 2009	V3-V5	Canada	N	M	Tr	550, 660, 700, 740, 780	NDVI							X		
				M	Hh	650, 770										
Varco et al., 2013	V6	MS, USA	N	M	Tr	450-900	Several		X			X				
Varvel et al., 1997	V8, V10, V12, V13, VT, R1	NE, USA	N	Cm	Hh	650, 940	SI (Cm)							X		
Varvel et al., 2007	V8, V10, V12	NE, USA	N	Cm	Hh	650, 940	SI (Cm)						X	X		
Wood et al., 1992; 1993	V10, Midsilk	AL, USA	N	Cm	Hh	650, 940	SPAD units		X				X			
Xia et al., 2015	V5, V6, V7, V8, V9, V10	China	N	M	Hh	650, 940			X		X	X				NNI
Zhao et al., 2003	15-42 DAE	MS, USA	N	H	Hh	350-2500		X	X							
Ziadi et al., 2008		Canada	N	Cm	Hh	650, 940	SPAD units						X			NNI

[a] DVS, crop development stage codified according to Ritchie et al. (1996) or recorded as days after sowing (DAS), days after emergence (DAE).
[b] F, main factor of variability (N=Nitrogen; W=Water; We=Weeds)
[c] Type of sensor used (Cm=chlorophyll meter, M=multispectral, H=hyperspectral)
[d] Vector (Hh=Hand-held, Tr=tractor-mounted, Ab=airborne, S=satellite, Gr=ground platform)
[e] VI, calculated vegetation indices. See the list in Appendix 1 for explanation of acronyms.
[f] Assessed variables (CC=chlorophyll content, Y=yield, B=above ground biomass, Nc=nitrogen concentration of above ground biomass, leaves or grain, Nu=nitrogen uptake, TONR=technically optimum nitrogen rate, EONR=economically optimum nitrogen rate, Other= green area index (GAI); nitrogen nutrition index (NNI)).
Empty cells indicate missing data in the original literature source.
The sufficiency index (SI) is always calculated as a ratio between a VI in the actual situation and the same VI in a N-rich condition. We indicated on which VI the SI is based.

APPENDIX 1. VEGETATION INDICES

Vegetation Index	Acronym	Equation
Normalized Difference Vegetation Index	NDVI	$(NIR - R)/(NIR + R)$
Green Normalized Difference Vegetation Index	GNDVI	$(NIR - G)/(NIR + G)$
Normalized Difference Red Edge	NDRE	$(NIR - RE)/(NIR + RE)$
Canopy Chlorophyll Content Index (Li et al.; 2014)	CCCI	$(\mathrm{NDRE} - \mathrm{NDREMIN})/(\mathrm{NDREMAX} - \mathrm{NDREMIN})$
Canopy Chlorophyll Content Index (Varco et al.; 2013)	CCCI	NDRE /NDVI
Double-peak Canopy Nitrogen Index	DCNI	$[(\mathrm{R720} - \mathrm{R700})/(\mathrm{R700} - \mathrm{R670})]/(\mathrm{R720} - \mathrm{R670} + 0.03)$
Dark Green Color Index	DGCI	$((HueG - 60)/[60 + (1 - SaturationG) + (1 - BrightnessG))\,)/3]$
Ratio Vegetation Index	RVI	NIR/R
Chlorophyll Index (NIR)	CI NIR	$(\mathrm{NIR/G}) - 1$
Chlorophyll Index (RE)	CI RE	$(\mathrm{NIR/RE}) - 1$
Red Edge Inflection Point	REIP	$700 + 40\,\mathrm{x}\left((\frac{(\mathrm{R670} + \mathrm{R780})}{2} - \mathrm{R700})\,/(\,\mathrm{R740} - \mathrm{R700}\right)$
Optimized Soil Adjusted Vegetation Index	OSAVI	$(R800 - R670)/(R800 + R670 + 0.16)$
Modified Chlorophyll Absorption Ratio Index	MCARI	$[(\mathrm{R700} - \mathrm{R670}) - 0.2\,\mathrm{x}\,(\mathrm{R700} - \mathrm{R550})]\,\mathrm{x}\,(\mathrm{R700/R670})$
Modified Triangular Vegetation Index 2	MTVI2	$1.5\,x\frac{[1.2\,x\,(R800 - R550) - 2.5\,x\,(R670 - R550)]}{\{(2\,x\,R800 + 1)^2 - [6\,\times\,R800 - 5\,x\,(R670)] - 0.5\}^{0.5}}$
Ratio between Modified Chlorophyll Absorption Ratio Index and Modified Triangular Vegetation Index 2	MCARI / MTVI2	MCARI/MTVI2
Triangular Greenness Index	TGI	$-0.5\,\mathrm{x}\,[(\mathrm{R670} - \mathrm{R480})\mathrm{x}(R_{670} \_\, R_{550}) - (\mathrm{R670} - \mathrm{R550})\mathrm{x}(R_{670} - R_{480})]$
Visible Atmospherically Resistant Index	VARI	$(G - R)/(G + R - B)$
Night-time Relative Brightness Index	NRBI	$\mathrm{NIR(night)\ x}\ 2^{-\left(2\,\mathrm{x}\log_2(\mathrm{F}_{NIR}) - \log_2(\mathrm{T}_{NIR}) - \log_2\left(\frac{ISO_{NIR}}{64}\right)\right)}$
Chlorophyll Absorption Integral	CAI	$\int_{R600}^{R735} Rs_I/Re_I$ Where $\mathrm{Rs_i}$ is the reflectance of vegetation spectrum at band I (%), and $\mathrm{Re_i}$ is the reflectance of the envelope at the band I (%)

Abbreviations used in the "Equation" column are: R followed by a number represents the reflectance in a wavelength specified by the number (expressed in nanometres); NIR=reflectance in near infrared; NIR(night)= reflectance in near infrared measured at night-time; R=reflectance in red; G=reflectance in green; B=reflectance in blue; RE=reflectance in red-edge; HueG, SaturationG and BrightnessG are the three cylindrical-coordinate representations of points in the most common RGB color model of the G band; F_{NIR}= the value of lens aperture, T_{NIR}=exposure time (shutter speed) and ISO_{NIR}=sensitivity of a digital camera when recording NIR reflectance.

CHAPTER 2

2. HYPERSPECTRAL IMAGING OF SPINACH CANOPY UNDER COMBINED WATER AND NITROGEN STRESS TO ESTIMATE BIOMASS, WATER, AND NITROGEN CONTENT

(Submitted to Biosystems Engineering, September 2016)

Martina Corti[1], Giovanni Cabassi[2], Daniele Cavalli [1], Pietro Marino Gallina[1]

[1] Department of Agricultural and Environmental Sciences - Production, Landscape, Agroenergy, Università degli studi di Milano; via Celoria 2, 20133 Milano (Italy)

[2] Consiglio per la ricerca in agricoltura e l'analisi dell'economia agraria, CREA-FLC; via Antonio Lombardo 11, 26900 Lodi (Italy)

ABSTRACT

This work had the goal to assess the capability of hyperspectral line scan imaging (400-1000 nm) to estimate crop variables in the greenhouse under combined water and nitrogen stress using multivariate data analysis and two data compression methods: canopy average spectra and hyperspectrogram extraction. Hyperspectral images contain far more information than do multispectral ones, which permits discrimination among minute pattern differences in canopy spectral reflectance.

A pot greenhouse experiment of eight treatments, from the combination of four nitrogen supply levels and two water supply levels, was designed to test widely varied spinach canopies. Using partial least square regression models, the fresh and dry weights of aboveground biomasses and water and nitrogen contents were estimated from a 76-sample dataset. Both the canopy reflectance-based and hyperspectrograms-based models performed

well in estimating variables strictly related to canopy leaf area index (m^2 of leaves/m^2 of soil) and geometry, *i.e.,* water content and fresh and dry weights, such that R^2 in independent validation reached values of 0.87, 0.65, 0.65, and 0.86, 0.74, 0.72, respectively. Estimation of nitrogen concentration from single leaf spectra hyperspectral images produced a high cross-validation R^2 (0.83), as opposed to the poor predictive results produced from canopy scans. This latter result arose from orientation effects due to canopy architecture. Finally, for estimation purposes, image hyperspectrogram compression without spatial information loss produced more encouraging results while considering canopy structure in crop variables than did average canopy spectra.

1 INTRODUCTION

Ineffective water and nitrogen (N) management is costly to both farmers and the environment, as it represents the main cause of agricultural pollution (Stirzaker, 2011). Such effects are avoidable by accurately estimating crop needs and properly scheduling the strongly linked managements of water (irrigation) and nitrogen (fertilization). Draining excess water from the root horizon carries away not only soluble and plant available mineral nutrients, but also nitrate, which reduces both their availability to plants and use efficiencies. Potential solution to this problem will match nitrogen and water supplies to variations in crop demand, both spatially and temporally, and that maintain yields while improving crop system environmental performance (Olfs et al., 2005). Remote sensing using optical scanners is one technique to investigate crop status quickly and without destruction because it captures spatialized crop information from crop radiative behavior. Moreover, when calibrated to describe crop response to water and nitrogen, precision crop management can be derived from sensor spectral information.

Multispectral sensors, whether handheld, ground vehicle-mounted, or airborne (aircraft or unmanned aerial vehicle), are the most common sensor types applied in agricultural settings. Multispectral sensors record reflectance in a few bands within the visible and near infrared (VIS-NIR) spectral region. From these reflectance signatures, vegetation indices are calculated and correlated to crop variables that reveal plant status, such as aboveground biomass, N uptake, and N concentration. These sensors are used most to detect N stress when N is the only limiting factor. However, studies conducted to discriminate the N stress of crops grown under different water availabilities have had difficulty distinguishing the effect of a single stress (Eitel et al., 2008; Schepers et al., 1996; Strachan et al., 2002; Wang et al., 2011; Zillmann et al., 2006). Among studies undertaken to separate nitrogen from water effects on various crops, only some authors have identified vegetation indices that related

more strictly to one stress over another. For instance, Peñuelas et al. (1993) found the ratio of reflectance at 970 and 900 nm to be indicative of plant water status; others found plant water status affected normalized difference vegetation indices (NDVI) of both the red and red-edge bands. A third vegetation index, described by the equation (R850-R710)/(R850-R680) and Meris terrestrial chlorophyll index (MTCI=(R760–R720)/(R720–R670)), were shown to be less affected by water stress (Shiratsuchi et al., 2011). Finally, the proposed MCARI/MTVI2 index, based on green, red, and red edge bands, was found to be highly correlated to chlorophyll content (and thus, to N status), but not affected by water on LAI (Eitel et al., 2008).

Other attempts to build a combined vegetative index univocally related to one of two stressors, *e.g.,* the Canopy Chlorophyll Content Index (CCCI) to estimate crop N status, were created from a combination of vegetation indices (Barnes et al., 2000; El-Shikha et al., 2007; Fitzgerald et al., 2007 and 2010; Rodriguez et al., 2006; Tilling et al., 2007). In some of these experiments that attempted to differentiate the effect of two stressors using vegetation indices (Rodriguez et al. 2006, Wang et al., 2011), it was suggested that confounding effects arose from changes in canopy architecture, leaf surface properties, and/or bare soil reflectance. Such effects would be particularly true for canopy cover-related indices in limited water, a time when soil moisture, not nitrogen availability, drives the variation in leaf optical properties (Eitel et al., 2008).

Combining optical and thermal indices (Barnes et al., 2000; Cohen et al., 2013) can be used to differentiate nitrogen and water stress effects, as Cohen et al. (2013) showed when they mixed thermal and hyperspectral imaging of potato. First, they categorized (using ANOVA) thermal images into water stress classes based on estimated leaf water potential, after which they used hyperspectral data to group water class-specific images according to crop nitrogen

concentration level. The two-step classification resulted in confusion matrices with accuracies of 83% and 65% on two potato varieties.

Hyperspectral sensors record hundreds of narrow bands in the VIS-NIR spectral region, and can be used to study combined two-stressor effects. With “across track” (whisk broom) or “along track” (push broom) scanning, the devices detect subtle differences in the patterns of canopy reflectance (Jones and Vhaughan, 2010) from the entire vegetation spectrum. Hyperspectral sensing can be of particular benefit to precision agriculture when it, employs imaging spectroscopy to extract spatialized information on canopy reflectance by combining the potential of digital images with hyperspectral measurements. To handle the large giga- or even tera-byte datasets produced from hyperspectral images, multivariate statistical analysis has proved a useful and affordable technique to reduce the data to a limited number of significant components (Stellacci et al., 2012).

Multivariate approaches can also help to overcome some of the limitations associated with vegetation indices. Principal Components Analysis (PCA; Schut and Ketelaars, 2003), Discriminant Analysis (Goel et al., 2003), and Partial Least Squares regression (PLS; Alchanatis et al., 2005; Hansen and Schjoerring, 2003; Li et al., 2014; Vigneau et al.; 2011) are promising multivariate techniques to assess vegetation nitrogen status separately from water status (Ullah et al., 2014; Zhang et al., 2012). However, their use in the presence of different stressors has yet to be deeply explored (Karimi et al., 2005; Ray et al., 2010; Strachan et al., 2002). Generation of a hyperspectrogram (HSG) is a data extraction and compression technique based on PCA that manage large numbers of hyperspectral images and retain spatial information (Ferrari et al. 2013). HSGs can then be used not only for calibration purposes—as opposed to the original image—but also for variable prediction by projecting them back into the image space or spectral domain to detect spatial and spectral regions carrying the most useful information.

Our goal in this work was to verify the capability of hyperspectral imaging in the VIS-NIR spectral range (400-1000 nm) in order to estimate crop variables with multivariate analysis using greenhouse spinach (as crop model) under combined water and nitrogen stresses. As a secondary product, this work compared the performances of two hyperspectral image data extraction methods—average spectra and HSGs calculated per Ferrari et al. (2013) with modifications.

2 MATERIALS AND METHODS

2.1 Experimental design and crop growing

A greenhouse pot experiment was carried out during April and May 2015 on dicotyledonous plant spinach (*Spinacia Oleracea*) at the Department of Agricultural and Environmental Sciences—Production, Landscape, Agroenergy (DiSAA), of Università degli Studi di Milano.

Eight treatments, resulting from combinations of four nitrogen supply levels and two water supply levels were compared. The four rates of nitrogen applied were No nitrogen (N0 = 0 kg N ha^{-1}), limiting (N1 = 28 kg N ha^{-1}), optimal (N2 = 132 kg N ha^{-1}) and redundant (N3 = 208 kg N ha^{-1}), and the two levels of water supplied were optimal (W+) and deficient (W-) via irrigation interruption to half of the experimental units at full crop development (30 days after sowing, DAS).

Treatments were assigned to pots following a completely randomized block design with four replications. Two of the four replicates were reserved for non-destructive optical measurements, while the other two replicates were destined for destructive reference analysis during the crop cycle. An extra replicate of the W- treatment (four nitrogen levels x one water level) was grown to allow for the high variability expected in plants in stressed *versus* optimal water conditions. The experiment considered a variety of treatments to simulate the variation in spinach canopies that results from differences in nitrogen and water availability.

Black rectangular polyethylene pots measured 35 cm (l) x 28 cm (w) x 20 cm (h) and were each filled with 18 litres of growing medium prepared by mixing equal parts (weight basis) of neutral silica sand (particle size 0.4-0.8 mm) and soil (sieved at 5 mm). The soil had the following characteristics: sand 52%, silt 39%, clay 9%, pH (H_2O) 7.44, 0.13 total nitrogen, and 1.35 organic carbon (% DM). The water content of the final mix had a field capacity of

0.12 kg H_2O kg^{-1} soil and a bulk density of 1.28 t m^{-3}. Powdered fertilizers containing micro- and macro-nutrients (other than nitrogen) were mixed with the soil before sowing. Triple superphosphate, potassium sulfate, and magnesium phosphate were added to supply equivalent amounts of 28 kg ha^{-1} of P_2O_5, 118 of K_2O, and 9 of Mg, as was the equivalent of 1 kg ha^{-1} of a balanced mix of micronutrients (Hortrilon, COMPO GmbH, Münster, Deutschland).

Spinach seeds (variety SV2157VB, Seminis, Italy) were sowed (seven plants on three rows, 21 plants each pot) on the 18th of April 2015 and grown under climatic greenhouse conditions (16- 22°C and 16 hrs of light daily). Nitrogen was applied weekly by fertigation, starting with the third week after sowing (three total applications). Soil water content was held between field capacity (water potential at -10 kPa) and 80% of total available water (spinach water stress threshold proposed by Allen et al. (1998)). Pots were weighed daily and water was added to reach the weight corresponding to field capacity. This procedure was followed by irrigation of all experimental pots until May 18 (30 DAS) when irrigation ceased for the W- treatment pots. The experiment was ended at 24 May 2016 (36 DAS).

2.2 Analytical reference measurements

We determined above ground biomass fresh weight (FW) and dry weight (DW) and its water content (Wc) and nitrogen concentration (Nc) by sampling five plants from each pot slated for destructive measurements during crop growth in four subsequent dates on May 18, 20, 22, and 24, 2015 corresponding to 30, 32, 34, and 36 DAS, respectively. On the final sampling date, the entire crop of pots cast for optical measurement were sampled, and from those we determined fresh weight and dry weight. Next, the dried (at 105 °C) plant samples were ground into powder with a ZM 100 centrifugal mill equipped with a 0.5 mm mesh sieve (Retsch Gmbh & Co., Germany) to determine total nitrogen concentration by dry combustion using a ThermoQuest NA1500 elemental analyser (Carlo Erba, Milan, Italy). At

the final sampling, six leaves—one each from six plants grown in treatment combinations derived from three nitrogen levels (N0, N2, and N3) and two water levels (W+ and W-)– were used to determine Nc. Last, volumetric soil water content was estimated first at 30 DAS and then throughout the experiment from soil weight after accounting for soil bulk density.

2.3 Crop image acquisition

Crop canopy hyperspectral diffuse reflectance images were acquired using a hyperspectral imaging line scan sensor equipped with a Specim V10 spectrometer and a Basler PiA190032gm sensor assembled by DV s.r.l., Padova (Italy) with 45°/0 reflectance geometry in respect to the line of view and active illumination. The spectral range of the sensor was 339 to 1094 nm with a 2.9 nm spectral resolution and 600 pixels along the spatial axis. A linear array sensor was used thus, in order to acquire the image of each experimental unit (the entire pot) we designed and fabricated a sliding platform (Figure 1).

Figure 1. – Image of the sliding platform and of the hyperspectral imaging sensor in the greenhouse.

It allowed each pot to be placed and then optical scans of the canopy to be taken (20 scans per second were averaged for a total duration of 120 s) in “push-broom” mode. From these

data resulted a hypercube with dimensions of 600 (x axis) x 120 (y axis) x 121 wavebands (λ axis). The optical scans were acquired on four sampling dates at midday on May 18, 20, 22, and 24, 2015, which corresponded to 30, 32, 34, and 36 DAS, respectively, at the same date of the destructive sampling. The images were taken under an active light source where the acquisition system was covered with a black box to eliminate any environmental light interference. On each date of image acquisition (total dates=4), 20 pots with undisturbed canopies assigned to the group for non-destructive optical measurements were scanned, such that 80 total images were acquired throughout the duration of the experiment.

On the last date for image acquisition, individual leaf scans were also taken. Six fully developed leaves from six plants representative of the different water and nitrogen nutritional status combinations were positioned onto a sheet of paper and scanned under optimal light exposure conditions. The average spectrum of each leaf was extracted while considering each leaf as a region of interest (ROI) for the subsequent data analysis.

We performed image correction by normalizing each image pixel to the white and black references (dark current signal) taken before each session. The dark current signal was acquired by putting a black cover in front of the sensor, whereas the white reference (white ceramic strip 60 cm wide) was acquired at a distance from the sensor equal to half of the spinach canopy height. We focused the Specim spectrometer on this plane with a paper sheet printed with black and white strips and a sensor aperture set to avoid light saturation. Images were adjusted per the formula (R_λ – dark current signal$_\lambda$)/(White ref$_\lambda$ – dark current signal$_\lambda$), where R_λ and White ref$_\lambda$ are the radiance values of each pixel of each pot scanned line and of the white reference, respectively, measured at each λ wavelength. The images were saved in HDR (High Dynamic Range image) format.

2.4 Image processing

We processed the hyperspectral data to identify spikes and dead pixels, which were eventually removed. Then, segmentation of the image background was performed to identify pixels that did not represent either vegetation or soil. We accomplished this by calculating the normalized difference vegetation index (NDVI= (R800-R680)/(R800+R680); Lichtenthaler et al., 1996), and then applied the Otsu segmentation algorithm (Otsu, 1975) to separate the canopy and pot from the sliding platform; we selected only soil and vegetation as ROI to be analyzed.

The resulting ROIs formed the basis for testing the two data extraction methods. To maintain image size without spatial information loss, NaN (Not a Number) values were assigned to each pixel falling in unselected regions, so that they were excluded from subsequent analysis and maintained only as position markers. The first compression method allowed extraction of the average spectra from the canopy of each experimental unit (Figure 2a), while the second method created HSGs following the Ferrari et al. (2013) procedure with modifications (Figure 2b).

2a 2b

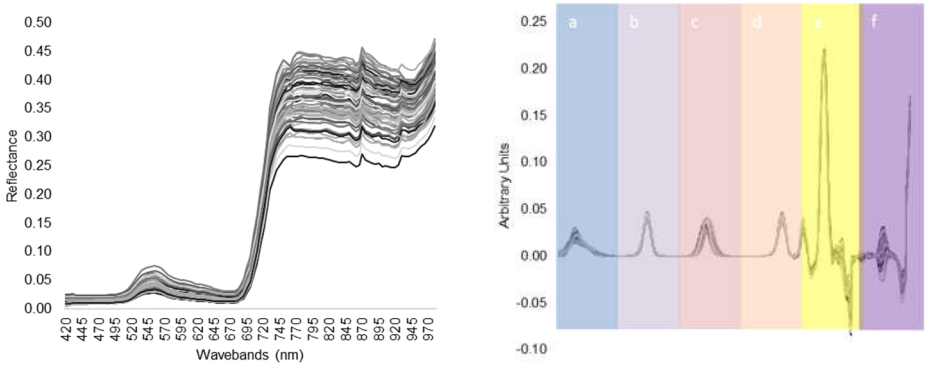

Figure 2. – Average spectra (2a) and hyperspectragram vectors (2b) of the pots (n=76) used in calibration. Figure 2b colour blocks indicate the different PCA statistics of the signal: frequency distribution curves of the first component scores (a), of the second component scores (b), of the Q residual scores (c), of the Hotelling T^2 values(d), loading vectors of the first component (e) and of the second component (f).

A schematic version of the original procedure presented by Ferrari et al. (2013) has been provided in the Figure 3.

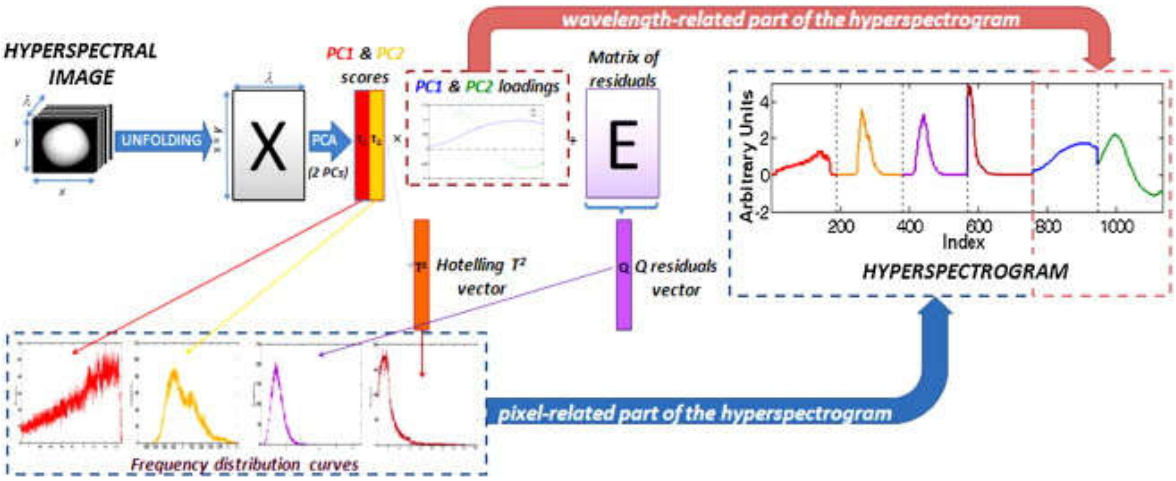

Figure 3. – Schematic procedure of hyperspectrogram exctraction as provided by the original paper[1].

Our first step to extract the HSGs was to unfold the ROIs to obtain an ROI image matrix of 600x120 rows (x and y axis of the original image) and 113 columns (λ axis). The number of wavebands included was 113 (from 420 to 980 nm) instead of 121 (from 339 to 1094) due to the low signal to noise ratio of the two tails of the spectra. The unfolded spectra were pre-processed using the first derivative calculation as described by Savitzky-Golay (1964) and mean centering. During the procedure, all hyperspectral images were processed sequentially with the same PCA options: the signs of loading vectors were adjusted to minimize the squared difference between loading the first image and each of the others. The first two PCA principal components were retained in the models. Then, to calculate the frequency distribution curves of the resulting score Q spectral residuals and Hotelling T^2 values, we chose a logarit[1]hmic distribution of the bins for its relatively symmetric distributions (average skewness = 2.5) of both PCA Q residuals and Hotelling T^2 values as compared to

[1] Reprinted from Analytica chimica acta 802, Ferrari, C., Foca, G., Ulrici, A., Handling large datasets of hyperspectral images: Reducing data size without loss of useful information, 29–39, Copyright (2013), with permission from Elsevier.

the skewed distribution curves (average skewness = 5.8) from the linear distribution of the bins proposed by Ferrari et al. (2013). Last, by combining the frequency distribution curves with the loadings corresponding to the selected scores, we derived a 678-long points vector HSG for each image of 113 x2 points for the frequency distribution curves of the two scores vectors + 113 points for the frequency distribution curve of the Q residuals vector + 113 points for the frequency distribution curve of the Hotelling T^2 vector + 113 x2 points of the loadings of the two principal components (Figure 2b).

Our choice of retaining two principal components in the image PCA was justified by the fact that third component loadings showed very different features from image to image, which made it difficult to recognize a common behavior or to explain the corresponding scores distributions.

Image processing, average vegetation spectra extraction, and HSG production were all performed with MATLAB (MathWorks, Natick, MA)

2.5 Statistical analysis

Firstly, the ANOVA-simultaneous component analysis (ASCA), according to Smilde et al. (2005) and Zwanenburg et al. (2011), was performed on both canopy average spectra and HSG datasets to determine which treatment(s), within the fixed effects of the experimental factors (water, nitrogen, and water x nitrogen interaction), were significant based on residual errors. As the normality assumption is not respected by spectral data, ASCA analysis performs a permutation test of samples with respect to treatments to build a distribution that compares the sum of squares to estimate p-values for significance of the effect of each factor or interaction.

Finally, PLS regression analysis allowed both the canopy average spectra and HSG dataset to be used as predictors for crop variable estimations: FW and DW of the above ground

biomass (AGB), the nitrogen concentration on a dry matter basis (Nc), and the AGB water content (Wc).

Non-averaged individual spectra or HSGs from the two replicate pots selected for non–destructive measurements were the basis of calibrations for the PLS model for these variables. They were regressed against the corresponding reference values (of the measured variables) calculated by averaging the results from the two biological replicates assigned to destructive analysis in agreement with Fearn (2015).

The cross-validation was planned considering all possible sources of variation: five different cancellation strategies were proposed (Table 1). This approach was adopted to ensure a robust estimation of the number of principal components and to avoid the effects of over-fitting from modeling noise.

Table 1. – Sample composition of the training-sets, cross-validation cancellation groups, and independent validation sets tested (N=nitrogen treatments, W=water treatments, R=replicates, D=DAS).

ID	Samples composing the Test Set	Number of samples of the Test Set	Number of samples of the Training-Set
C-Val1	1N x 2W x 2R x 1D	5* or 4	71 or 72
C-Val2	4N x 1Wx 2R x 1(2)D	22-11* or 8	54-65 or 68
C-Val3	4N x 2W x 2R x 1D	19*	57
C-Val4**	4 samples x 2R	11*-8	65-68
C-Val5**	8 samples x 2R	21*-16	55-60
Val-Ind	1N x 2W x 1D x 2R + extra replicates	28	48

* The size of the cancellation group varied due to the presence, in some, of a third replicate arranged for the thesis (W- x 4N treatments)
** The test set was set up by sorting the samples by variable value and using contiguous block cross-validation

The errors of the cross-validation strategies were also used to give a robust estimation of the true error. Three of the five cross-validation strategies evaluated different model sensitivities: model sensitivity to the effects of nitrogen treatments (C-Val1), model sensitivity to crop water status (C-Val2), model sensitivity to the effect of acquisition date

(C-Val3). The fourth and fifth cross-validation strategies (C-Val4 and C-Val5) were obtained with consideration of the variability in measured nitrogen concentrations and AGB production, as opposed to a classification based on the applied treatments of the experimental design. The cancellation groups of C-Val4 and C-Val5 consisted of four and eight samples, respectively, per iteration, covering the entire range in variation of the measured crop variable. Finally, an independent validation set was also selected; it was composed of all the replicates arising from a combination of one nitrogen level and the two water levels on each acquisition date as shown in Table 1. Spectra coming from the extra replicate (n=12) were also included. The resulting training set contained 48 samples and the validation set contained 28 samples. Data were split into cancellation groups and test sets, cross-validation and independent validation respectively, by grouping all replicates from one treatment to assure the independence of all outlying subgroups (Fearn, 2015).

The PLS model results from application of the different cross-validation methods were tested for all predicted crop variables using the Snedecor and Cochran (1967) method of SECV pairwise comparison.

In the cross-validation step, the number of principal components retained was based on the significance of the explained variance by each latent variable. In the independent validation step following significance testing of the SECV differences, the number of principal components to estimate each variable was done by minimizing RMSECV and the number of latent variables.

Statistical parameters to evaluate the predictive ability of the various models were then calculated. The determination coefficient (R^2), root-mean-square error of calibration (RMSEC), cross validation, and independent validation were calculated. RMSE is defined as RMSE=$\sqrt{\frac{\sum_{i=1}^{n}(\hat{y}_i - y_i)^2}{n}}$ in which $\hat{y}_i$ are the estimated values, y_i are the measured values, and n is the number of observed data. The ratio of prediction to deviation (RPD) was calculated

as the ratio of the standard error of prediction to the standard deviation of the samples. Finally, the reference data reproducibility score was calculated as the pooled standard deviation of biological replicates. The reference data reproducibility (Rep) was used to estimate the maximum R^2 achievable with the actual dataset as $R^2_{max} = \frac{std^2 - Rep^2}{std^2}$ where *std* is the standard deviation of each dataset as proposed by Dardenne (2010).

Multivariate data analysis was carried out using PLS Toolbox (Eigenvectors Research, Inc., Manson, WA) for MATLAB.

3 RESULTS AND DISCUSSION

3.1 Measured crop variables

Until 18 DAS, all spinach plants underwent homogenous treatment. Next, the different nitrogen treatments were applied and water stress was imposed at 30 DAS. Plant Wc was unaffected by nitrogen treatment. In fact, regardless of the nitrogen level, the date of 22 May, corresponding to 34 DAS, (four days after the interruption of irrigation) was considered the onset of water stress according to plant Wc and soil volumetric Wc measurements (Figure 4).

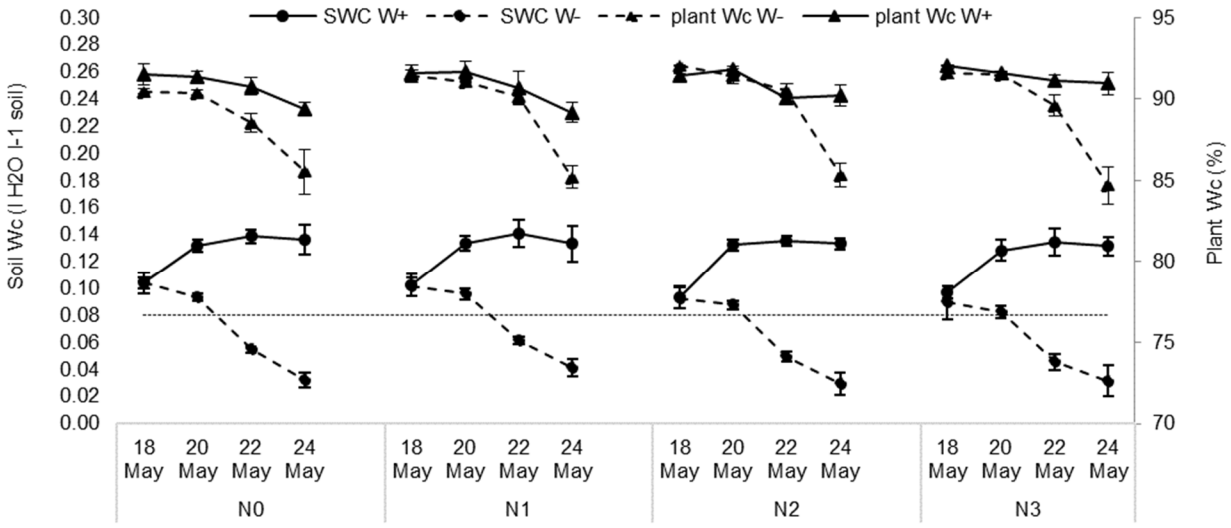

Figure 4. – Soil water content (SWC) and plant water content (Plant Wc) dynamics of pots under combination treatments of four nitrogen levels with optimal water conditions (W+) and water stress conditions (W-) during different acquisition times.

From that moment, the plants subjected to water stress were characterized by a drop of plant Wc in line with the increase of time from the last irrigation. Furthermore, plants under N0 and N1 treatments resulted in slightly lower AGB production compared to those under N2 and N3 treatments with average weights of 8.63-16.27 *vs* 10.34-18.94 g DW pot^{-1}, respectively (Table 2).

Table 2. – Mean and standard deviation (std) of the above ground biomass dry weight (AGB DW) and nitrogen concentration (Nc) measured at each acquisition time, for each combination of water and nitrogen levels.

N levels	Date	W -				W +			
		AGB DW (g pot^{-1})		Nc (% DM)		AGB DW (g pot^{-1})		Nc (% DM)	
		mean	std	mean	std	mean	std	mean	std
N0	30 DAS	11.06	0.478	2.87	0.057	8.97	1.004	2.84	0.479
	32 DAS	14.05	0.013	2.94	0.374	12.56	1.190	3.03	0.080
	34 DAS	14.46	2.066	2.52	0.162	13.97	1.129	2.50	0.194
	36 DAS	13.60	0.222	2.53	0.083	15.47	0.139	2.23	0.040
N1	30 DAS	8.63	0.512	3.15	0.349	9.89	1.373	3.26	0.679
	32 DAS	12.83	0.851	2.88	0.148	10.65	1.527	3.06	0.390
	34 DAS	11.14	0.619	2.62	0.153	13.40	2.272	2.42	0.155
	36 DAS	13.99	0.288	2.62	0.083	16.27	0.855	2.25	0.098
N2	30 DAS	10.34	0.179	3.52	0.085	13.03	1.226	3.10	0.111
	32 DAS	14.88	0.395	3.39	0.132	14.78	2.383	3.30	0.194
	34 DAS	15.24	0.022	3.12	0.116	17.42	0.809	2.59	0.122
	36 DAS	15.38	0.375	3.01	0.145	16.42	0.536	2.75	0.025
N3	30 DAS	12.14	0.186	3.48	0.006	11.54	1.049	3.71	0.254
	32 DAS	14.27	0.331	3.70	0.102	13.36	1.888	3.04	0.165
	34 DAS	13.65	1.514	2.94	0.025	15.92	2.394	3.04	0.051
	36 DAS	15.61	0.318	3.54	0.380	18.94	1.380	2.91	0.334

Water stress also affected AGB. In fact, the water stressed plants decreased in DW probably due to diminished photosynthetic activity and leaf senescence from the water status. On the contrary, the plants with an optimum water status were characterized by a constant increase in their DW.

Measured Nc (Table 2), expressed as a percentage of dry matter (DM), decreased as time increased from the dilution effect on older tissues. This trend was more evident at lower nitrogen availabilities (N0, N1), which may arise from N moving from older to younger leaves before senescence. Nitrogen treatments also affected canopy nitrogen concentrations,

which separated into two average N concentration groups of 0.23 g N g DW^{-1} for N0-N1 and 0.37 for N2-N3. In addition, the treatments produced wide variation in FW (12.39 g DW pot^{-1}) and Nc (2% DM), representing 61% and 48% of the variation, respectively.

3.2 Spectral features of spinach leaves and canopies under nitrogen or water stress

Canopy leaf reflectance was studied from ROIs in canopy leaf samples taken from several hyperspectral datasets: well-watered green leaves under various nitrogen treatments (N0 and N3; Figure 5a), green and yellow leaves under the two water levels (Figure 5b), and soils of various water contents (Figure 6). Leaf ROIs directly illuminated and directly shadowed by the lamp were also selected for sampling (Figure 7). Results showed that the most relevant nitrogen treatment effects (Figure 5a) were found in either the visible or NIR spectral regions. Specifically, the canopy of N stressed plants showed higher reflectance in the green and red bands of the visible region with respect to a canopy under optimal N. This was indicated by a leaf colour change from green to yellowish-green (Schlemmer et al., 2005). In the NIR region, an increase of non-specific scattering at all wavebands was observed in N-deficient plants.

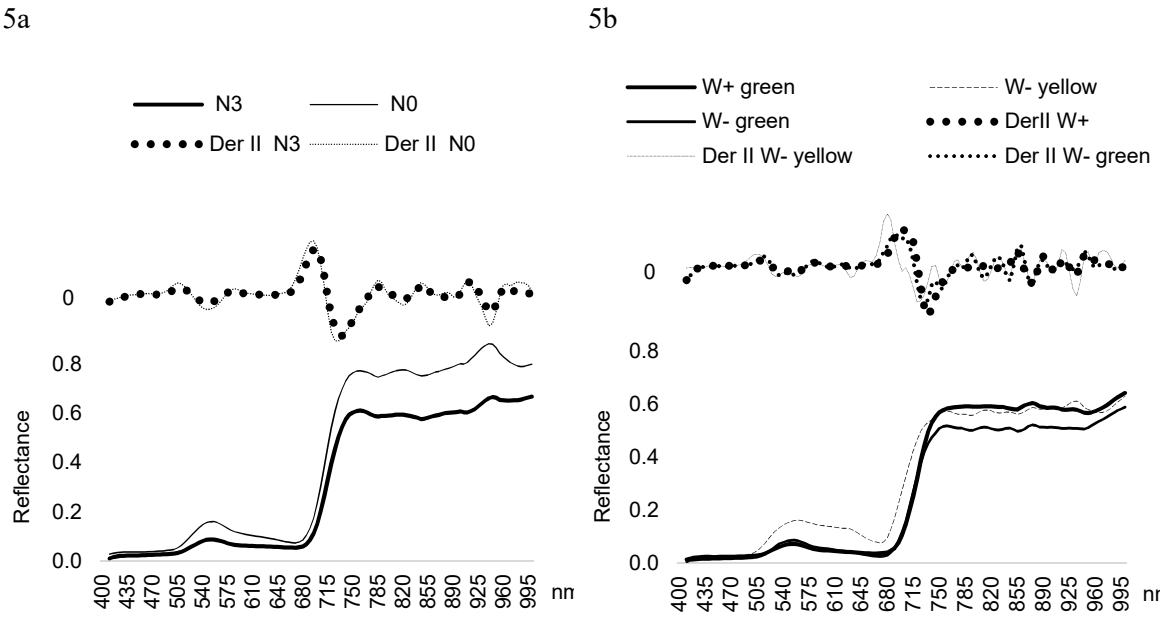

Figure 5. – Average spectra and second derivatives (Der II) of ROIs of different leaves under N0 and N3 treatments (5a). Average spectra and second derivatives of ROIs of green leaves at optimal water status (W+) and of green and yellow leaves under water stress (W-) (5b).

Green canopy leaves under water limited and optimal water status show reflectance differences (Figure 5b) in the NIR region of the spectrum. According to various authors (Hunt and Rock, 1989; Jackson and Ezra; 1985; Peñulas et al., 1993), values are lower in water-stressed leaves. On the contrary, others have reported the opposite (Schut and Ketelaars, 2003). Yellow water-stressed leaves display high reflectance in the green and red parts in the visible region of the spectrum, which is likely due to the old age/low N concentration of the leaves. Finally, worth noting is the so-called "red-edge" region in the transition from visible to NIR wavelengths. In the presence of a yellow leaf, the feature characteristically shifts to lower wavelengths, an easily observed phenomenon in the second derivative of the spectra in green and yellow leaves (Figure 5b). The behavior relates to chlorophyll content (Filella and Peñulas, 1994; Scotford and Miller, 2004) and is more strictly correlated to nitrogen concentration as suggested by Perry and Roberts (2008) and

observed by Schlemmer et al. (2005) in red edge shift from longer to shorter wavelengths in nitrogen-stressed plants.

Soil (Figure 6) was included in the ROI samples and its signal was not separated from that coming from the vegetation in yet to be fully developed canopies, which caused its contribution to the reflectance to be considered and used as a predictor of crop variables. As can be seen in Figure 6, soil reflectance values were low overall, except in the slight higher reflectance at all wavelengths in dry soil *versus* wet soil due to back scattering (albedo), also suggested by Daughtry et al. (2000).

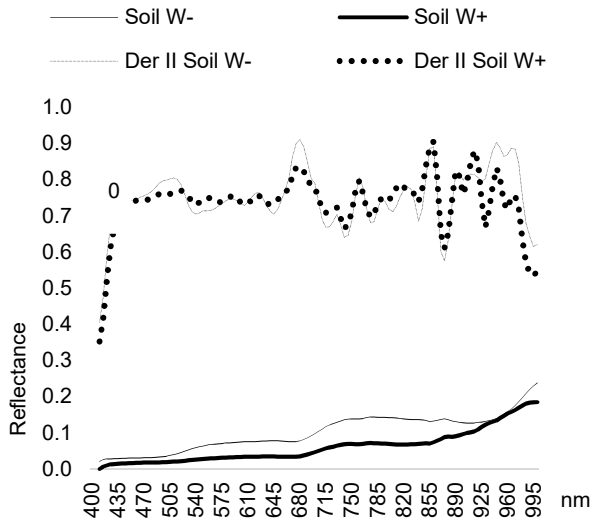

Figure 6. – Average spectra and second derivatives (Der II) of the soil mix used in the experiment at two water contents: at field capacity (W+) and at the wilting point (W-).

Since the canopy constituents are not coplanar, different leaves experience different exposure levels. Moreover, during canopy scanning all leaves are not planar positioned to ensure the correct and ideal 45°/0 reflectance geometry necessary to eliminate specular reflection. Leaves oriented to different angles results in direct reflection and shading that affects the spectra and increases both noise and the degree of offset. In fact, in this work, differences between illuminated and shadowed leaves had a relevant effect (sharp decrease of the red-edge) on spectral variability (Figure 7).

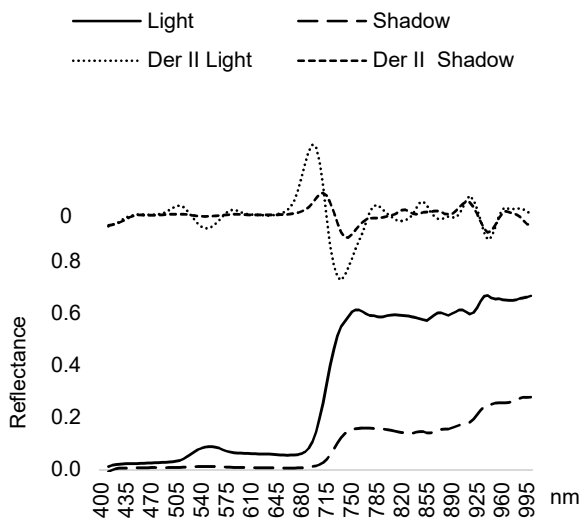

Figure 7. – Average spectra and second derivatives (Der II) of a ROI of different leaves directly under the sensor light (Light) or shadowed leaves (Shadow).

Undoubtedly, the spectral variability due to different illuminations of different canopy areas is one of the biggest sources of spectral variability that has to be taken into account when modeling spectral response.

ASCA analysis was applied to the mean spectra and HSGs to test the significance of collected spectral data with respect to experimental design factors. Results are summarized in Table 3.

Table 3. – Results of ASCA two-way interaction models calculated for mean spectra and HSG datasets.

	Canopy average spectra			**HSGs**		
Factor	**PCs**	**Effect %**	**p-value**	**PCs**	**Effect %**	**p-value**
Nitrogen	3	13.44	*0.001*	3	6.56	*0.029*
Water	1	2.95	*0.057*	1	5.14	*0.002*
Nitrogen x Water	7	47.88	*0.128*	7	19.58	*0.573*
Residuals		35.73			68.72	

Overall, nitrogen treatment had a bigger effect than water and was highly significant. Water treatment (with only two levels) affected HSGs highly significantly, and reached a maximum

significance near 5% with the mean spectrum approach. No significant interaction (NxW) effects, subjected to permutation test, were found.

3.3 Development and performance of prediction models

3.3.1 Canopy reflectance-based estimation models

Different models were built to predict each studied variable from testing the average spectra with the five cross-validation and independent validation strategies. Autoscaling was used to pre-process the spectra; the results are summarized in Table 4.

Table 4. – Performances of the five cross-validation methods for each estimated variable by canopy reflectance-based models. The number of selected principal components (N PC), R^2 obtained in the calibration step (R^2 CAL) and cross-validation step (R^2 CV), root-mean-square errors in calibration and cross-validation (RMSEC and RMSECV, respectively), cross-validation bias, and RPD and theoretical R^2_{MAX} are each reported.

Predicted Variable	*Strategy*	*N PC*	*R^2 CAL*	*R^2 CV*	*RMSE C**	*RMSE CV**	*BIAS CV**	*RPD*	*R^2_{MAX}*
AGB FW (g pot^{-1})	C-Val1	5	0.75	0.61	14.011	0.854	-0.039	1.59	0.84
	C-Val2	7	0.79	0.60	12.689	0.920	-0.133	1.47	
	C-Val3	Poor performance							
	C-Val4	5	0.75	0.65	14.011	0.797	-0.032	1.70	
	C-Val5	5	0.75	0.68	14.011	0.771	-0.033	1.76	
AGB DW (g pot^{-1})	C-Val1	6	0.69	0.57	1.296	1.531	0.002	1.53	0.74
	C-Val2	Poor performance							
	C-Val3	Poor performance							
	C-Val4	6	0.69	0.60	1.296	1.483	-0.026	1.57	
	C-Val5	5	0.68	0.60	1.306	1.478	-0.084	1.58	
Wc (%)	C-Val1	4	0.89	0.87	0.755	0.827	-0.004	2.76	0.91
	C-Val2	5	0.90	0.89	0.710	0.770	0.077	2.96	
	C-Val3	2	0.78	0.65	1.062	1.429	0.414	1.60	
	C-Val4	4	0.89	0.87	0.755	0.827	-0.004	2.76	
	C-Val5	3	0.87	0.84	0.804	0.903	-0.056	2.53	
Nc (% DM)	C-Val1	3	0.49	0.32	0.290	0.338	-0.003	1.21	0.64
	C-Val2	4	0.54	0.30	0.278	0.375	-0.068	1.10	
	C-Val3	Poor performance							
	C-Val4	4	0.54	0.44	0.278	0.307	-0.005	1.34	
	C-Val5	4	0.54	0.46	0.278	0.300	-0.003	1.37	

* The statistical parameter is expressed using the same unit measure of the corresponding predicted variable

Only the water content prediction models produced, all, acceptable results. The worst performances for all predicted variables were observed using C-val3 when the test set was composed of samples coming from each acquisition time separately, although the result was expected because water stress appeared four days after irrigation interruption (34 DAS), and was recognized only during the last two acquisition times. In fact, the sub-models resulting from water stress treatment cancellation led to low estimation performances. Although variability was shown by the regression coefficients, the SEP of the PLS models failed to show significant differences (alfa=0.05) among the cross-validation methods for all predicted variables. This proved consistency among the models built. Therefore, the independent validation models for the prediction of AGB FW and AGB DW were built from five components, the Nc prediction model was built from four principal components and the model for Wc prediction was built from three components.

Table 5. – Results of canopy reflectance-based models performing the independent validation. The number of selected principal components (N PC), R^2, root-mean-square errors of prediction (RMSEP), bias, RPD, and theoretical R^2_{max} are each reported.

		AGB FW (g pot^{-1})	***AGB DW (g pot^{-1})***	***Wc (%)***	***Nc (% DM)***
Canopy reflectance-based models	N PC	5	5	3	4
	R^2	0.65	0.65	0.87	0.41
	RMSEP*	19.08	1.80	0.85	0.26
	BIAS*	3.28	0.36	-0.088	0.034
	RPD	1.49	1.30	2.67	1.56
	R^2_{max}	0.84	0.74	0.91	0.64

* The statistical parameter is expressed using the same unit measure of the corresponding predicted variable

The canopy LAI and geometry-related variables Wc, AGB FW, and AGB DW were estimated with independent validation R^2 values 0.87, 0.65, and 0.65, respectively, and RMSEP values 0.85%, 19.08, and 1.80 g pot^{-1} (Table 5). The Nc estimate results were the worst (R^2= 0.41).

A discussion of variable influence on projection (VIP) scores informed the determination of model coefficient weights (Figure 8).

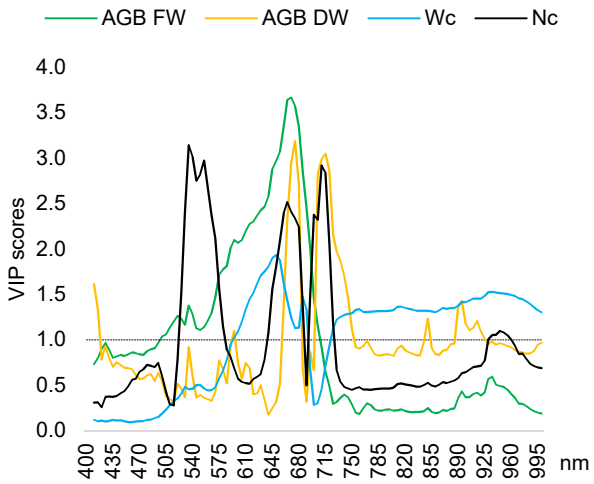

Figure 8. – VIP scores of the canopy reflectance-based models for estimation of the studied variables. The line indicates the threshold value (VIP=1) chosen to select the variables that played a role in variable estimation.

The highest VIP values for the estimating AGB FW in the model were in the green to red (500 to 705 nm) visible region. This finding agrees with the fact that the highest correlation coefficients (average r = -0.78) between single wavebands and AGB FW were found along the 470 to 715 nm visible region. The red, and particularly the red-edge, portions of the spectrum (660-750 nm) also resulted in high VIP scores for estimating AGB DW, while the green region was found not meaningful for the projection loadings on which the model relies. For the estimation of Wc, the highest VIP scores came from the yellow to red region (595-690 nm), however, the red-edge and NIR regions (725 to 980 nm) also had high VIP scores, which indicated a role for NIR scattering. This unique feature confirmed that the variability induced by water stress is mainly explained by reflectance changes across the entire NIR region (Figure 5b), as various authors have highlighted (Govender et al., 2009).

From these results, we conclude that the roles played by the red—red-edge spectral regions in estimating AGB DW and Wc completely reflect the very high correlations found between variables AGB DW and Wc and the red—red-edge wavebands (r=-0.77 and -0.80, respectively). This phenomenon might emanate from other relationships to chlorophyll content. Nitrogen is not the only factor to affect chlorophyll concentrations; indeed, water stress also affects leaf chloroplast light absorbance and leads to increased red reflectance (Jackson and Ezra, 1985).

3.3.2 Single leaf reflectance-based estimation models

A model was also built to estimate Nc from single leaf spectra to study estimation performance when spectra are recorded at optimal reflectance geometry and light exposure conditions for all leaves, without effects due to canopy architecture orientation. Such a model would then be considered to perform at the upper limit achievable using this experimental setup and instrumentation. For this model, the cross-validation was performed using cancellation blocks from six samples; leaves from a single plant comprised a single block. The R^2 values of the model during calibration and cross-validation were 0.84 and 0.83, respectively, and the RMSE values were 0.29 and 0.32% DM, respectively. The single leaf reflectance-based model, showed the highest VIP score values (Figure 9) in the red-edge region of the spectrum, which is attributable to the fact that reflectance in the red-edge changes considerably with yellow and green leaves (Figure 5b). As might be expected, this relates strongly to chlorophyll content and so, to Nc as well, given the canopy measurements displayed in Figure 5a and to the findings of others (Blackmer et al., 1996; Graeff and Claupein, 2003; Schepers et al., 1996; Schlemmer et al., 2005; Zaho et al., 2003).

Figure 9. – VIP scores of the single leaf spectra-based model for the estimation of leaf Nc. The line indicates the threshold value (VIP=1) chosen to select the variables that played a role in variable estimation.

Some similarities and differences can exist between the VIP scores of the model built on average canopy spectra and of those built on single leaf spectra (Figure 8 and 9). The green, red, and red-edge regions of the spectrum were consistent in both models, although the regressors in the red region had lower VIP score values than did those in the green and red-edge. Model regressors of the average canopy model had a VIP score profile with sharper bands than did regressors of the single leaf model.

Finally, Figure 10 contains two detached leaf spectra that demonstrate how signal quality improves when correct reflectance geometry occurs during scanning, especially in the NIR region where the weak water band (950-970 nm, OH 3rd overtone) is easily recognized. In fact, this signal is often used to calculate the water band index ($WI=Ref_{970}/Ref_{900}$, Peñuelas et al., 1993), which is almost completely masked by noise in canopy measurements.

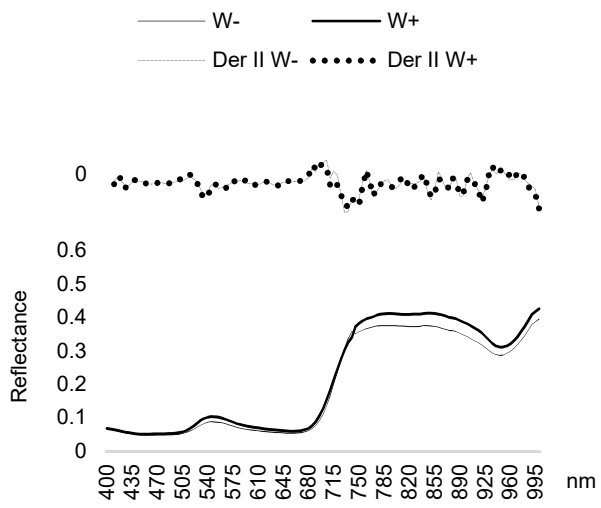

Figure 10. – Average spectra and second derivatives (Der II) of ROIs of single detached leaves scanned separately at optimal water status (W+) and under water stress (W-).

3.3.3 HSG-based estimation models

Different models were built to predict each variable from the HSGs, by first testing the five cross-validation methods, and then performing independent validation. The HSGs were pre-processed using smoothing and autoscaling. Model performances are reported in Table 6.

Table 6. – Performances of the five cross-validation methods for each estimated variable by the HSG-based models. The number of selected principal components (N PC), R^2 obtained in the calibration step (R^2 CAL) and cross-validation step (R^2 CV), root-mean-square errors in calibration and cross-validation (RMSEC and RMSECV, respectively), cross-validation bias, RPD, and theoretical R^2_{max} are each reported.

Predicted Variable	*Strategies*	*N PC*	*R^2 CAL*	*R^2 CV*	*RMSE C**	*RMSE CV**	*BIAS CV**	*RPD*	*R^2_{max}*
AGB FW (g pot^{-1})	C-Val1	3	0.70	0.54	1.268	1.582	-0.060	1.48	
	C-Val2	3	0.70	0.49	1.268	1.668	-0.146	1.40	
	C-Val3	Poor performance							0.84
	C-Val4	3	0.70	0.53	1.268	1.610	-0.091	1.45	
	C-Val5	3	0.70	0.57	1.268	1.530	-0.039	1.53	
AGB DW (g pot^{-1})	C-Val1	3	0.78	0.62	13.180	17.616	-0.383	1.62	
	C-Val2	2	0.73	0.37	14.658	22.546	0.308	1.26	
	C-Val3	Poor performance							0.74
	C-Val4	2	0.73	0.62	14.658	17.536	-0.548	1.62	
	C-Val5	3	0.78	0.66	13.180	16.466	-0.760	1.73	
Wc (%)	C-Val1	5	0.91	0.78	0.670	1.081	-0.030	2.11	
	C-Val2	2	0.83	0.47	0.930	1.654	0.197	1.38	
	C-Val3	4	0.89	0.52	0.739	1.623	0.136	1.40	0.91
	C-Val4	5	0.91	0.78	0.670	1.073	0.016	2.12	
	C-Val5	5	0.91	0.78	0.670	1.083	-0.010	2.11	
Nc (% DM)	C-Val1	3	0.70	0.47	0.223	0.298	-0.001	1.38	
	C-Val2	3	0.70	0.3	0.223	0.391	-0.048	1.05	
	C-Val3	Poor performance							0.64
	C-Val4	3	0.70	0.48	0.223	0.296	-0.003	1.39	
	C-Val5	3	0.70	0.48	0.223	0.298	-0.007	1.38	

* The statistical parameter is expressed using the same unit measure of the corresponding predicted variable

For the independent validation procedure, models based on three components were selected for the prediction of AGB FW, AGB DW and Nc, whereas two principal components were used to build the Wc-predicting model (Table 7).

Table 7. – Results of the HSG-based models performing the independent validation. The number of selected principal components (N PC), R^2, root-mean-square errors of prediction (RMSEP), bias, RPD, and theoretical R^2_{max} are each reported.

		AGB FW (g pot^{-1})	*AGB DW (g pot^{-1})*	*Wc (%)*	*Nc (% DM)*
HSG-based models	N PC	3	3	2	3
	R^2	0.74	0.72	0.86	0.48
	RMSEP*	17.33	1.74	0.875	0.249
	BIAS*	0.68	0.20	-0.166	0.047
	RPD	1.64	1.34	2.61	1.65
	R^2_{max}	0.84	0.74	0.91	0.64

* The statistical parameter is expressed using the same unit measure of the corresponding predicted variable

The model to predict AGB FW yielded an R^2 of prediction of 0.74 and an RMSEP = 7.33 g pot^{-1}. The VIP scores of the waveband-related part of the HSGs, presented in Figure 11, identified wavebands 650, 780-790, and 800-840 nm as the most informative for variability estimation of AGB FW.

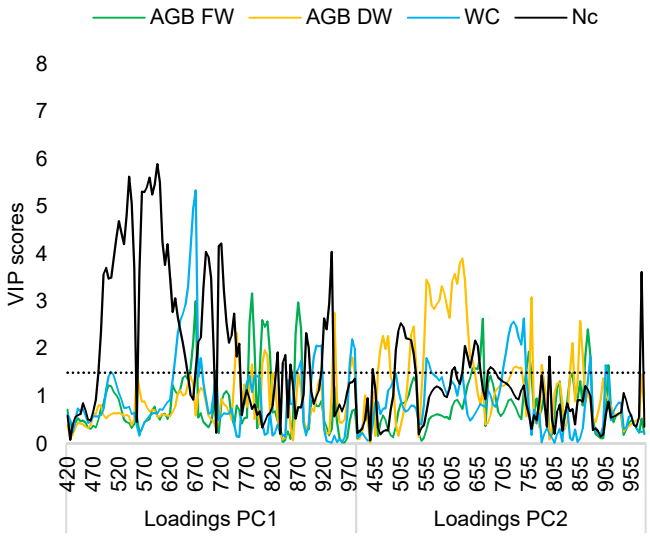

Figure 11. – VIP scores of the spectral-related portion of the HSG-based models for estimation of the studied variables. The line indicates the threshold value (VIP=1.5) chosen to select the variables that played a role in variable estimation.

The red band from 650 to 670 nm, with coefficients that recorded the highest VIP scores, participated in AGB FW estimation by both the model built on canopy average spectra and

the one built on HSGs. The R^2 and RMSEP values estimated by the model for AGB DW were 0.72 and 1.74 g pot^{-1}, respectively. The model also focused on variability in the same NIR region (780-795 nm and 825-835 nm) for AGB FW estimation, and a selection of bands that might have reflected the water treatment-induced variability and produced better AGB on FW and DW estimates using the HSG-based model as opposed to the one bases on canopy reflectance (R^2 in prediction = 0.74 and 0.72 *vs* 0.65 and 0.65, respectively).

In the visible spectral range, we selected measured reflectance from the green to red region (560-650 nm) for its information of AGB DW variation. This was also true for Nc estimation, despite an unsatisfactory prediction performance (R^2 = 0.48) in the visible (470 to 695 nm) region of the spectrum. The model also highlighted an NIR region band (895 to 960 nm). The main difference between the AGB coefficient model and the Nc estimation model was in the red-edge portion of the spectrum (715-760 nm) that was selected for its very high VIP scores in the case of Nc estimation only. The VIP scores of the HSG-based model β-coefficients behaved very similarly to those of the canopy reflectance-based model built on canopy average spectra except for the NIR band that played a greater role in HSG-based prediction than in reflectance-based prediction. HSG-based estimation of Wc relied on different wavebands than the estimation based on canopy reflectance, despite producing very similar results (R^2 = 0.86 and RMSEP = 0.88%. Both green (560 nm) and red (640-650 nm) bands took part in estimation, but not in scattering in the NIR region.

As was observed in the canopy reflectance-based model, the C-val3 method performed poorest for all predicted variables.

Model results were tested following Snedecor and Cochran (1967); no differences were found ($\alpha = 0.05$) among the models performances.

As HSGs rely on PCA performed on hyperspectral images, Figure 12a-d shows PCA results when performed on a simple image.

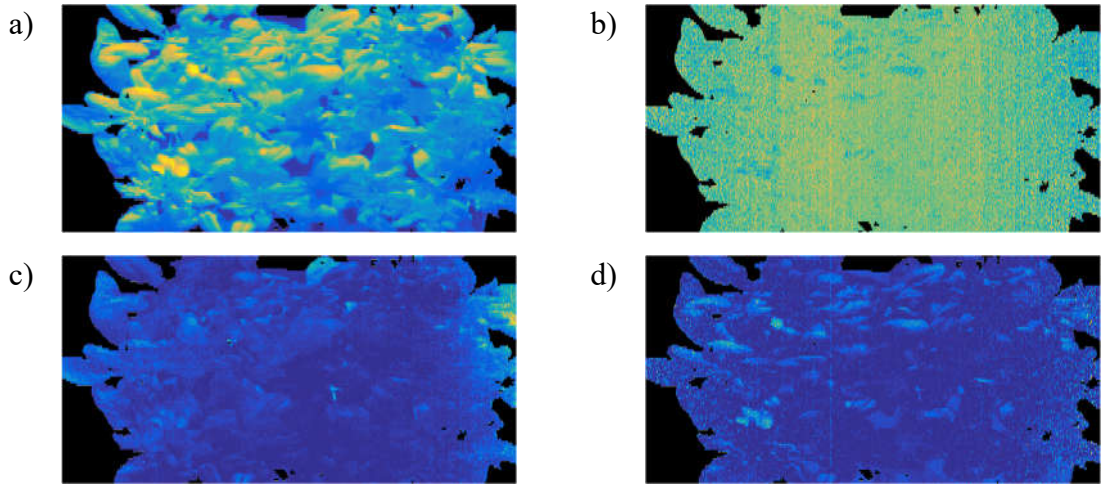

Figure 12. – Results of image PCA applied to a pot under optimal nitrogen and water levels (N3 W+) at the first step of HSG creation, and reporting the first principal component scores (a), the second principal component scores (b), and the Q residuals and the Hotelling T^2 values (d). The lowest values are displayed in blue and the highest ones in yellow.

The first component of the image-PCA, which explained 44% of variability, contained canopy structure information that discriminated between illuminated and shadowed leaves (Figure 12a). On the other hand, the second component explained 27% of the variability, but revealed no specific structural features in the image (Figure 12b). The pixels with the highest Q residuals (Figure 12c) and Hotelling T^2 residuals (Figure 12d) represented the canopy area with better sensor lamp illumination.

In the pixel-related portion of the HSGs, original image pixels that contributed to predicting the studied variables were identifiable.

To explain model behaviour, Figure 13 presents four example images of a pot under N3 and W+ combined treatment for predictive models AGB FW, AGB DW, Wc, and Nc. The canopy pixels carrying the most useful information for estimating all tested crop parameters, selected by imposing a 1.5 threshold on the VIP scores, are highlighted in white.

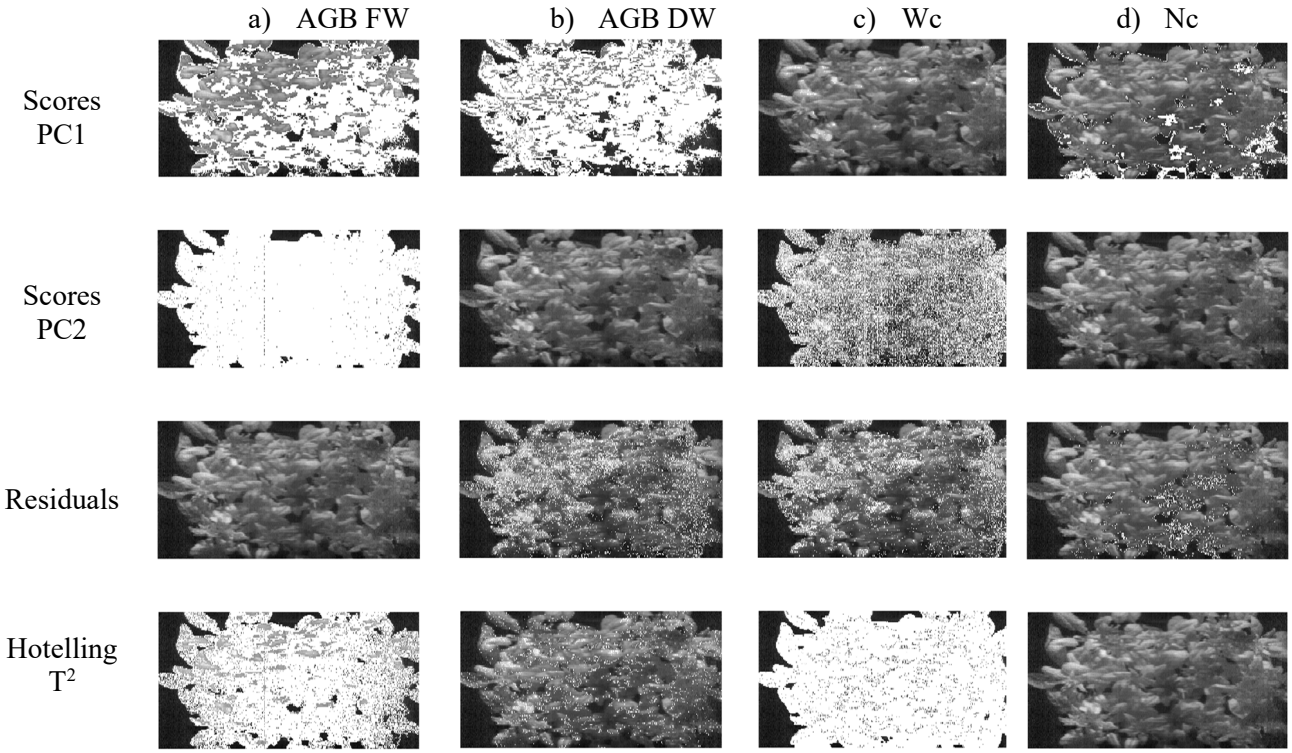

Figure 13. – Maps of the pixels containing information used by the HSG-based estimation models (white pixels). Each column represents an estimated variable: AGB FW (a), AGB DW (b), Wc (c), and Nc (d). Each row contains the HSG element used as a predictor in the estimation models.

Most relevant to an overall evaluation of HSG-based models to predict crop variables, is that the HSG pixel-related portion of the Nc estimate is represented by the scores of the first principal component (coefficients had the highest VIP scores of all predictors) and by the residuals, indicating their key role in canopy structure. The average reflectance spectra of the white pixels and the average reflectance of pixels with low VIP scores were calculated and presented in Figure 14a-d.

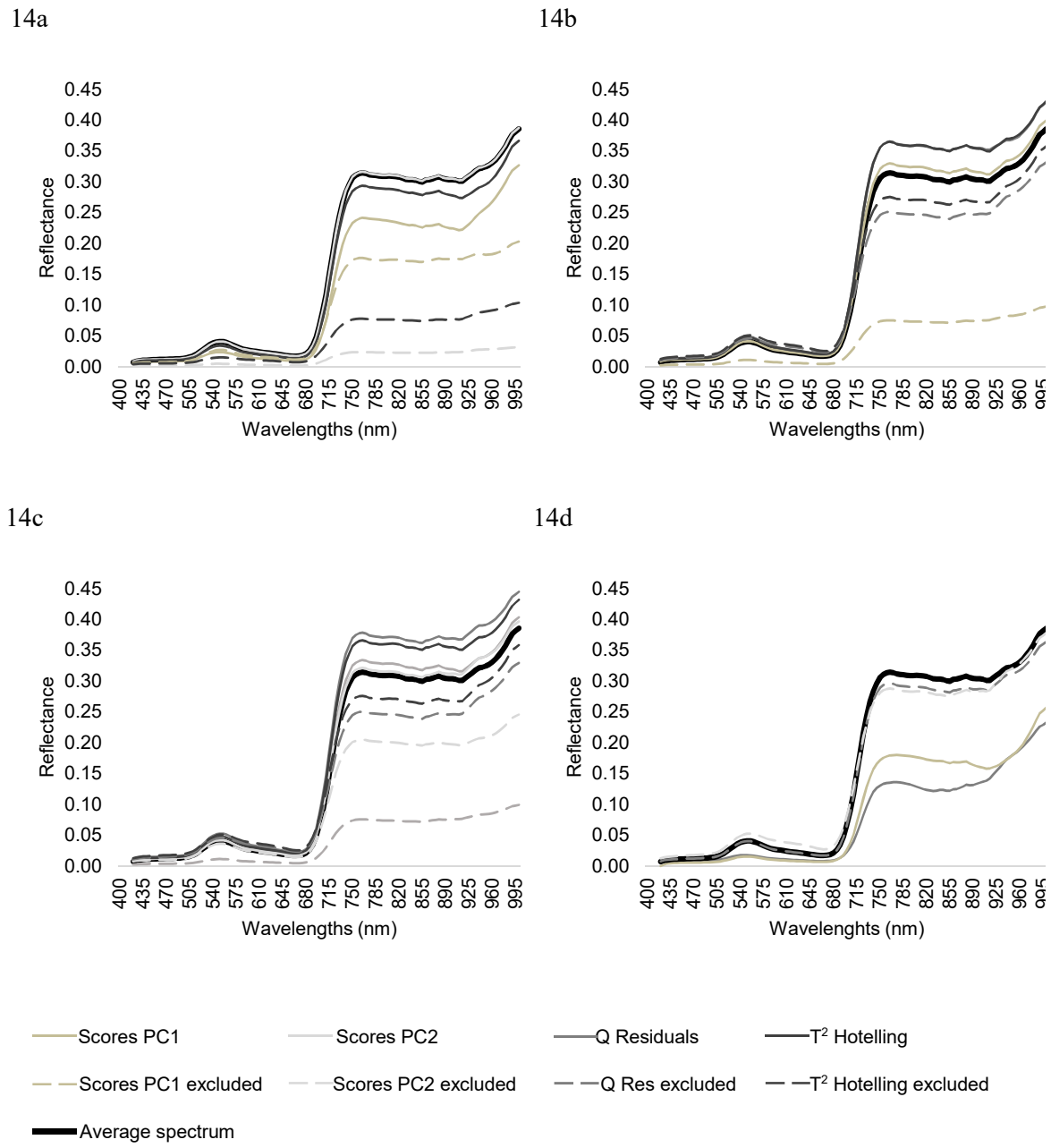

Figure 14. – The average spectra of the pixels retained by the estimation models and the average spectra of the pixels excluded from each image PCA statistic composing the HSGs for all estimation models: AGB FW (a), AGB DW (b), Wc (c), and Nc (d).

The AGB DW estimation model showed the highest VIP value predictors corresponded to the first component scores. Comparing the selected pixels from the first principal component scores (PC1) (Figure 13b) with the image PCA scores (Figure 12a) caused pixels across a wide range of PC1 scores to be selected, from both illuminated and shadowed leaves. However, the average spectra of the selected pixels (Figure 14b) showed that the AGB DW

estimation model explained the encountered variability using the spectra characterized by high Hotelling T^2 values, corresponding to leaves illuminated directly by the lamp in the image PCA (Figure 12d). Also, the selected pixels displayed higher reflectance (NIR region) than on average for the pot (Figure 14b).

As with the AGB DW estimation model, Wc estimation was depended on spectra with very high NIR reflectance (Figure 14c). The pixels selected along the second component (Figure 13c) had the highest VIP scores, and were characterized by an average reflectance comparable to that of the whole pot. The estimation of the AGB FW relied on pixels covering a large area of the image, but in contrast to results from the Wc estimation model (Figure 13c), the pixels with the highest Hotelling T^2 values and brightest areas of the canopy had reduced weights (Figure 12d and Figure 13c). In fact, the high-weight pixels in this model were generally characterized by average reflectance, approximating the whole pot average reflectance or slightly lower in both the visible and NIR regions (Figure 14c). The greater role of the second component (PC2) in Wc and AGB FW estimation relative to other variables probably depend on its relationship to reflectance in the spectral region with the highest PC2 loading values (970-980 nm) (data not shown) that corresponds to a water absorption region (Peñuelas et al., 1993).

The estimation of Nc depended on leaf spectra characterized by a dark green colour (Figure 14d). Of interest is that only the Nc estimation model used information linked to darker leaves, often the youngest and richest in Nc, but also related to the shadow effect of leaf layers and wet soil. Shadows and soil might have had a confounding effect, which would have diminished the estimation of nitrogen concentration (Schut and Ketelaars, 2003; Sripada et al., 2006). Noh and Zhang (2012) described that spectral information coming from shadowed leaves might result in a higher chlorophyll content (at different nitrogen levels)

and reflectance correlation, as they recorded with a multispectral sensor in shadowed maize leaves.

4 CONCLUSION

The aim of this work was to verify the capability of hyperspectral imaging data in the VIS-NIR range of the spectrum (400-1000 nm) to estimate crop variables under combined water and nitrogen stress using multivariate data analysis. Both the canopy reflectance-based and HSG-based models used in the study performed well in estimating variables strictly related to canopy LAI and geometry, such as Wc, AGB FW, and AGB DW. An estimation of the maximum R^2 achievable with no error or noise in the spectral measurement or in the models, using the repeatability of reference data as proposed by Dardenne (2009) yielded values of 0.91, 0.84, 0.74, and 0.64 for Wc, AGB FW, AGB DW, and Nc estimations, respectively. Both the canopy reflectance-based and HSG-based estimations nearly achieved these upper limits with R^2 of prediction values of 0.87, 0.65, 0.65, 0.41 and 0.86, 0.74, 0.72, 0.48 respectively. The red and red-edge spectral regions played the greatest roles in estimation of these variables, in both the canopy reflectance-based and HSG-based models as summarized in Table 8. The Wc estimation model, which relied principally on the red region, represented an exception. Scattering in the NIR region contributed to AGB FW and DW, but not to Wc, in HSG-based estimation. However, the opposite occurred in canopy reflectance-based estimation, despite the selection of different NIR portions. Canopy-based Nc estimation produced poor predictive results. On the contrary, the prediction from single leaf spectra produced very good results with an R^2 in cross-validation of 0.83 and an RMSECV of 0.32 g DW $plant^{-1}$. This estimation relied on the visible and red-edge portion of the spectrum, and was possibly due to optimal light exposure for all leaves, without any orientation effects due to canopy architecture. More studies are needed on canopy geometry modeling to consider canopy structure in estimation models, and on the collection of multiple angle measurements of the canopy to reduce structural effects.

Finally, image data extraction proved successful to untangle water and nitrogen supply effects. In particular, hyperspectrograms, in place of average canopy spectra for variable estimation, produced encouraging results. Data compression dramatically reduced the size of analyzed datasets and the amount of segmented field data. The original hyperspectral images were 1.25 GB in size, the unfolded images built for the analysis 922 MB, while the resulting hyperspectrograms used in calibration procedures was 300 kB and an average spectra just 68 kB. This work represented the first step in the application of HSG-based estimations of plant variables for agricultural purposes and demonstrates that HSG extraction is a reliable technique.

Table 8. – Summary of the wavebands retained by the models for estimation of the studied variables based on single leaf reflectance (Average spectrum), canopy reflectance (Average spectrum), and canopy hyperspectrograms.

Level of acquisition	Set of predictors	Spectral region	AGB FW	AGB DW	Wc	Nc
LEAF	**Average Spectra**	*Blue*				420-495 nm
		Green				495-590 nm
		Red				590-680 nm
		Red-Edge				680-715 nm
		NIR				
CANOPY	**Average Spectra (soil + vegetation)**	*Blue*				
		Green	500-590 nm	595 nm		525-580 nm
		Red	590-680 nm	660-680 nm	595-690 nm	640-685 nm
		Red-Edge	680-705 nm	705-750 nm	725-750 nm	695-725 nm
		NIR			750-980 nm	930-960 nm
	Hyperspectrograms	*Blue*		420-425 nm		470-495 nm
		Green		560-590 nm	560 nm	495-555, 570-590 nm
		Red	650 nm	590-650 nm	640-650 nm	590-645, 655-680 nm
		Red-Edge	710, 780 nm	780 nm		680-695, 715-760 nm
		NIR	780-790, 800-840 nm	780-795, 825-835 nm	900-910, 970-980 nm	895-960 nm

5 ACKNOWLEDGMENTS

The Department of Agricultural and Environmental Sciences of Università degli studi di Milano (UNIMI) through Development Plan UNIMI 2014 funded this research. Moreover, we thank Dr. Daniele Masseroni, Dr. Alessandro Ferri, Domenico Ditto and all the other colleagues for their precious help in managing the greenhouse experiment.

6 REFERENCES

Allen, R.G., Pereira, L.S., Raes, D., Smith, M., others, 1998. Crop evapotranspiration-Guidelines for computing crop water requirements-FAO Irrigation and drainage paper 56. FAO, Rome 300, D05109.

Barnes, E.M., Clarke, T.R., Richards, S.E., Colaizzi, P.D., Haberland, J., Kostrzewski, M., Waller, P., Choi, C., Riley, E., Thompson, T., 2000. Coincident detection of crop water stress, nitrogen status and canopy density using ground based multispectral data, in: Proc. 5th Int. Conf. Precis Agric. Bloomington, MN, USA.

Blackmer, T.M., Schepers, J.S., Varvel, G.E., 1994. Light reflectance compared with other nitrogen stress measurements in corn leaves. Agronomy Journal 86, 934–938.

Cohen Yafit, Rosen Carl, Alchanatis V., Mulla D., Heuer Bruria, Dar Zion, Ronit Rud, and Tyler Nigon, 2013. Fusion of Hyperspectral and Thermal Images for Evaluating Nitrogen and Water Status in Potato Fields for Variable Rate Application. Final Scientific Report of BARD Project, Number: IS-4255-09.

Dardenne, P., 2010. Some considerations about NIR spectroscopy: Closing speech at NIR-2009. NIR news 21, 8–14.

Daughtry, C.S.T., Walthall, C.L., Kim, M.S., De Colstoun, E.B., McMurtrey, J.E., 2000. Estimating corn leaf chlorophyll concentration from leaf and canopy reflectance. Remote sensing of Environment 74, 229–239.

Eitel, J.U.H., Long, D.S., Gessler, P.E., Hunt, E.R., 2008. Combined Spectral Index to Improve Ground-Based Estimates of Nitrogen Status in Dryland Wheat. Agronomy Journal 100, 1694. doi:10.2134/agronj2007.0362

El-Shikha, D.M., Waller, P., Hunsaker, D., Clarke, T., Barnes, E., 2007. Ground-based remote sensing for assessing water and nitrogen status of broccoli. Agricultural water management 92, 183–193.

Fearn, T., 2015. Chemometric Space: How to use replicate spectra, NIR news 26, 18–18. doi: 10.1255/nirn.1535

Ferrari, C., Foca, G., Ulrici, A., 2013. Handling large datasets of hyperspectral images: Reducing data size without loss of useful information. Analytica chimica acta 802, 29–39.

Filella, I., Penuelas, J., 1994. The red edge position and shape as indicators of plant chlorophyll content, biomass and hydric status. International Journal of Remote Sensing 15, 1459–1470.

Fitzgerald, G., Rodriguez, D., O'Leary, G., 2010. Measuring and predicting canopy nitrogen nutrition in wheat using a spectral index—The canopy chlorophyll content index (CCCI). Field crops research 116, 318–324.

Fitzgerald, G.J., Rodriguez, D., Christensen, L.K., Belford, R., Sadras, V.O., Clarke, T.R., 2006. Spectral and thermal sensing for nitrogen and water status in rainfed and irrigated wheat environments. Precision agriculture 7, 233–248.

Goel, P.K., Prasher, S.O., Patel, R.M., Landry, J.A., Bonnell, R.B., Viau, A.A., 2003. Classification of hyperspectral data by decision trees and artificial neural networks to identify weed stress and nitrogen status of corn. Computers and Electronics in Agriculture 39, 67–93. doi:10.1016/S0168-1699(03)00020-6

Govender, M., Dye, P.J., Weiersbye, I.M., Witkowski, E.T.F., Ahmed, F., 2009. Review of commonly used remote sensing and ground-based technologies to measure plant water stress. Water SA 35, 741–752.

Graeff, S., Claupein, W., 2003. Quantifying nitrogen status of corn (Zea mays L.) in the field by reflectance measurements. European Journal of Agronomy 19, 611–618. doi:10.1016/S1161-0301(03)00007-8

Hansen, P.M., Schjoerring, J.K., 2003. Reflectance measurement of canopy biomass and nitrogen status in wheat crops using normalized difference vegetation indices and partial least squares regression. Remote Sensing of Environment 86, 542–553. doi:10.1016/S0034-4257(03)00131-7

Hunt, E.R., Rock, B.N., 1989. Detection of changes in leaf water content using near-and middle-infrared reflectances. Remote sensing of environment 30, 43–54.

Jackson, R., Ezra, C.E., 1985. Spectral response of cotton to suddenly induced water stress. International Journal of Remote Sensing 6, 177–185.

Jones, H., Vaughan, R., 2010. Remote Sensing of Vegetation: Principles, Techniques and Applications. Oxford University Press, New York.

Karimi, Y., Prasher, S.O., McNairn, H., Bonnell, R.B., Dutilleul, P., Goel, P.K., 2005. Discriminant analysis of hyperspectral data for assessing water and nitrogen stresses in corn. Transactions of the Asae 48, 805–813.

Li, F., Mistele, B., Hu, Y., Chen, X., Schmidhalter, U., 2014. Reflectance estimation of canopy nitrogen content in winter wheat using optimised hyperspectral spectral indices and partial least squares regression. European Journal of Agronomy 52, 198–209.

Lichtenthaler, H. K., Gitelson, A., & Lang, M. (1996). Non-destructive determination of chlorophyll content of leaves of a green and an aurea mutant of tobacco by reflectance measurements. Journal of Plant Physiology, 148(3), 483-493.

Liu, J., Miller, J.R., Haboudane, D., Pattey, E., 2004. Exploring the relationship between red edge parameters and crop variables for precision agriculture, in: Geoscience and Remote Sensing Symposium, 2004. IGARSS'04. Proceedings. 2004 IEEE International. IEEE, pp. 1276–1279.

Noh, H., Zhang, Q., 2012. Shadow effect on multi-spectral image for detection of nitrogen deficiency in corn. Computers and Electronics in Agriculture 83, 52–57.

Olfs, H.-W., Blankenau, K., Brentrup, F., Jasper, J., Link, A., Lammel, J., 2005. Soil- and plant-based nitrogen-fertilizer recommendations in arable farming. Journal of Plant Nutrition and Soil Science 168, 414–431. doi:10.1002/jpln.200520526

Osborne, S.L., Schepers, J.S., Francis, D.D., Schlemmer, M.R., 2002. Use of spectral radiance to estimate in-season biomass and grain yield in nitrogen-and water-stressed corn. Crop Science 42, 165–171.

Otsu, N., 1975. A threshold selection method from gray-level histograms. Automatica 11, 23–27.

Peñuelas, J., Filella, I., Biel, C., Serrano, L., Save, R., 1993. The reflectance at the 950–970 nm region as an indicator of plant water status. International journal of remote sensing 14, 1887–1905.

Peñuelas, J., Gamon, J.A., Fredeen, A.L., Merino, J., Field, C.B., 1994. Reflectance indices associated with physiological changes in nitrogen-and water-limited sunflower leaves. Remote Sensing of Environment 48, 135–146.

Perry, E.M., Roberts, D.A., 2008. Sensitivity of narrow-band and broad-band indices for assessing nitrogen availability and water stress in an annual crop. Agronomy journal 100, 1211–1219.

Ray, S.S., Singh, J.P., Panigrahy, S., 2010. Use of hyperspectral remote sensing data for crop stress detection: ground-based studies. International Archives of Photogrammetry, Remote Sensing and Spatial Information Science 38.

Rodriguez, D., Fitzgerald, G.J., Belford, R., Christensen, L.K., 2006. Detection of nitrogen deficiency in wheat from spectral reflectance indices and basic crop eco-physiological concepts. Crop and Pasture Science 57, 781–789.

Savitzky, A., Golay, M.J., 1964. Smoothing and differentiation of data by simplified least squares procedures. Analytical chemistry 36, 1627–1639.

Schepers, J.S., Blackmer, T.M., Wilhelm, W.W., Resende, M., 1996. Transmittance and Reflectance Measurements of CornLeaves from Plants with Different Nitrogen and Water Supply. Journal of Plant Physiology 148, 523–529.

Schlemmer, M.R., Francis, D.D., Shanahan, J.F., Schepers, J.S., 2005. Remotely measuring chlorophyll content in corn leaves with differing nitrogen levels and relative water content. Agronomy Journal 97, 106–112.

Schut, A.G.T., Ketelaars, J.J.M.H., 2003. Imaging spectroscopy for early detection of nitrogen deficiency in grass swards. NJAS - Wageningen Journal of Life Sciences 51, 297–317. doi:10.1016/S1573-5214(03)80021-0

Scotford, I.M., Miller, P.C.H., 2005. Applications of Spectral Reflectance Techniques in Northern European Cereal Production: A Review. Biosystems Engineering 90, 235–250. doi:doi: DOI: 10.1016/j.biosystemseng.2004.11.010

Shiratsuchi, L., Ferguson, R., Shanahan, J., Adamchuk, V., Rundquist, D., Marx, D., Slater, G., 2011. Water and Nitrogen Effects on Active Canopy Sensor Vegetation Indices. Agronomy Journal 103, 1815–1826. doi:10.2134/agronj2011.0199

Smilde, A.K., Jansen, J.J., Hoefsloot, H.C., Lamers, R.-J.A., Van Der Greef, J., Timmerman, M.E., 2005. ANOVA-simultaneous component analysis (ASCA): a new tool for analyzing designed metabolomics data. Bioinformatics 21, 3043–3048.

Snedecor, G.W., Cochran, W.G., 1967. Statistical methods. Iowa State University Press 327.

Sripada, R.P., Heiniger, R.W., White, J.G., Meijer, A.D., 2006. Aerial color infrared photography for determining early in-season nitrogen requirements in corn. Agron. J. 98, 968–977. doi:10.2134/agronj2005.0200

Stellacci, A.M., Castrignanò, A., Diacono, M., Troccoli, A., Ciccarese, A., Armenise, E., Gallo, A., Vita, P.D., Lonigro, A., Mastro, M.A., Rubino, P., 2012. Combined approach based on principal component analysis and canonical discriminant analysis

for investigating hyperspectral plant response. Ital J Agronomy 7, e34. doi:10.4081/ija.2012.e34

Stirzaker, R.J., 2009. Strategy, tactics and heuristics for managing solutes in horticultural crops, in: VI International Symposium on Irrigation of Horticultural Crops 889. pp. 59–65.

Strachan, I.B., Pattey, E., Boisvert, J.B., 2002. Impact of nitrogen and environmental conditions on corn as detected by hyperspectral reflectance. Remote Sensing of Environment 80, 213–224.

Tilling, A.K., O'Leary, G.J., Ferwerda, J.G., Jones, S.D., Fitzgerald, G.J., Rodriguez, D., Belford, R., 2007. Remote sensing of nitrogen and water stress in wheat. Field Crops Research 104, 77–85. doi:10.1016/j.fcr.2007.03.023

Ullah, S., Skidmore, A.K., Ramoelo, A., Groen, T.A., Naeem, M., Ali, A., 2014. Retrieval of leaf water content spanning the visible to thermal infrared spectra. ISPRS Journal of Photogrammetry and Remote Sensing 93, 56–64. doi:10.1016/j.isprsjprs.2014.04.005

Vigneau, N., Ecarnot, M., Rabatel, G., Roumet, P., 2011. Potential of field hyperspectral imaging as a non destructive method to assess leaf nitrogen content in Wheat. Field Crops Research 122, 25–31. doi:10.1016/j.fcr.2011.02.003

Wang, T.-C., Ma, B.L., Xiong, Y.-C., Saleem, M.F., Li, F.-M., 2011. Optical sensing estimation of leaf nitrogen concentration in maize across a range of water-stress levels. Crop and Pasture Science 62, 474–480.

Zhang, Q., Li, Q., Zhang, G., 2012. Rapid determination of leaf water content using VIS/NIR spectroscopy analysis with wavelength selection. Journal of Spectroscopy 27, 93–105.

Zhao, D., Reddy, K.R., Kakani, V.G., Read, J.J., Carter, G.A., 2003. Corn (Zea mays L.) growth, leaf pigment concentration, photosynthesis and leaf hyperspectral reflectance properties as affected by nitrogen supply. Plant and soil 257, 205–218.

Zillmann, E., Graeff, S., Link, J., Batchelor, W.D., Claupein, W., 2006. Assessment of Cereal Nitrogen Requirements Derived by Optical On-the-Go Sensors on Heterogeneous Soils. Agronomy Journal 98, 682–690. doi:10.2134/agronj2005.0253

Zwanenburg, G., Hoefsloot, H.C., Westerhuis, J.A., Jansen, J.J., Smilde, A.K., 2011. ANOVA–principal component analysis and ANOVA–simultaneous component analysis: A comparison. Journal of Chemometrics 25, 561–567.

3. LOW-COST MULTISPECTRAL CAMERA ON BOARD A UAV: ESTIMATION OF MAIZE NITROGEN-RELATED VARIABLES TO SUPPORT NITROGEN FERTILIZATION

ABSTRACT

Maize, characterized by high nitrogen fertilization rates, is the main crop in Northern Italy, a territory vulnerable to nitrate leaching. In this context, matching maize nitrogen demands with the correct timing and amount of nitrogen fertilizers would be crucial. Nowadays, it could be possible thanks to the development of new technologies that allow the monitoring of in-field crop variability at very high spatial and temporal resolutions. In particular, the development of small unmanned aerial vehicles (UAVs) and the advancement in sensors technology that made the consumer digital cameras suitable for the remote-sensing of vegetation (if properly modified to become visible and near-infrared cameras) have increased the interest of the use of these devices for agriculture applications.

This work aimed to test the opportunities of this low-cost sensor technology to map within-field variability to support nitrogen fertilization decisions. An experimental field with six different nitrogen organic fertilizer treatments was surveyed the year 2014 and 2015. The crop was sampled at V6 and V9 development stages and the above ground biomass dry weight, its nitrogen concentration and uptake were determined. At the same time, the UAV mounting a modified consumer digital camera surveyed the field to record the aerial image. The average BNDVI, GNDVI and the estimated fraction cover were then calculated for each experimental plot and regressed against the measured variables. The estimation of the above ground biomass at V9 was the most satisfactory. Estimations at V6 were not possible due to

the low level of crop biomass which represented a limitation to the sensing. The best predictor was found to be the estimated fraction cover: regression equation built using the data recorded at V9 in the two years of experiment resulted in R^2=0.87 and rRMSE of 17%. The low cost imaging system led to very good performance in AGB estimation thanks to the very high spatial resolution of the imaging sensor that allowed a reliable estimation of AGB through the assessment of the canopy fraction cover.

1 INTRODUCTION

The efficient use of agronomic inputs represents an answer to the increasing attention of public opinion to agriculture intended as a source of environmental pollution, especially referring to fertilization that could cause water pollution with drawbacks on human health. A more efficient preservation of environmental resources in agriculture can be gained taking into account field variability when applying external inputs. Both between and within-field variability can be evidenced with maps describing crop status at specific phenological stages. Maps could be obtained as outputs of remote-sensing techniques involving the use of optical sensors and then used to interpret the dynamics of plant nitrogen demand during the growing season, rapidly and accurately substituting destructive and time-consuming analytical measurements. Remote sensing is usually referred to satellite sensors. Different satellite sensors are suitable to monitor nitrogen status of the vegetation but satellite-collected data requires post-processing to make atmospheric correction and to calculate vegetation indicators. Furthermore, some authors have underlined the limited operational flexibility of such techniques for real time field monitoring or management due to low temporal and spatial resolution of acquired images, long satellite re-visit times, cloud cover and total cost of the service (Berni et al., 2009; Swain et al., 2007). However, nowadays, the improvements of satellite spatial and temporal resolution and the availability of free images renew the interest in satellite remote sensing for agricultural purposes applied to large surfaces.

On the other hand, tractor-mounted proximal sensors have been already developed and commercialized and widely use to assess nitrogen status. They acquire reflectance variably from two to twenty wavebands in the visible (VIS) and near-infrared (NIR) range of the spectrum. Tractor-mounted sensors have their own light source to avoid sunlight dependence. Moreover, the normalization of the vegetation indices by using a N-rich

reference strip is suggested and it allows to avoid the dependence of reflectance on environmental specific factors. In this way, calculated vegetation indices can be better related to variables revealing crop status (*e.g.,* above ground biomass, N uptake, N concentration), by using site- and crop-specific calibration algorithms.

Between the satellite- and tractor-mounted optical sensors, in these recent years, new opportunities for crop monitoring were opened by the innovative use of unmanned aerial vehicles (UAVs). UAVs, opportunely equipped with multi-spectral digital cameras, can be used to periodically fly over the field to acquire crop spectral information in VIS and NIR bands in order to calculate vegetation indices. Recent attempts to construct crop-specific calibration curves between UAV-derived vegetation indices and crop variables are recorded in literature (Geipel et al., 2016; Huang et al., 2010; Lebourgeois et al., 2008;). Digital cameras mounted on UAVs are devices of increasing interest in precision agriculture because of the opportunity to collect images with high spatial and temporal resolution throughout the season, even when the use of tractor-mounted sensors is logistically and economically difficult. Moreover, UAV-based monitoring is a flexible tool in terms of the timing of the surveys and in terms of possible applications: nutrient and water management, weed control, disease and pest detection, estimation of grain yields (Wójtowicz et al., 2016). However, the ability of the UAV-mounted sensors to assess vegetation status hangs on images calibration and processing that implies to retrieve reflectance and to compensate for ambient light variation (Noh et al., 2005; Kim et al., 2008), to manage soil background noise (Noh et al, 2005), as well as for the other passive sensors. Finally, one or more vegetation indices are calculated and related to the crop variables within the field through site-specific calibration curves.

The surveyed literature highlighted the use of different modified digital cameras mounted on UAVs to monitor crop nitrogen status. In particular, the relationships between the vegetation indices acquired using digital cameras or modified digital cameras and leaf chlorophyll concentration (R^2>0.7, Lebourgeois et al., 2008; Noh and Zhang, 2012; Miao et al., 2009), above ground biomass (R^2=0.70-0.85, Geipel et al., 2016; Reyniers e Vrindts, 2005), plant nitrogen concentration (R^2=0.4-0.8, Geipel et al, 2016; Lebourgeois et al., 2012; Reyners e Vrindts, 2005) and grain yield (R^2>0.7, Huang et al., 2010) were proved in different works on different cereals.

Maize is the main crop in Northern Italy and it is characterized by high nitrogen fertilization rates (average 300 kg N ha^{-1}, provided either with animal manures and fertilizers) in a territory that is vulnerable to nitrate pollution of water. In this context, matching maize nitrogen demands would be crucial to optimize yields and to decrease environmental pollution. Thus, crop monitoring at high spatial and temporal resolution with the aim to map crop variability linked to nitrogen nutrition would be crucial to support site-specific fertilization. Furthermore, since side dress fertilization is applied on maize crop between V6 and V9 development stages, UAV-based monitoring is particular interesting to monitor maize crop in this short time window. Regarding the UAV-based monitoring of maize crop, different attempts were made to estimate maize above ground biomass (Osborne et al., 2004; Sakamoto et al., 2012a and 2012b), nitrogen concentration (Osborne et al., 2004; Rorie et al., 2010 and 2011) and uptake (Tomer et al., 1997). The authors agreed in finding green band-based vegetation indices as the best predictors for the studied maize nitrogen-related variables: R^2 ranged between 0.5-0.98 for the estimation of the above ground biomass, 0.49-0.7 for the estimation of nitrogen concentration and 0.38-0.59 for the estimation of nitrogen uptake. However, it must be considered that these recorded experiences were carried for one

or two years and often, at later development stages than the ones identified as the best time window for nitrogen side dress fertilization (V6-V9). Furthermore, if V6 and V9 development stages were sensed, the dataset used for regression analysis were not specific for those stages but comprehensive of vegetative and reproductive stages (Osborne et al., 2004; Sakamoto et al., 2012a and 2012b). Due to the lack of specific information about maize UAV-based monitoring in the time window suitable for maize side dress fertilization, we present a two years-case study where a modified consumer digital camera mounted on board a UAV was used to estimation maize nitrogen-related variables (above ground biomass, plant nitrogen concentration and plant nitrogen uptake). To this end, an experimental field with an induced fertilization gradient was used to test the opportunities of a low-cost technology to map within-field variability, to calculate vegetation indices, and to support nitrogen fertilization decisions.

2 MATHERIALS AND METHODS

The UAV survey was carried out on an experimental field located at Montanaso Lombardo (Lodi), Italy (45°20'32" N, 9°26'43" E, altitude 80 m asl) during 2014 and 2015 maize growing seasons. The experiment (Cavalli et al., 2016) started during 2011 with the aim of studying livestock manure-N use efficiency in a crop rotation silage-maize and Italian Ryegrass (*Lolium perenne*, Lam.). Six treatments (four manures plus an ammonium sulphate and an unfertilized treatment) were arranged in a randomized block design with four replicates. Plots were 15 m long and 7.5 m wide, with ten meters spacing between adjacent blocks. The four manures comprised an unseparated anaerobically-digested dairy cow slurry (co-digested with silage maize), its liquid and solid fractions, and an unseparated anaerobically-stored dairy cow slurry. For more details about the experiment refer to Cavalli et al. (2016). This on-going experiment provided a wide range of variability in N availability and thus it was chosen to be surveyed by the UAV mounting the modified camera, for calibration purposes. In the year 2015 the same experimental design of the previous year was replicated, but no treatments were applied because the aim of the original experiment was to quantify the residual N effects of previous fertilizations. Thus, in order to rise further available plant-N variability, during 2015, four treatments were added to the original experimental design: ammonium sulphate at 35, 70 and 150 kg N ha^{-1}, and calcium nitrate at 150 kg N ha^{-1}. These treatments were applied to small plots (8 m long and 7.5 m wide) in the strips between blocks.

2.1 Crop sampling and analysis

Maize samples were collected on two different maize phenological stages: at V6 (maize with six fully expanded leaves) and V9 (maize with nine fully expanded leaves), in both the years of the experimentation corresponding to 18 July and 1 August 2014 and 3 July and 13 July

2015, respectively. Above ground biomass (AGB) of maize was estimated by collecting 15 plants per plot (three plants row^{-1} of the five inner rows of each plot). Moreover, during 2015, eight small areas outside experimental plots were sampled (1 m of two maize rows) in order to further increase variability in the collected samples. Plants were oven dried (105°C), ground with a rotary-knife mill equipped with a sieve of 4 mm mesh; subsequently, a part was ground with a ZM 100 centrifugal mill equipped with a sieve of 0.2 mm mesh (Retsch Gmbh & Co., Haan, Germany). Total nitrogen was determined by dry combustion using a ThermoQuest NA1500 elemental analyser (Carlo Erba). Nitrogen uptake was also determined multiplying the measured above ground biomass by the corresponding nitrogen concentration.

2.2 Image acquisition and processing

The prototype UAV was a coaxial octocopter in carbon fiber, a maximum take-off mass of 12kg and equipped with a GNSS (Global Navigation Satellite System) NEO-M8N (u-blox, Thalwil, Switzerland) and a gimbal platform. A consumer digital camera Canon® Powershot SX260 HS was manually modified by removing the infrared-blocking filter and adding a Super Blue IR filter to be transformed in VIS-NIR digital camera acquiring 8-bit spectral information in three channels: blue (B), green (G) and NIR. The image acquisition was carried out in the same dates of plant sampling for destructive analysis (before plant collection).

The modified camera was mounted on board the UAV that surveyed the field at a low flight speed (5 m/s). The images were acquired with the autofocus mode and with 75% forward and sideward overlap, under clear sky conditions, at 35 m altitude, between 11:00 and 13:00 a.m. solar time. The output images were 12.1 MP (Mega pixel) 3-band 8-bit per band JPEG files with a spatial resolution of 1.5 cm.

The orthomosaics of the field were made using the software Pix4Dmapper (Pix4D SA, Lausanne, Switzerland). No radiometric calibration was carried out at this step. Images of each experimental plot were then selected from the orthoimages acquired in the year 2014, by sampling the area corresponding to the inner five rows of each plot. Only half a plot was cropped from the orthoimages acquired in the year 2015, in order to sample the same number of pixels for all the plots (according to the fact that the 2015 extra blocks areas treated with mineral fertilizers were half the size of the original plots). Moreover, the eight areas collected out of the experimental blocks were also sampled in the image by cropping only the collected rows (a small blue tile was positioned at the beginning of the sampled area to be recognized from the aerial images). Figure 1 represents the regions of interest of the image (ROIs) collected in both the years of experimentation.

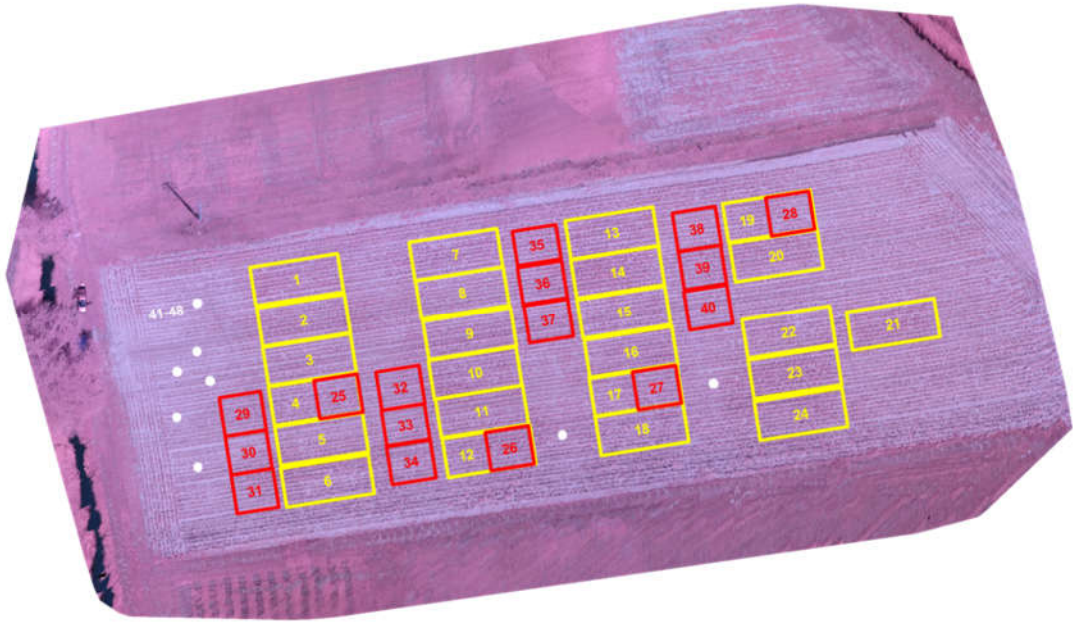

Figure 1. – Aerial orthomosaic of the field acquired at 18 July 2014 (maize at V6 stage), as example. The areas in yellow identify the ROIs of the image collected for the calibration of the first year (2014, n=24), while the yellow+red areas+white points identify the ROIs sampled for the calibration of the second year (2015, n=48).

A black and a white tile were positioned in each plots and used for the radiometric calibration of the plots by normalizing each pixel intensity of each channel by the value of the white reference, after subtracting the black reference.

Using MATLAB (MathWorks, Natick, MA), two vegetation indices were calculated for each sampled plot: the Blue Normalized Difference Vegetation Index (BNDVI= (NIR – B)/(NIR + B)) and the Green Normalized Difference Vegetation Index (GNDVI= (NIR – G)/(NIR + G)). Then, the canopy fraction cover (fraction cover=number of vegetation pixels/total number of pixels) was calculated following two different segmentation strategies: the canopy fraction cover was estimated applying image segmentation using the Otsu algorithm (Otsu, 1975) to obtain image masking based on i) the BNDVI (Fc_{BNDVI}); ii) the GNDVI (Fc_{GNDVI}). Finally, two new vegetation indices ($BNDVI_{veg}$ and $GNDVI_{veg}$, respectively) were proposed joining the spectral information (classical vegetation indices, BNDVI and GNDVI) with the information about the canopy fraction cover. We obtained the vegetation indices of the fraction cover following the equation:

$$VI_{veg} = \frac{\sum_{i=1}^{n} VI_{masked\ (i)}}{N_p}$$

where VI_{masked} is the value of the vegetation index of the pixels of vegetation only, N_p is the total number of pixels of the image.

2.3 Statistical analysis

Simple linear regression models were built to estimate above ground biomass (g D.M. m^{-2}), nitrogen concentration (Nc, g N 100 g $D.M.^{-1}$) and nitrogen uptake (Nu, g N m^{-2}) from the six predictors: BNDVI and GNDVI of the plots, the fraction cover calculated from BNDVI and from GNDVI, BNDVI and GNDVI of the vegetation fraction. The determination

coefficient (R^2) and the relative root mean squared error (rRMSE) were calculated according to the following equations:

$$R^2 = 1 \quad \frac{\sum_{i=1}^{n}(\hat{y}_i \quad y_i)^2}{\sum_{i=1}^{n}(y_i \quad \bar{y})^2}$$

$$rRMSE = \frac{\sqrt{\frac{\sum_{i=1}^{n}(\hat{y}_i \quad y_i)^2}{n}}}{\bar{y}} x100$$

Where $\hat{y}_i$ are the estimated values, y_i are the measured values, n is the number of observations and $\bar{y}$ is the mean value of the experimental data.

3 RESULTS AND DISCUSSION

Table 1 summarizes the variability showed by the measured variables in the two phenological stages of the two years of experimentation.

Table 1. Statistics of the reference variables (AGB, Nc and Nu) measured in the maize field at the different sampling dates.

Statistic[a]	2014						2015					
	V6[b]			V9			V6			V9		
	AGB[c] (g/m^2)	Nc (%DM)	Nu (g/m^2)	AGB[c] (g/m^2)	Nc (%DM)	Nu (g/m^2)	AGB[c] (g/m^2)	Nc (%DM)	Nu (g/m^2)	AGB[c] (g/m^2)	Nc (%DM)	Nu (g/m^2)
Mean	48	3.5	1.7	244	2.4	5.9	42	3.6	2.6	121	1.5	3.3
Std Dev	8	0.30	0.3	35	0.3	1.3	8	0.3	0.4	57	0.4	1.8
Min	35	2.8	1.1	171	1.7	2.9	26	3.0	2.0	12	0.9	0.4
Max	70	3.9	2.6	320	2.9	7.9	61	4.1	3.5	297	2.2	9.4
CV (%)	17	9	20	14	13	21	19	7	14	47	23	56

[a]Std Dev, standard deviation; Min, minimum; Max, maximum; CV, coefficient of variation (%).
[b]V6 and V9 maize phenological stages according to Ritchie et al., (1998).
[c]AGB, above ground biomass; Nc, plant N concentration; Nu, plant N uptake.

As a general observation, the average data measured at V6 and V9 on the year 2015 showed percent reduction in accumulation of -10% and -50% compared to 2014, of both AGB and Nu, if compared to correspondent variables measured in the year 2014.

This happened because the year 2015 was characterized by no application of organic fertilization in order to study, as aim of the original experiment, the residual effects of the different fertilizers nitrogen. However, thanks to the introduction of the extra blocks of mineral fertilizers treatments, a very high range of variability in maize canopies was recorded, reflecting a high variation in AGB and, consequently, Nu (figure 2a).

Distributions of the two vegetation indices calculated from data collected by the modified digital camera are shown in Figures 2a and 2b.

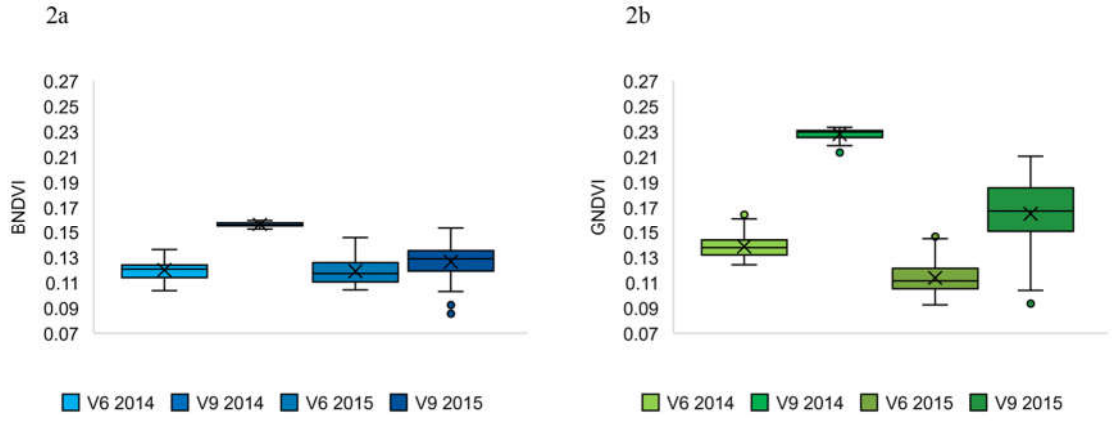

Figure 2. – Box and whiskers plots indicating the distributions of BNDVI (2a) and GNDVI (2b) at the sampling dates of both the years.

Distributions of BNDVI (Figure 2a) were characterized by lower values than those of GNDVI (Figure 2b) and also by less variation. Both the indices showed increasing values from V6 to V9 stage, according to the observed increase of AGB. However, BNDVI recorded a less variation between the two phenological stages in both the years, revealing a possible saturation of the blue channel at higher biomass levels. Saturation might have also affected the green band at V9 in the year 2014, when GNDVI had a very short range of variation (0.02).

The similar statistics of the two indices, and their reduced range of variability, provided unsatisfactory estimates of maize nitrogen-related variables at V9 in 2014: the coefficients of determination of linear regression models were less than 0.4 and 0.3 for the estimation of AGB and Nu, respectively. Moreover, both indices regressed poorly with plant-nitrogen concentration in both years and phenological stages (data not shown), with best performance achieved with GNDVI at V9 in 2014 (R^2 of 0.43). This result was expected because the ability of the vegetation indices derived by optical sensors (like those used in this study) to assess vegetation biomass relies on the strong relationship existing between vegetation indices and the canopy fraction cover related to AGB (Hunt et al., 2010; Li et al., 2010).

Therefore, vegetation indices can only indirectly estimate factors affecting biomass production (*e.g.,* nitrogen availability). Thus, the lack of a strong biochemical relationship between the broad bands collected with the modified consumer digital camera and plant-N concentration and the reduced variation range of Nc resulted in poor regressions between the calculated indices and plant-N concentration. Table 2 summarizes the performances in calibration of the linear regression models built in this work.

In order to isolate the signal coming from plants from those of soil and shadows, segmentation processes were proposed (Kim et al., 2008; Pauly, 2014). Given the high resolution of the collected images (1.5 cm per pixel), a segmentation procedure was applied and the fraction cover (fraction of ground cover by vegetation) was calculated and regressed with the AGB. The BNDVI resulted in a better separation between soil and vegetation compared to GNDVI. Conversely, GNDVI led to a wrong estimation of the fraction cover in both years because it did not satisfactory discriminate shadows from leaves as showed in Figure 3.

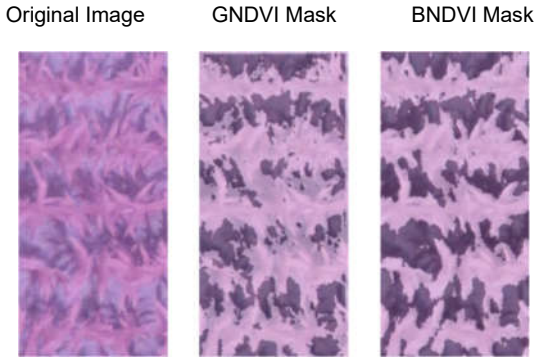

Figure 3. – From the left to the right are reported the original image showing maize leaves, soil under the sunlight (bright gray areas) and shadowed soil, the vegetation masks built using GNDVI and BNDVI. The darker part of the masks identifies soil pixels, the original image is seen in transparency.

Table 2. Calibration performances in terms of R^2 and rRMSE of the calculated linear regression models: two years (2014 and 2015) x two development stages (V6 and V9) x 3 estimated variables (AGB, Nc and Nu) x six predictors (BNDVI, GNDVI, Fc_{BNDVI}, Fc_{GNDVI}, $BNDVI_{veg}$, $GNDVI_{veg}$). The determination coefficients are in different colors, based on the following scale: R^2<0.3=dark red, 0.31-0.5=red, 0.51-0.6=orange, 0.61-0.8=green, R^2>0.81=dark green. The relative root mean squared errors are reported for R^2>0.55.

Year	Development stage	Estimated variable	Statistics	BNDVI	GNDVI	Fc_{BNDVI}	Fc_{GNDVI}	$BNDVI_{veg}$	$GNDVI_{veg}$
2014	*V6*	*AGB*	R^2	**0.37****	**0.57****	**0.57****	**0.30****	**0.56****	**0.57****
			rRMSE	-	11%	11%	-	11%	11%
		Nc	R^2	ns	ns	ns	ns	ns	ns
			rRMSE	-	-	-	-	-	-
		Nu	R^2	**0.25***	**0.4****	**0.17***	**0.35****	**0.37****	**0.39****
			rRMSE	-	-	-	-	-	-
	V9	*AGB*	R^2	ns	**0.27****	**0.50****	**0.27****	**0.52****	**0.44****
			rRMSE	-	-	-	-	-	-
		Nc	R^2	**0.26***	**0.43****	**0.35****	ns	ns	**0.41****
			rRMSE	-	-	-	-	-	-
		Nu	R^2	ns	**0.43****	**0.56****	**0.17***	**0.4****	**0.55****
			rRMSE	-	-	14%	-	-	14%
2015	*V6*	*AGB*	R^2	**0.23****	**0.34****	**0.33****	**0.24****	**0.38****	**0.41****
			rRMSE	-	-	-	-	-	-
		Nc	R^2	ns	ns	ns	ns	ns	**<0.1***
			rRMSE	-	-	-	-	-	-
		Nu	R^2	**0.17****	**0.29****	**0.26****	**0.18****	**0.32****	**0.36****
			rRMSE	-	-	-	-	-	-
	V9	*AGB*	R^2	**0.58****	**0.68****	**0.73****	**0.52****	**0.72****	**0.74****
			rRMSE	30%	24%	24%	-	25%	27%
		Nc	R^2	ns	ns	ns	ns	ns	ns
			rRMSE	-	-	-	-	-	-
		Nu	R^2	**0.41****	**0.53****	**0.60****	**0.41****	**0.57****	**0.61****
			rRMSE	-	-	35%	-	37%	36%
2014+2015	*V9*	*AGB*	R^2	**0.75****	**0.82****	**0.87****	**<0.1***	**0.86****	**0.87****
			rRMSE	24%	20%	17%	-	18%	17%
		Nc	R^2	**<0.1***	ns	ns	**<0.1***	ns	ns
			rRMSE	-	-	-	-	-	-
		Nu	R^2	**0.56****	**0.66****	**0.71****	ns	**0.67****	**0.71****
			rRMSE	33%	29%	27%	-	29%	27%

* p<0.05
** p<0.01
ns= non-significant

The correlation between the Fc_{BNDVI} and AGB was the most satisfactory at less at V9, R^2 ranged between 0.30 (at V9) and 0.51 (at V6) in the year 2014 and between 0.33 (at V6) to 0.73 (at V9) in the year 2015.

Due to the better segmentation results gained using the BNDVI, the "GNDVI of the vegetation fraction" ($GNDVI_{veg}$) was re-calculated using the vegetation mask based on the BNDVI values and it resulted in very similar performances of Fc_{BNDVI} for the estimation of both, AGB and Nu, in all the stages of both the years. This finding supports the underlying principle on which imaging sensors basically acquire information about the canopy fraction cover: as canopy fraction cover increases, the portion of vegetation pixels increases until canopy closure. When sensor spatial resolution increases, the correlation between the estimated fraction cover and AGB becomes stronger because soil signal could be successfully separated from the signal coming from the vegetation (Hunt et al., 2010). Thus, in the time window from emergence to canopy closure, very high spatial resolution imagery could play a role in the assessment of AGB variability even if the sensors are characterized by low spectral and radiometric resolutions. This is the case of the consumer digital cameras characterized by very high spectral resolution (12-18 MP) in comparison to professional multispectral cameras (1.2-3.2 MP), as showed in Figure 4a and 4b, indeed the Fc_{BNDVI} resulted the best estimator thus, only its results will be discussed.

4a 4b

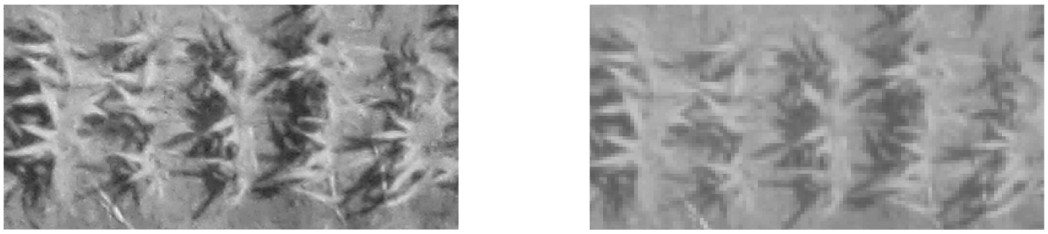

Figure 4. – Detail of an aerial image of maize plants (V9-2015) as in the original NIR channel (12 MP) of the modified Canon camera (4a) and the same detail simulated at low spatial resolution (1.2 MP; 4b).

The AGB estimation by Fc_{BNDVI} was less satisfactory at V6 than V9 in both the years of experimentation: R^2 =0.57 and rRMSE=11% in the year 2014, R^2 =0.33 and rRMSE=24% in the year 2015. Linear regression models, built to estimate Nu from Fc_{BNDVI}, also gave poor performances (R^2<0.44) at V6 in both the years. These results were probably caused by a low AGB and thus low spectral response of the canopy at this stage. In fact, higher regression performance was reached at V6 in the year 2014 in presence of higher AGB production.

The Fc_{BNDVI} showed the strongest correlations to AGB and pant-N uptake at V9 in 2015 (Figure 5).

In fact, AGB and the Nu were estimated with R^2 of linear regression of 0.75 and 0.63 and with rRMSE of 24% and 36%, respectively. These are very positive results but their use seems to be limited to a specific phenological stage (V9).

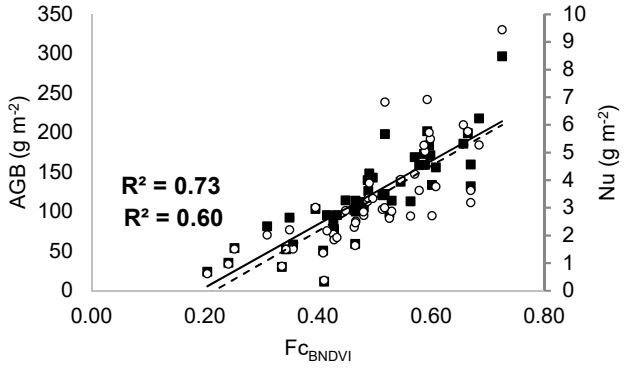

Figure 5. – Linear regression model between Fc_{BNDVI} and AGB (black squares) and between Fc_{BNDVI} and plant-N uptake (white dots). Both the models refer to maize at phenological stage V9 in the year 2015.

These stage-specific calibration models limit their use on maize at different phenological stages, it can be noted also by the variation of the slope of the models built at V6 and V9 in both the years (Table 3).

Table 3. Slope and intercept of the linear regression models for the estimation of the above ground biomass based on Fc_{BNDVI} and $GNDVI_{veg}$.

Year	**2014**				**2015**				**2014+2015**	
Development stage	**V6**		**V9**		**V6**		**V9**		**V9**	
Statistics	*Intercept*	*Slope*	*Intercept*	*Slope*	*Intercept*	*Slope*	*Intercept*	*Slope*	*Intercept*	*Slope*
$BNDVI_{fc}$	-9.8	138.9	-204.9	561.7	21.1	89.4	-61.8	370.5	-70.7	390.8
$GNDVI_{veg}$	4.1	598.3	-60.2	1728.3	25.2	455.7	-17.5	1436.6	-20.2	1496.9

Further studies must be done exploring the correlations between optical data and crop measured variables at each stage of the whole time window considered useful for fertilization applications.

Considering that the best performances in the estimation of AGB and Nu were obtained at the V9 stage, an attempt to build a unique regression equation suitable for the estimation of AGB and Nu at V9 in the two years of the experiment was done (Figure 6). As expected,

AGB was better estimated by Fc_{BNDVI} with a rRMSE of 17%. Improvement in the estimation of Nu was also obtained (R^2 =0.71). However, AGB remained the only variable that could be satisfactory predicted (R^2>0.8). Thus, it is the only to be used to drive an in-field application to support fertilization plans.

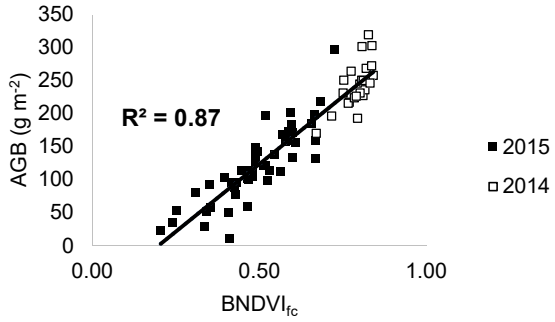

Figure 6. Linear regression model between Fc_{BNDVI} and AGB of maize at phenological stage V9 in both years

Estimating AGB with good performances represented a valuable result because of the strong correlation found between AGB production and nitrogen uptake (r=0.95) that can be used, in turn, to derive maize nitrogen status and its requirements.

4 CONCLUSION

A modified consumer digital camera mounted on a UAV surveyed an experimental maize field for two years, at V6 and V9 phenological stages (a time window useful for fertilizer application) in order to estimate nitrogen-related maize variables. Maize above ground biomass and nitrogen uptake were estimated from the average BNDVI and GNDVI of the plots and from the average $BNDVI_{veg}$ and $GNDVI_{veg}$ of the vegetation cover. Fraction cover was also estimated and regressed against the above ground biomass and it was found that BNDVI was the best estimator of the fraction cover that was positively and well correlated with the AGB. Very good performances in AGB and Nu estimation were found only at the V9 stage of the 2015, when a larger range of variation in the measured variables was explored. Moreover, the regression equation built using the data recorded at V9 in the two years of experiment gave encouraging results: Fc_{BNDVI} regressed against AGB with R^2=0.87 and rRMSE of 17%. The calibration procedures carried out in this work are stage-specific and this represents a limit in the application of the regression equations at different development stages of the time window V6-V9, suitable for side-dress fertilization.

Finally, the low cost imaging system, even with the limitations due to a low dynamic range and JPEG compression (that could cause channels overlap and saturation also at early development stages), led to very good performance in AGB estimation. This was possible thanks to the very high spatial resolution of the imaging sensor that allowed a reliable estimation of AGB through the assessment of the canopy fraction cover. Then, AGB may be used to assess maize nitrogen status, thanks to the correlation between AGB and Nu, when data, from more than one year, are available for index calibration.

5 REFERENCES

Berni, J.A.J., Zarco-Tejada, P.J., Suárez, L., González-Dugo, V., Fereres, E., 2009. Remote sensing of vegetation from UAV platforms using lightweight multispectral and thermal imaging sensors. Int. Arch. Photogramm. Remote Sens. Spatial Inform. Sci 38, 6.

Cavalli, D., Cabassi, G., Borrelli, L., Geromel, G., Bechini, L., Degano, L., Marino, P., 2016. Nitrogen fertilizer replacement value of undigested liquid cattlemanure and digestates. European Journal of Agronomy 73, 34–41.

Geipel, J., Link, J., Wirwahn, J.A., Claupein, W., 2016. A Programmable Aerial Multispectral Camera System for In-Season Crop Biomass and Nitrogen Content Estimation. Agriculture 6, 4. doi:10.3390/agriculture6010004

Huang, Y., Thomson, S.J., Lan, Y., Maas, S.J., 2010. Multispectral imaging systems for airborne remote sensing to support agricultural production management. International Journal of Agricultural & Biological Engineering 3.

Hunt, E.R., Hively, W.D., Fujikawa, S.J., Linden, D.S., Daughtry, C.S., McCarty, G.W., 2010. Acquisition of NIR-green-blue digital photographs from unmanned aircraft for crop monitoring. Remote Sensing 2, 290–305.

Kim, Y., Reid, J.F., Zhang, Q., 2008. Fuzzy logic control of a multispectral imaging sensor for in-field plant sensing. Computers and electronics in agriculture 60, 279–288.

Lebourgeois, V., Bégué, A., Labbé, S., Houlès, M., Martiné, J.F., 2012. A light-weight multi-spectral aerial imaging system for nitrogen crop monitoring. Precision agriculture 13, 525–541.

Lebourgeois, V., Bégué, A., Labbé, S., Mallavan, B., Prévot, L., Roux, B., 2008. Can commercial digital cameras be used as multispectral sensors? A crop monitoring test. Sensors 8, 7300–7322.

Lelong, C.C., Burger, P., Jubelin, G., Roux, B., Labbé, S., Baret, F., 2008. Assessment of unmanned aerial vehicles imagery for quantitative monitoring of wheat crop in small plots. Sensors 8, 3557–3585.

Noh, H., Zhang, Q., 2012. Shadow effect on multi-spectral image for detection of nitrogen deficiency in corn. Computers and Electronics in Agriculture 83, 52–57.

Noh, H., Zhang, Q., Han, S., Shin, B., Reum, D., 2005. Dynamic calibration and image segmentation methods for multispectral imaging crop nitrogen deficiency sensors. Transactions-American Society Of Agricultural Engineers 48, 393–401.

Osborne, S.L., Schepers, J.S., Schlemmer, M.R., 2004. Using multi-spectral imagery to evaluate corn grown under nitrogen and drought stressed conditions. Journal of Plant Nutrition 27, 1917–1929. doi:10.1081/LPLA-200030042

Otsu, N., 1975. A threshold selection method from gray-level histograms. Automatica 11, 23–27.

Pauly, K., 2014. Applying conventional vegetation vigor indices to UAS-derived orthomosaics: issues and considerations. Proceedings of the 12th International Conference for Precision Agriculture. July 2014, Sacramento, California, USA.

Reyniers, M., Vrindts, E., 2006. Measuring wheat nitrogen status from space and ground-based platform. International Journal of Remote Sensing 27, 549–567. doi:10.1080/01431160500117907

Rorie, R.L., Purcell, L.C., Karcher, D.E., King, C.A., 2011a. The Assessment of Leaf Nitrogen in Corn from Digital Images. Crop Sci. 51, 2174–2180. doi:10.2135/cropsci2010.12.0699

Rorie, R.L., Purcell, L.C., Mozaffari, M., Karcher, D.E., King, C.A., Marsh, M.C., Longer, D.E., 2011b. Association of "Greenness" in Corn with Yield and Leaf Nitrogen Concentration. Agronomy Journal 103, 529. doi:10.2134/agronj2010.0296

Swain, K.C., Jayasuriya, H.P.W., Salokhe, V.M., 2007. Low-altitude remote sensing with unmanned radio-controlled helicopter platforms: A potential substitution to satellite-based systems for precision agriculture adoption under farming conditions in developing countries.

Tomer, M.D., Anderson, J.L., Lamb, J.A., 1997. Assessing corn yield and nitrogen uptake variability with digitized aerial infrared photographs. Photogrammetric engineering and remote sensing 63, 299–307.

Sakamoto, T., Gitelson, A.A., Nguy-Robertson, A.L., Arkebauer, T.J., Wardlow, B.D., Suyker, A.E., Verma, S.B., Shibayama, M., 2012a. An alternative method using digital cameras for continuous monitoring of crop status. Agricultural and Forest Meteorology 154, 113–126.

Sakamoto, T., Gitelson, A.A., Wardlow, B.D., Arkebauer, T.J., Verma, S.B., Suyker, A.E., Shibayama, M., 2012b. Application of day and night digital photographs for estimating maize biophysical characteristics. Precision Agric 13, 285–301. doi:10.1007/s11119-011-9246-1

Wójtowicz, M., Wójtowicz, A., Piekarczyk, J., 2016. Application of remote sensing methods in agriculture. Communications in Biometry and Crop Science 11, 31–50.

CHAPTER 4

4. COMPARISON OF SIGNALS COMING FROM A MODIFIED DIGITAL CAMERA AND A PROFESSIONAL MULTISPECTRAL CAMERA FOR IN-FIELD AIRBORNE APPLICATIONS

ABSTRACT

The innovative use of unmanned aerial vehicles (UAVs) in agriculture has opened a great interest in the use of digital cameras to monitor vegetation. Digital cameras can be consumer digital cameras (three visible channels) or multichannel professional cameras (more than three channels in the visible and near-infrared regions of the spectrum). In the first case digital cameras have to be modified to acquire reflectance in the near-infrared channels. Self-modified or not, details about wavelengths acquired after the modification are not known. The presented work was thought to provide quantitative information about the differences between signals acquired by a consumer modified- digital camera (Canon® Powershot SX260 HS by Canon Inc., Tokyo, Japan), and processed by the user through a stand-alone orthomosaicking program, and signals acquired by a professional multispectral camera (MicaSense RedEdge™ by MicaSense, Inc., Seattle, WA, USA), treated by a processing service offered by the camera producer, in order to understand the feasibility of the use of the studied devices for practical in-field applications also taking into account the costs of the technologies.

Firstly, the modified camera spectral sensitivity was measured in the laboratory and it was found out that the signal is not acquired in pure bands. Then, from the comparison of signals coming from a field survey made with both the cameras, the signal of the modified camera

resulted characterized by a short dynamic range and by correlated signals between the visible bands and the NIR band. These findings led to the conclusion that this modified camera should be used for quantitative analysis only in presence of high within-field variability (so differences in vegetation spectral responses could be acquired by this camera) and not saturating conditions. The professional digital camera gave the most reliable results.

1 INTRODUCTION

The innovative use of unmanned aerial vehicles (UAVs) in agriculture has opened new possibilities for crop monitoring. Digital cameras mounted on UAVs are devices of increasing interest in precision agriculture because of their flexibility and the possibility to map between-field and within-field crop variability with high spatial and temporal resolution. Digital cameras usually employed in crop imaging are multispectral cameras, with dedicated optics and detectors for specific bands, both in the visible (blue, green and red) and near infrared spectral regions (red-edge and near-infrared).

Alternatively, consumer digital cameras, properly modified to acquire reflectance in the near-infrared (NIR) region of the spectrum, are widespread used for aerial imaging of vegetation because are cheaper if compared to more complex multispectral cameras. However, details about wavelengths acquired by modified consumer digital cameras are not known *a priori* (Berra et al., 2015). Moreover, filters applied do not guarantee a pure signal per band (Pauly, 2014) and the registered output is usually a broad-band signal of three bands. Due to the uncertainty in camera specifications of the modified commercial digital cameras, some professional digital cameras for agricultural applications have been commercialized and they are characterized by acquiring narrow-band signals (from ±10 to ±40 nm of full width at half maximum) in more than three channels in the visible and NIR region of the spectrum. Both the types of digital cameras are widely used and some studies were carried out identifying some issues concerning their practical applications for vegetation monitoring: digital cameras are passive sensors and thus they are affected any changing in environmental light conditions; characterization of their spectral sensor is often lacking (Pauly, 2014). Some solutions to the issues arisen were then found focusing on the best way to apply radiometric correction to mitigate the distortions linked to camera optics

and environmental light conditions (Lebourgeois et al., 2008). Such techniques comprise irradiance sensors mounted on UAVs; white calibration panels (Pauly, 2014); acquiring images in the native camera format (RAW), in order to avoid effects of JPEG compression; and proposing a workflow for the processing of the RAW images data (Verhoeven, 2010). These solutions find some difficulties to be applied by farmers and agronomists because of a lack of knowledge in remote sensing techniques or because the proposed methods were expensive, difficult to apply and time-consuming. For this reason, professional digital cameras are usually sold together with an images processing service that provides image correction and orthomosaic composition. For example, the ATLAS service by MicaSense (MicaSense, Inc., Seattle, WA, USA) takes one day to deliver the processed orthomosaic, the digital elevation model of the surveyed area, and maps of different vegetation indices at a relatively low cost (0.60 USD per acre). Alternatively, to these support services, image stitching and orthomosaicking software (*e.g.,* Pix4Dmapper, Pix4D SA, Lausanne, Switzerland; Agisoft Photoscan, Agisoft LLC, St. Petersburg, Russia) could be used to process aerial images acquired by both multispectral and modified cameras. Such software allows generating good quality orthomosaics with rapid processing time (Wulfsohn and Lagos, 2014) when the effects of angular variation in reflectance, stitching and ambient light fluctuations are taken into account (Rasmussen et al., 2016).

Given the issues presented above, it seems mandatory to improve our knowledge for practical use of modified consumer digital cameras in crop monitoring, on sensors characterization and image processing. To this end, the objective was to provide quantitative information about the differences between signals acquired by a consumer modified- digital camera, and processed by the user through a stand-alone orthomosaicking program, and signals acquired by a professional multispectral camera, treated by a processing service

offered by the camera producer, in order to understand the feasibility of the use of the studied devices for practical in-field applications also taking into account the costs of the technologies.

2 MATHERIALS AND METHODS

The experiment started in autumn 2015 on a field located in Sant'Angelo Lodigiano (Lodi), Italy (45°14'20"40 N, 09°24'34"92 E, altitude 73 m asl) cultivated with barley (*Hordeum vulgare* L.). The field had a surface of 10 hectares and has been selected due to its great variability in above ground biomass. Barley was sown on 10 October 2015 and it was surveyed with a UAV carrying two different digital cameras, in March 17 and 18, immediately before crop fertilization. At those dates, plants were at the development stage of 25 according to the BBCH scale (Witzenberger et al., 1989 and Lancashire et al., 1991). The UAV (Figure 1) was a coaxial octocopter in carbon fiber, a maximum take-off mass of 12kg and equipped with a GNSS (Global Navigation Satellite System) NEO-M8N (u-blox, Thalwil, Switzerland) and a gimbal platform.

Figure 1. – Picture of the UAV used.

2.1 Digital cameras

Two different cameras were used to acquire multispectral images of the barley field. The first was a commercial digital camera Canon® Powershot SX260 HS (Canon $_{BNDVI}$Inc., Tokyo, Japan) and the second was a MicaSense RedEdge™ (MicaSense, Inc., Seattle, WA, USA) specifically commercialized for agricultural applications (five bands camera: blue, green, red, red-edge and near-infrared).

The Canon Powershot was modified to acquire light in the visible and near-infrared (VIS-NIR) in three channels (blue (B), green (G) and NIR). Modifications consisted in removing the infrared-blocking filter and in the addition of a Super Blue IR filter that blocked the red light and enabled the original red channel to capture the infrared light. Spectral sensitivity of the camera was measured in the laboratory using a dispersive monochromator applied to a Xenon lamp in order to record single waveband measurements for the range 400-800 nm, every 10 nm (Figure 2).

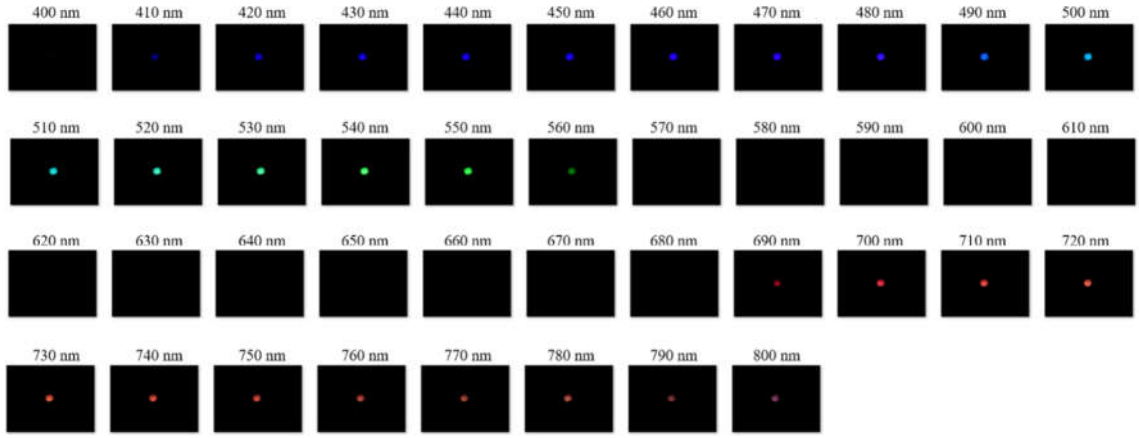

Figure 2. – JPEG images of each monochromatic waveband (from 400 to 800 nm) as recorded by the modified Canon.

Images were acquired in a dark room, at a distance of 7 cm from the light source, with the camera sensor perpendicular to the monochromatic ray. The camera was manually set up to eliminate saturated values in any band with the following settings: focus, 8.0, exposure time 1/60 s and sensitivity ISO100. The images were recorded in the JPEG format.

Finally, the average digital number for each channel of the camera recorded at each studied wavelength was calculated and normalized in a range of values from 0 to 1. The resulting graphic, presented in Figure 3, shows each channel sensitivity. The channel sensitivity of the

Micasense RedEdge was provided by the producer and it was also included in Figure 3 as a comparison.

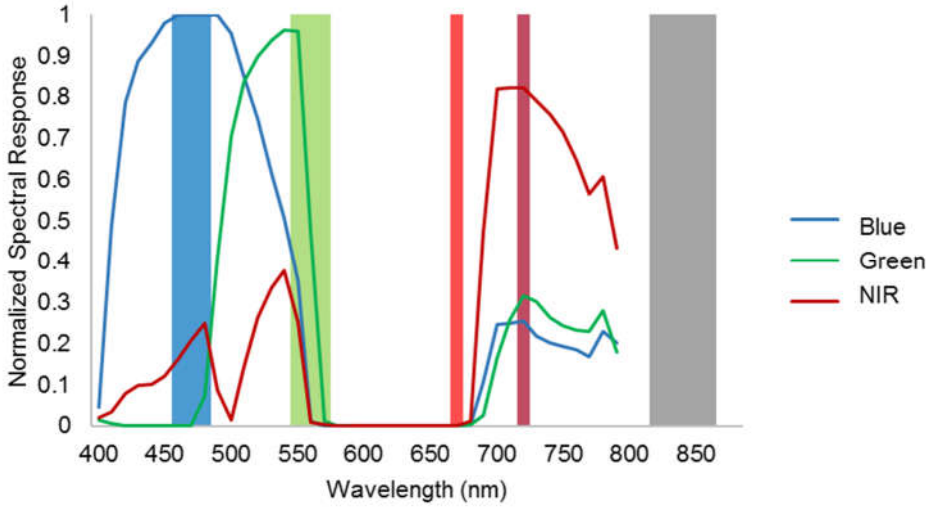

Figure 3. – Comparison between the spectral response of the modified Canon and of the five channels of the MicaSense RedEdge, represented as overlaying blocks of blue, green, red, red-edge and NIR, respectively.

2.2 Data acquisition

The Canon Powershot acquired images of the field at March 17, while the MicaSense at March 18. Both cameras were mounted on board the UAV on a gimbal platform and they were pointed in the same direction, in horizontal mode (landscape orientation). The UAV had a flight speed of 10 m/s at an altitude of 100 m, enabling to have 75% forward and sideward overlaps. Images were acquired in autofocus mode under clear sky conditions between 11:00 and 13:00 a.m. solar time. The ground resolution of the images was 4.3 and 6 cm per pixel for the Canon Powershot and MicaSense RedEdge, respectively.

2.1 Image processing

The modified Canon PowerShot was set to store 12.1 MP 3-band 8-bit per band JPEG files. The orthomosaic of the field was obtained using the software Pix4Dmapper (Pix4D SA, Lausanne, Switzerland), and five ground control points were used to assure the correct georeferencing and geometric calibration. Images of a reference white panel (the MicaSense white calibration panel) were acquired before the UAV flight with the Canon Powershot. They were used for radiometric calibration of field images: the intensity of each channel was normalized according to the corresponding average value measured in the reference panel. This procedure applied to all pixels of the images of the field. Geometric adjustments and georeferencing was carried out using five ground control points.

The MicaSense RedEdge stored 1.2 MP 12-bit uncompressed TIFF image files for each of the five channels. The white reference panel was acquired before and after the flight by the MicaSense RedEdge. All the images collected during the flight (included the images of the white reference panel) were uploaded to the MicaSense Atlas cloud, a processing service that provided all the pre-processing activities and produced the final orthomosaic: a 5-band 16-bit image containing the reflectance values expressed as digital numbers properly scaled. The pixel alignment between the two orthomosaics obtained with the two cameras was guaranteed by reprojecting, in the QGIS environment, the Atlas orthomosaic using the same ground control points used for the orthomosaic of the modified Canon PowerShot images.

Starting from the two orthomosaics, the region of the entire field was identified and then it was divided into a regular grid of 2 m tiles by using QGIS. The average intensity values of the three channels common to both cameras (B, G and NIR) were recorded for each tile of the grid. Thereafter, frequency and cumulative frequency distributions of the intensities of

the pixels were calculated, separately for each channel, and discussed. Finally, the GNDVI maps were calculated from the signals of two cameras and compared.

$$GNDVI = \frac{(NIR \quad GREEN)}{(NIR + GREEN)}$$

3 RESULTS AND DISCUSSION

A comparison of the frequency distribution curves of the two cameras are presented in figure 4a and 4b.

The absolute distribution curves (figure 4a) showed similar amplitude and positive skewness values, ranging from 1.9 to 2.3. However, the MicaSense acquired a range of intensities lower than the modified Canon PowerShot in all the channels (figure 4a and 4b).

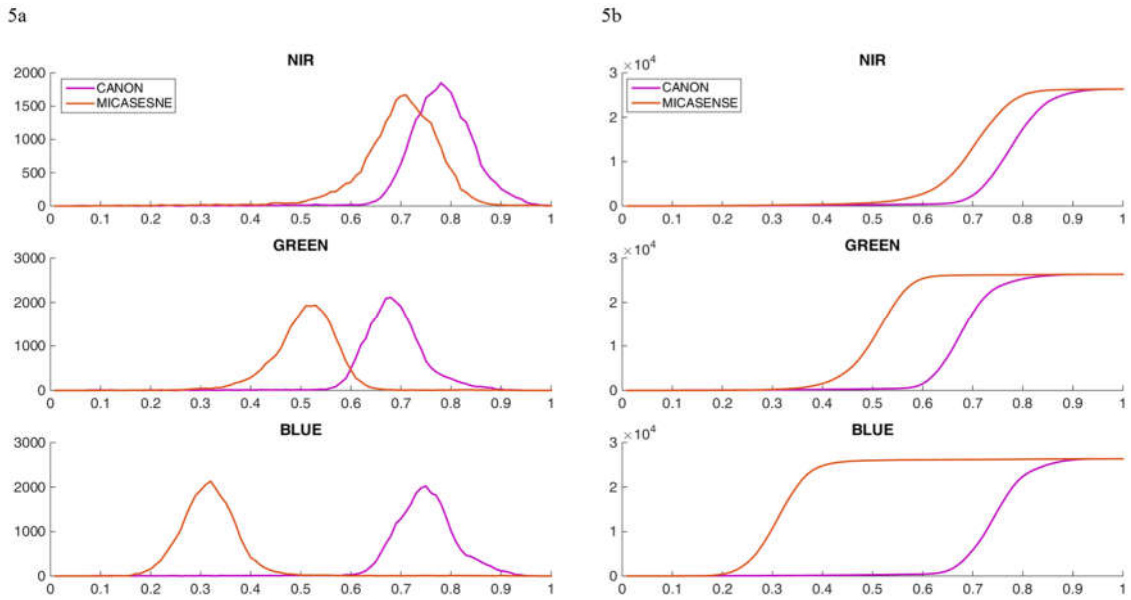

Figure 4. – The absolute (4a) and cumulative (4b) frequency distribution curves of the pixels of the two tested cameras for the three corresponding channels. The intensity values are normalized by the maximum reached by each camera in order to calculate the frequencies in the same number of classes (100 bin from 0 to 1).

This means that the signals of the Canon PowerShot saturate earlier than the signal recorded by the MicaSense. Moreover, a greater difference in channel intensity between the two cameras was observed in the visible channels (in particular in the blue one) than in the NIR channel. The saturation occurred using the Canon PowerShot is also visible at single pixel level, considering the pixels that recorded the highest intensity values (figure 5). These

saturating pixels are more present in the NIR channel and in the B channel of the modified Canon PowerShot than in the G channel of the same camera, in agreement with the lower intensity values recorded in the G channel (figure 4a and 4b).

The NIR channel is the most saturating one also in the MicaSense camera, while the visible channels recorded lower intensity values.

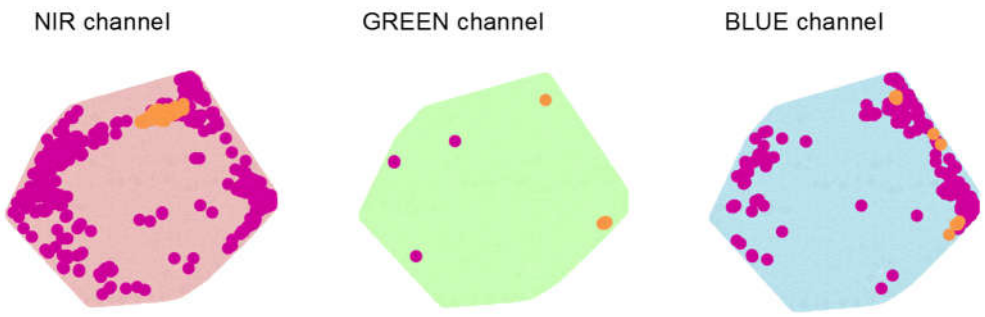

Figure 5. – The map of the barley field split into the three channels showing the highest intensity values recorded by the two tested cameras (pink dots identify the modified Canon PowerShot and the orange dots identify the MicaSense).

Finally, the effects of the modification of the Canon PowerShot caused a very high correlation between the visible bands and the NIR channel (figure 6) due to the fact that the visible channels also record some NIR light and *vice versa*, it was also observed by Pauly (2016).

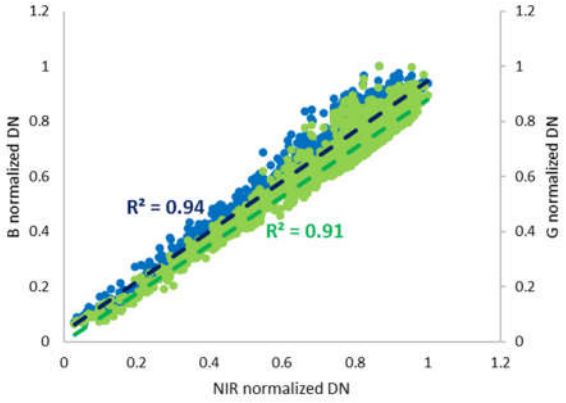

Figure 6. – Scatterplot of the NIR band versus the B the G band. Linear regression determination coefficients were calculated.

This behavior, together with the short dynamic range, intended as the ratio between the maximum and minimum measurable light intensities, of the modified Canon, affected the calculation of the vegetation indices. In figure 7 are presented the maps of the Green Normalized Difference Vegetation Index (GNDVI=(NIR-G)/(NIR+G)) calculated from the two cameras. The map of the differences between the GNDVI calculated from both the camera was also produced.

The GNDVI map built from the modified Canon PowerShot signal showed lower values of the index, in some cases negative values, than the MicaSense-based GNDVI map moreover, no correlation was found between the two indices (figure 7).

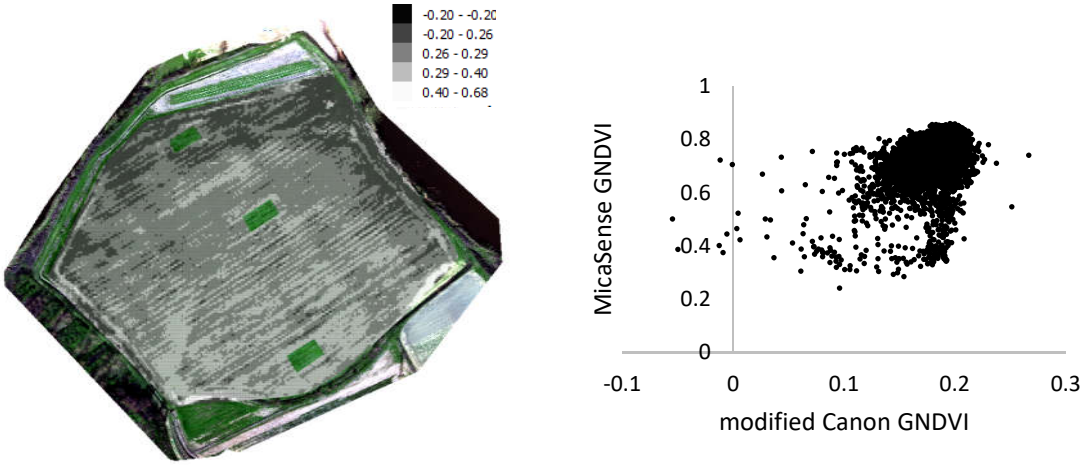

Figure 7. – Ratio of the GNDVI measured with the Canon by the GNDVI measured with the Micasense. The scatterplot shows the relationship between the two vegetation indices.

The lower range of variation of the modified Canon GNDVI resulted in a more uniform map that did not explain the total in-field variability. This result, due to the saturation of the camera channels and to the limited dynamic range of the JPEG files can represent a problem when mapping the vegetation at later development stages when the soil effects on reflectance will be negligible and the vegetation will be darker. These findings suggest that the MicaSense RedEdge camera could be used during the whole season, even at higher development stages when the crop is characterized by canopy closure and by a dark green color. On the contrary, slightly better performances could be gained using the modified Canon images in RAW format (Pauly, 2016). In this case, more storage memory and more complex and time-consuming image processing would be required (Verhoeven, 2010).

These findings should be interpret also taking into account the costs of the devices. The modified Canon costed 260€ and the Infragram DIY Filter Pack (Public Lab Online Store), applied to modify the camera, costed 10$; Pix4D software needed for image processing could be rent for 260€/month but it needs a PC with minimum system requirements of CPU (Intel i5, i7 or Xeon) and of RAM ranging from 8 to 32 GB (it depends on the number of

images to be processed, thus on the surveyed area) whose total cost starts from 900€; finally, a calibration panel of known reflectance (60-1000€) is needed to standardize the acquired reflected radiation. The cost of the MicaSense Red-Edge is 5900$ (the cost is comprehensive of its white calibration panel), while the cost of the Atlas cloud processing service ranged between 50 to 250$/month (it depends on the dimensions of the surveyed area); finally, internet connection is required. Following both the image elaboration workflows, less than 24 hours are required to obtain the orthomosaics and maps of vegetation indices. This is particularly true when using the Atlas service whereas, only one orthomosaic at a time could be made using Pix4D (or similar) software if one PC is available. The modified-camera represents a very low-cost solution if compared to the professional multispectral camera however, the image processing workflows is more time-consuming and a higher knowledge about sensor and image processing software is required by the user. Furthermore, the sensor has some limitation due to the uncertainty about its spectral response after the modification applied. On the other hand, even if the professional camera requires less specific knowledge in image analysis, it is a very expensive and a study on its economical sustainability should be carried out in the future.

4 CONCLUSION

The professional digital camera was found to be a more reliable device to be used for vegetation monitoring due to its higher spectral (more recorded bands) and radiometric (more brightness level acquired) resolutions that would allow its use along the whole season. The modified digital Camera was characterized by a short dynamic range and by correlated signals between the visible bands and the NIR band. The acquisition of signals of not pure bands was also confirmed by the characterization of its spectral sensitivity. These findings led to the conclusion that this modified camera should be used for quantitative analysis only in presence of high within-field variability (so differences in vegetation spectral responses could be acquired by this camera) and not saturating conditions (lower amount of plant biomass). Moreover, every time a consumer digital camera is modified, its spectral sensitivity has to be measured (Pauly, 2014) in order to determine the reliability of its signals when used to support agronomic decisions. Finally, if this modified cameras have to be used, the processing of the RAW signals should be considered (Verhoeven, 2010).

5 REFERENCES

Berra, E., Gibson-Poole, S., MacArthur, A., Gaulton, R., Hamilton, A., 2015. Estimation of the spectral sensitivity functions of un-modified and modified commercial off-the-shelf digital cameras to enable their use as a multispectral imaging system for UAVs. The International Archives of Photogrammetry, Remote Sensing and Spatial Information Sciences 40, 207.

Lancashire, P.D.; H. Bleiholder; P. Langeluddecke; R. Stauss; T. van den Boom; E. Weber; A. Witzen-Berger, 1991. A uniform decimal code for growth stages of crops and weeds. Ann. Appl. Biol., 119 (3), 561–601. doi:10.1111/j.1744-7348.1991.tb04895.x.

Lebourgeois, V., Bégué, A., Labbé, S., Mallavan, B., Prévot, L., Roux, B., 2008. Can commercial digital cameras be used as multispectral sensors? A crop monitoring test. Sensors 8, 7300–7322.

Pauly, K., 2014. Applying conventional vegetation vigor indices to UAS-derived orthomosaics: issues and considerations. Proceedings of the 12th International Conference for Precision Agriculture. July 2014, Sacramento, California, USA.

Pauly, K., 2016. Towards Calibrated Vegetation Indices from UAS-derived Orthomosaics. Proceedings of the 13th International Conference on Precision Agriculture. July 31 – August 3, 2016, St. Louis, Missouri, USA.

Rasmussen, J., Ntakos, G., Nielsen, J., Svensgaard, J., Poulsen, R.N., Christensen, S., 2016. Are vegetation indices derived from consumer-grade cameras mounted on UAVs sufficiently reliable for assessing experimental plots? European Journal of Agronomy 74, 75–92. doi:10.1016/j.eja.2015.11.026

Verhoeven, G.J.J., 2010. It's all about the format – unleashing the power of RAW aerial photography. International Journal of Remote Sensing 31, 2009–2042. doi:10.1080/01431160902929271

Witzenberger, A.; H. Hack; T. van den Boom (1989). Erläuterungen zum BBCH-Dezimal-Code für die Entwicklungsstadien des Getreides - mit Abbildungen. Gesunde Pflanzen, 41, 384–388.

Wulfsohn, D., Lagos, I.Z., 2014. The use of a multirotor and high-resolution imaging for precision horticulture in Chile: an industry perspective, in: In Proceedings of the 12th International Conference on Precision Agriculture, Sacramento, CA.

CHAPTER 5

5. HOMOGENEOUS ZONES DEFINITION FOR NITROGEN MANAGEMENT IN WINTER WHEAT: APPLICATION OF A UAV-MOUNTED MULTISPECTRAL IMAGING SENSOR

ABSTRACT

Winter wheat is one of the most relevant crop in Europe and also it requires a large amount of nitrogen fertilizers. In this context it becomes decisive to adopt new techniques that would allow a more efficient use of fertilizers. A crucial role could be played by remote-sensing techniques including small unmanned aerial vehicles mounting light imaging sensors which could take information about crop status at high spatial and temporal resolution. This work studied the capability of a multispectral camera (the MicaSense RedEdge™ recording five channels: blue 475 nm, green 560 nm, red 668 nm, red-edge 717 nm, and near-infrared 840 nm), on board a UAV, to map the within-field variability for nitrogen fertilizers management aims. The experiment started on a wheat field (11.3 ha) on March 2016. The experimental design consisted in three randomized blocks with three nitrogen levels (0, 72, 144 kg N ha^{-1}) with three replications. The remainder of the field received 144 kg ha^{-1} of nitrogen. The experiment was replicated in three different areas of the field showing marked variability in soil properties and potential productivity. The field aerial surveys were carried out at three phenological stages suitable for nitrogen fertilizer applications: at 25, 31 and 45 BBCH stages with the aim to identify the best period to classify the field in homogenous zones for nitrogen management. Three “normalized difference” vegetation indices were calculated from the field aerial images (NDVI, GNDVI and NDRE). They were regressed against ground measurements of grain yield and above ground biomass, taken at the moment of the

flight (nitrogen concentration in plants and nitrogen uptake were also determined). The NDRE gave the best performances for the estimation of both grain yield (R^2 0.76-0.91) and above ground biomass (R^2 0.37-0.9) at all phenological stages. The GNDVI performed similarly to NDRE, whereas NDVI showed saturation dynamics. The most suitable period for crop monitoring was found to be at 31. At this stage, three areas of the field with similar aboveground biomass were identified, BBCH. Three homogenous zones of the field were identified based on the estimation error of above ground biomass estimation. We were able to identify the average biomass production and its nitrogen uptake for each zone, putting the basis for an accurate prescription map for fertilizer applications.

1 INTRODUCTION

Intensive agriculture adopted in recent decades has led to serious negative environmental consequences due to sub optimal management of the agronomic inputs like irrigation water, fertilizers and agrochemicals. In this context, precision farming was developed as a system based on a network of site-specific information about crop, soil, atmosphere, biotic and abiotic factors and designed to increase long-term site-specific and whole farm crop efficiency, productivity and profitability taking into account both, between-field and within-field variabilities retrieving and minimizing negative externalities (Taylor and Whelan, 2005). In this system, getting accurate information on crop status and crop variability is crucial to determine application times and site-specific amounts of agronomic inputs.

Site-specific management of nitrogen fertilizers, in particular, is still an open issue of precision agriculture. Nitrogen, in fact, plays a fundamental role in crop production and crop yield is greatly affected by nitrogen fertilization. However redundant use of nitrogen fertilizers leads to negative environmental impacts, such as water eutrophication and contamination, acid rain and nitrous oxide gas emissions in the atmosphere (Geipel et al., 2016).

Optical sensors are the most interesting sensors for precision agricultural. Among tools used to get site-specific information about soil and crop status and to guide nitrogen fertilization, remote sensing is the most suitable. In particular, imaging multispectral sensors are the most used.

Multispectral sensors collect from two to tens wavebands and they could be active or passive sensors, depending on their source of light. Both punctual and imaging sensors, those that record images, can be mounted on ground or aerial platforms (drones and satellites).

Winter wheat is one of the most important crop in Europe and it requires a large amount of nitrogen fertilizers. Due to economic and environmental impacts of N fertilization, numerous studies were carried out to test the reliability of optical sensors to support fertilization (Schmidhalter et al., 2003; Reyniers and Vrindts, 2005; Moges et al., 2006; Rodriguez et al, 2006; Zhu et al., 2006; Eitel et al., 2007; Li et al., 2009; Hunt et al, 2010; Erdle et al., 2011; Cao et al., 2014; Geipel et al, 2016). Applications of remote sensing to support nitrogen fertilization of winter wheat have been intensively studied because of both the economic importance and the high nitrogen demand of this crop. Variability of winter wheat fields has been mainly investigated using active multispectral sensors mounted on tractors. The workflow of the information from the signal of the sensor to the map showing variability of the measured vegetation index is characterized by the following steps:

a) Acquisition of spectral data. The tractor is driven through the field to detect the reflectance of the crop. A complete mapping of the field requires multiple trips over the field, due to sensor spatial resolution (tens of cm) (Price, K-State Extension and Research). No radiometric image correction is required if the tractor is equipped with active sensors. An N-rich strip, is often used to standardize the measurements taken into the field to avoid the effects of local conditions other than N, such as weather, soil fertility, hybrid, and crop management on crop status;
b) Vegetation indices are calculated and mapped

Tractor-mounted acquisition systems are the most used, they are already commercialized, and dedicated algorithms have been developed to retrieve nitrogen fertilizers rates. However, these systems often rely on punctual multispectral signal acquisitions and thus require interpolation techniques to build a map that continuously cover the investigation area. Moreover, tractors are not flexible platforms in terms of timings of monitoring campaigns

because they cannot be used for field surveys along the entire growing season, but only in specific time windows.

Another approach that could be used for field surveys is based on multispectral images acquired by satellites. Satellite images, representing the area of interest (when properly cloud-free) are downloaded, atmospheric and topographic correction procedures are applied and finally, vegetation indices are calculated and mapped. The new satellites allow to avoid the problems linked to low spatial and temporal resolution of the older ones but they still have some problems due to cloud cover. For instance, Reyniers and Vrindts (2005), in a comparison between ground-based and satellite sensors to retrieve wheat nitrogen status, were able to use only one satellite image of the experimental field during the whole growing season due to cloudy conditions. New satellite constellations, with very short revisit times and high spatial resolution, could solve the identified issues concerning satellite data.

Finally, the recent interest of agriculture in the use of unmanned aerial vehicles (UAVs) as platform mounting optical sensors to support precision fertilization led, in the last years, to numerous studies aiming to test the potential of this new technology. The workflow that leads to a UAV-derived map of the sensed vegetation indices is summarized in the following steps:

a) Spectral data acquisition. The UAV is driven automatically, following a flight plan which is designed to ensure the survey of the entire area of interest with an image overlap that guarantees a correct mosaicking process;
b) Mosaicking process that merges the captured image in a unique image of the entire field. Different types of software or cloud services are available and usually they also perform a geometric and radiometric correction (using a calibration panel characterized by known reflectance);

c) Vegetation indices are calculated and mapped.

The main advantage of using airborne spectral data collected with a multispectral sensor coming from an UAV rather than satellite-mounted sensors is the high spatial and temporal resolution. This feature makes UAV-derived spectral data more flexible in terms of timing and use. Indeed, the very high spatial resolution can allow shape analysis and their use also for site-specific application of pesticides and herbicides. Moreover, imaging optical sensors mounted on UAV are characterized by the highest spatial resolution achievable. However, the professional multispectral cameras capable of recording red-edge and near-infrared bands are still expensive. Finally, digital cameras are passive sensors and thus the quality of images is not constant and must be assured to retrieve quantitative information as well as proper post-processing techniques (*i.e.,* radiometric and geometric correction and georeferencing).

Irrespective of the platform used for field survey, the main output of the summarized workflows is usually a map of the variability of the chosen vegetation index. A large number of experiments were carried out on winter wheat giving satisfactory results in the calibration of regression models for the estimation of the above ground biomass, plant nitrogen content and plant nitrogen uptake from both, tractor and UAV platforms (Erdle et al, 2011; Li et al, 2009; Schmidhalter et al, 2003; Reyniers and Vrindts, 2005; Geipel et al., 2016). However, the resulting calibration curves are rarely translated in operative maps. Only in a few cases the developed algorithms have been already implemented to define the level of the fertilizers (Raun et al., 2005) that can be applied with the use of variable rate technology. Differently, several types of software have been developed to identify homogenous management zones relying on soil samples analysis (Schenatto et al., 2016) and their use has been recently extended also to spectral data (Bazzi et al., 2015; Schenatto et al., 2015). These algorithms

are usually based on cluster analysis (Basnyat et al., 2001; Schenatto et al., 2016; Sona et al., 2016). Furthermore, in recent years, geostatistics techniques have been used to map soil and crop variables (Stewart et al., 2002; Zhang et al., 2011) and for the definition of homogeneous management zones (Buttafuoco et al., 2016) as well. Although clustering and, in particular, geostatistics are valuable in accounting spatial patterns of variation of crop and soil variables, they require in-depth knowledge of statistics (Schenatto et al., 2016). Furthermore, using geostatistics would require a high computational cost when very high spatial resolution is gained by the optical sensors involved in field monitoring (Benítez et al., 2016).

In this framework, we propose an experiment on winter wheat in which a very high spatial resolution imaging sensor recording five bands (blue, green, red, red-edge and near-infrared) was used to map the variability in above ground biomass production in a cost-effective and prompt way, suitable for in-field applications. Then, a robust quantification of the number of homogeneous zones was performed on the basis of the estimation errors. Finally, the best timing for the UAV survey of the field will be discussed taking into account the phenological stage, identifying a time that allows an effective fertilizer application while informing about the variability in grain yield.

2 MATERIALS AND METHODS

The experiment started in March 2016 on a field of 11.3 hectares located in Sant'Angelo Lodigiano (Lodi), Italy (45°14′20″ N, 9°24′35″ E, altitude 73 m asl) at Cascina Belfuggito (owned by the Morando Bolognini Foundation). The field was cultivated with of winter wheat (*Triticum aestivum*, var. Basmati).

Three different areas of the field were identified because they were characterized by within-area homogeneity and between-area heterogeneity of soil physical and chemical properties (Table 1).

Table 1. – Soil physical and chemical properties of three areas of the same field. Mean values with standard deviations are reported.

Measured soil variable	Area 1	Area 2	Area 3
Gravel % FM	0.2±0.0	0.5±0.2	6.2±2.1
Sand %	46.2±4.1	54.8±2.6	76.6±0.3
Silt %	36.8±4.1	30.8±2.4	12.7±0.5
Clay %	17.0±0.3	14.3±0.2	10.7±0.4
pH	6.8±0.2	6.5±0.3	7.5±0.2
Total organic carbon %DM	0.79±0.96	0.99±0.01	0.60±0.01
Total Nitrogen %	0.09±0.10	0.11±0.13	0.06±0.11

The experiment was established in plots of 35 m^2 (5 x 7 m) arranged in a randomized block design with three replicates, and involving three levels of N fertilization: an unfertilized control (N0), 72 kg N ha^{-1} (N1), and 144 kg N ha^{-1} (N2). Three experimental sub-fields were put inside each identified area (Figure 1). An additional plot fertilized with 288 kg N ha^{-1} was included in each area, out of the experimental design, in order to increase variability in the dataset.

Figure 1. – The experimental field (on the left), white rectangles identify the position of the experimental sub-plots (on the right).

The remainder received 144 kg ha^{-1} of nitrogen, corresponding to the fertilization rate calculated through a simplified nitrogen balance.

The winter wheat was sown on 10 November 2015. Its fertilization was split into two applications: 36% of the total target nitrogen level was applied on 13 February 2016 as ammonium nitrate when wheat development stage was 23 BBCH; the remaining 64% of total N was applied on 18 March 2016 as urea, at phenological stage 25 of the BBCH scale. Fertilizers were hand-spread on experimental plots.

The crop was harvested on 28 June 2016 with a Claas Lexion 570 (CLAAS KGaA mbH, Harsewinkel, Germany) harvester equipped with yield sensors which carried out the yield mapping of the entire field, whereas the experimental plots were hand-harvested the following day. Harvested grain was collected in a wagon and weighted, in order to correct yeld data obtained with the harvester.

2.1 Image acquisition and processing

The platform used for image acquisition was a coaxial octocopter self-made in carbon fiber, with a maximum take-off mass of 12 kg and equipped with a GNSS (Global Navigation

Satellite System) NEO-M8N (u-blox, Thalwil, Switzerland) and a gimbal platform mounting a MicaSense RedEdge™ camera which is a professional digital camera for agriculture applications. The camera acquires reflectance in five discrete bands centered at the following wavelength: blue band, 475 nm; green band, 560 nm; red band, 668 nm, red-edge band, 717 nm; near-infrared band, 840 nm. Image acquisition was carried out in three different dates during wheat vegetative growth: at 25, 31 and 45 BBCH phenological stages, corresponding to early tillering, beginning of stem elongation, and late boot stage respectively (Witzenberger et al., 1989; Lancashire et al., 1991). Images of a white reference panel of known reflectance were acquired before and after each flight in order to perform radiometric calibration of images collected with the MicaSense RedEdge. The survey of the field was done at an altitude of 120 m and at low flight speed (8 m s^{-1}). The flight plan guaranteed 75% of forward and sideward overlap, needed for the mosaicking process. All the images collected during the flight (included the images of the white reference panel) were uploaded to the MicaSense Atlas cloud, a processing service that provided all the pre-processing activities and the production of the orthomosaic: a single 5-band 16-bit image containing the reflectance values expressed as digital numbers.

2.2 Samples collection and analysis

An area corresponding to 0.5 m^2 was sampled from each the day after each flight. Samples were cut just above the collar and oven dried at 105°C and. After weighing, the samples were ground with a rotary-knife mill equipped with a sieve of 4 mm mesh. A subsample was further ground with a ZM 100 centrifugal mill equipped with a sieve of 0.2 mm mesh (Retsch Gmbh & Co., Haan, Germany). Total nitrogen of samples was then determined by dry combustion using a ThermoQuest NA1500 elemental analyzer (Carlo Erba, Milano, Italy).

2.3 Image analysis

Image analysis was carried out following two different spectral data extraction of vegetation indices from the image of the entire field in order to build regression models for the estimation of grain yield provided by the harvester; the second step consisted in the procedures depending on the aim. The extraction of vegetation indices from the experimental plots was performed in order to build regression models to estimate above ground biomass of wheat at the time of the UAV survey while, the extraction of vegetation indices from the image of the entire field was carried out in order to build regression models for the estimation of the grain yield.

Three normalized difference vegetation indices (ND) were used as predictors of both grain yield and above ground biomass: the normalized difference vegetation index (NDVI), the green normalized difference vegetation index (GNDVI) and the normalized difference red-edge index (NDRE). The equation is common to all indices:

$$ND = \frac{NIR \quad Band}{NIR + Band}$$

Where *NIR* is the reflectance recorded by the near-infrared band and *Band* is the reflectance recorded in a specific band, different for each index: the red band for the NDVI, the green band for the GNDI and the red-edge band for the NDRE.

In both the cases, vegetation indices were calculated using QGIS while, the statistical analysis was carried out using MATLAB (MathWorks, Natick, MA).

2.3.1 Vegetation indices extraction from the experimental plots and estimation of above ground biomass at the time of each flight

The flight for crop monitoring were made at 25, 31 and 45 BBCH. Before every flight, in each plot, the area to be sampled was identified by putting white tiles at each vertex of the

sampled areas in order to recognize the pixels corresponding to the sampled plants. Sampled areas were identified and then the average vegetation indices were calculated for each experimental plot (N=30) using the QGIS software. Linear regression models for the estimation of above ground biomass were built using ordinary least squares method, and their prediction errors were calculated using leave-one-out cross-validation.

The coefficient of determination in calibration and cross-validation were calculated, as well as the RMSE and BIAS (see the following equations).

$$R^2 = 1 \quad \frac{\sum_{i=1}^{n}(\hat{y}_i \quad y_i)^2}{\sum_{i=1}^{n}(y_i \quad \bar{y})^2}$$

$$RMSEP = \sqrt{\frac{\sum_{i=1}^{n}(\hat{y}_i \quad y_i)^2}{n}}$$

$$BIAS = \frac{\sum_{i=1}^{n}(\hat{y}_i \quad y_i)}{n}$$

Where $\hat{y}_i$ are the estimated values, y_i are the measured values, n is the number of observations.

Finally, the homogeneous zones were identified taking into account the RMSE in cross-validation for the estimation of above ground biomass. The number of zones was calculated by dividing the range of estimated above ground biomass by the doubled RMSECV, which represents the step used for class definition.

2.3.2 Vegetation indices extraction from the entire field and estimation of grain yield

The harvester yield map consisted in a vector file of points containing the coordinates and the associated grain yield measurements as recorded by the harvester sensor. The first step consisted in the elimination of outliers and the correction of the yield data (total yield was adjusted taking into account for measured total grain in the wagon; while humidity was considered equal to that measured in experimental plots). Then, a process of homogenization

of the vectorial data of the yield map and those collected using multispectral camera (as a raster) was necessary in order to build regression models for the estimation of the grain yield. Three methods were tested for the homogenization of spatial resolutions: 1) Voronoi polygons; 2) a regular grid of 5x5 m; 3) a regular grid of 15x15 m.

First, Voronoi polygons were calculated from the vector point file of the yield maps then, the mean values of the three tested vegetation indices were calculated for each polygon. By doing this, each record of the grain yield map had a corresponding vegetation index value for every acquisition time. However, Voronoi polygons showed to be too sensitive to the drift of the yield sensor and biased by harvester unevenness of covered area thus two other methods were tested in order to reduce these noise sources. Two regular grids of 5x5 m and 15x15 m were also used to sample grain yield data and the corresponding average vegetation index. The resulting datasets were then split into two subsets according to the stripes depicted on figure 2: one set was used for the calibration procedure while the second set was used for the independent validation of the built regression models (Table 2).

Figure 2. – Picture of the wheat field. The data underlying the green areas were used in calibration whereas the data underlying the red areas were used for the independent validation.

Table 2. – Sample size of the dataset used for calibration (building-set) and independent validation (test-set) of the regression models for grain yield estimation. The data are reported for the three types of tested spatial resolution.

	Number of polygons (Voronoi, squares of the grid)	
Resolution type	**Building-set**	**Test-set**
Voronoi polygons	8597	6286
Regular grid 5 m	1962	1388
Regular grid 15 m	248	159

The relationships between the vegetation indices, acquired in the three different crop growth stage, and the grain yield were built using the ordinary least squares (OLS) regression models. For each model the determination coefficients of calibration and prediction (R^2) and the root mean squared error in prediction (RMSEP) were calculated.

3 RESULTS AND DISCUSSION

3.1 Measured data

Figure 3 shows wheat above ground biomass and its nitrogen concentration as affected by soil properties (field areas), nitrogen treatments and growth stage.

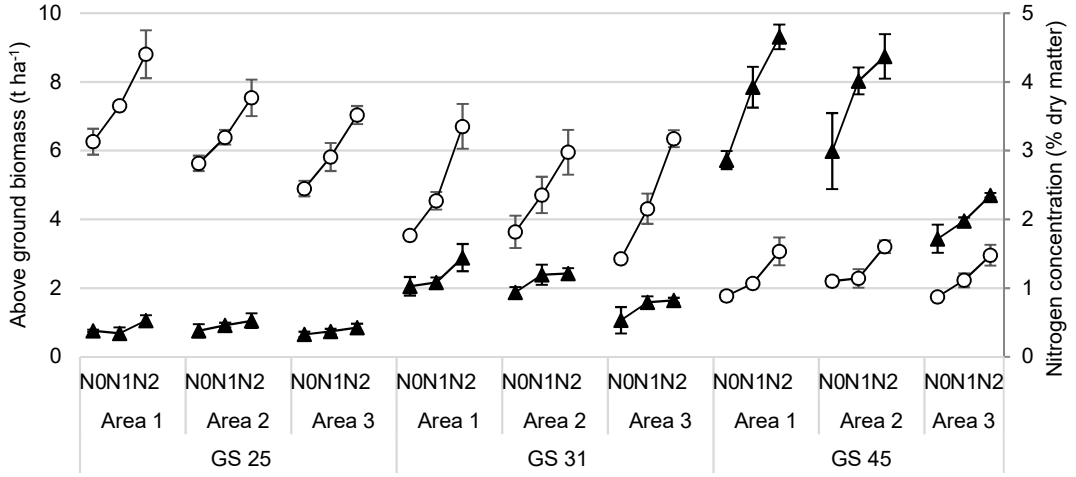

Figure 3. – Measured above ground biomass (black triangles) and nitrogen concentration (white dots) differentiated for field areas, nitrogen treatment and growth stage (GS).

As expected, above ground biomass showed an increasing trend during progress crop development. Biomass ranged from 0.54 t ha^{-1} to 1.23 t ha^{-1} at GS 25, from 0.84 t ha^{-1} to 3.2 t ha^{-1} at GS 31 and from 3.2 t ha^{-1} to 9.6 t ha^{-1} at GS 45. Considering data separately for each phenological stage, it was possible to distinguish crop response to N fertilizer in relation to the area of the field. Differences in above ground biomass among N treatments and field areas were detectable from GS 31, while at GS 25, neither soil physical-chemical properties neither N fertilization levels markedly affected plant biomass. Indeed, at GS 31 and 45, crop biomass positively responded to N fertilization rate, and was higher in areas 1 and 2

compared to area 3. It could be that the lower percentage of silt and clay in area 3 compared to other areas (Table 1) gave rise to higher water stress.

As a consequence of plant growth and N dilution in plant, plant N concentration decreased from GS 25 to GS 45 (Figure 3). Differently from above ground biomass, differences among treatments regarding plant N concentration arose already from GS 25. Plant N concentration increased proportionally to applied N at all stages, while it responded to differences in soil properties only at GS 25, when it was in the order area 1 > area 2 > area 3. After GS 25, average plant N concentration was very similar in all areas (Figure 3).

Results of Figure 3 confirmed that a large range of variability in crop biomass and N concentration was gained, and thus collected data represented a suitable data set wide range of values for calibration purposes. Finally, the linear regression models were built in order to estimate the above ground biomass because a very high correlation between measured above ground biomass and nitrogen uptake was found (r=0.84). Considering that the first information gained by an imaging sensor is the fraction cover and secondarily intensities of absorptions, above ground biomass is the main variable detectable by these sensors, while nitrogen nutrition status of the crop could be only indirectly detected (because it affects crop growth and greenness simultaneously). Thus, in order to retrieve a reliable information from the optical sensor we chose to estimate crop above ground biomass directly from the sensor signal while the crop nitrogen status was assessed with a second step from its relationship with the estimated above ground biomass.

3.2 Above ground biomass estimation and definition of homogeneous zones for nitrogen fertilization management

Linear regression models were built, using the data aroused from the experimental subfields, between the values of the tested vegetation indices and the above ground biomass measured

at GS 25 and 31, identified as the best moments to map crop variability linked to nitrogen crop demands. The dataset of each tested phenological stage consisted in 30 samples collected from the experimental plots. The robustness of the OLS linear regression models was tested using the leave-one-out cross-validation method. Results of the performances of the vegetation indices are reported in table 3.

Table 3. – Performances of the linear regression models for the estimation of the above ground biomass using NDVI, GNDVI and NDRE in terms of R^2, of root mean squared error (RMSE), of BIAS, in calibration and cross-validation (C and CV, respectively).

	NDVI		***GNDVI***		***NDRE***	
	GS 25	***GS 31***	***GS 25***	***GS 31***	***GS 25***	***GS 31***
R^2 *C*	0.36	0.68	0.38	0.80	0.37	0.83
R^2 *CV*	0.30	0.60	0.31	0.75	0.34	0.82
RMSE C	0.14	0.45	0.14	0.41	0.14	0.27
RMSE CV	0.15	0.47	0.15	0.42	0.15	0.28
BIAS C	0.002	0.026	0.003	0.032	-0.005	0.024
BIAS CV	0.002	0.025	0.003	0.031	-0.005	0.023

No differences were found in estimation performances between the three vegetation indices at GS 25. Furthermore, the performances of all the indices were not satisfactory at this phenological stage. At GS 25, the average above ground biomass production may have been too low to be sensed (average value of 0.83 t ha^{-1}) due to the confounding effect of soil on the camera signal. Anyway, it must be observed that the differences in soil properties and consequently, in nitrogen (and water) availability, started to affect the crop already at this early stage (even if not sensed by the camera), for example in terms of nitrogen concentration (figure 3). Furthermore, at GS 25 phenological stage, the vegetation indices showed higher

correlation with the nitrogen concentration (r=0.72 for NDVI, r=0.75 for GNDVI, r=0.75 for NDRE) and nitrogen uptake (r=0.69 for NDVI, r=0.73 for GNDVI, r=0.72 for NDRE) than with the biomass (r=0.61 for NDVI, r=0.61 for GNDVI, r=0.63 for NDRE) confirming the establishment of the variability which would be later translated in different potential grain yields.

At GS 31 the performances in above ground biomass estimation were satisfactory, the GNDVI and the NDRE were the best predictors. Different authors found out that the best results in estimation performances were gained using red-edge and green vegetation indices from both tractor- and UAV-mounted multispectral sensors (Cao et al. ,2014; Erdle et al., 2011; Geipel et al., 2016) reaching very similar performances. The same authors attributed the less satisfactory estimation performances of the NDVI as predictor of the above ground biomass to the saturation of the index at higher biomass levels. Although our results confirmed the better performances of the GNDVI and NDRE if compared to NDVI, a saturation phenomenon was observed for all the tested indices *i.e.,* the vegetation indices lost linearity in their relationships with the above ground biomass at higher biomass values (figure 4).

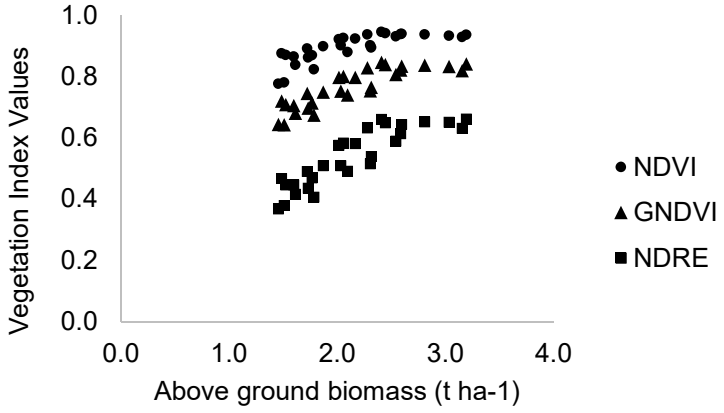

Figure 4. – The studied vegetation indices *vs* the measured above ground biomass at GS 31.

This phenomenon was probably due to both the effects of soil buffering properties (field areas) and nitrogen levels. Differences in above ground biomass production were detectable among the field areas where the crop showed variable level of soil canopy coverage: the fertilized experimental plots of the areas 1 and 2 reached a full soil canopy cover, while the control plots (no nitrogen applied) and the experimental plots of area 3 (low water availability) showed sparse vegetation, irrespective of the nitrogen levels. Then, in the experimental plots characterized by sparse vegetation, the vegetation indices were able to detect changes proportionally to the fraction cover whereas, in the experimental plots characterized by full canopy cover, the vegetation indices were no longer able to recognize changes in the above ground biomass production. The better estimation performances of the GNDVI and particularly, of the NDRE could be explained by the ability of these indices of discriminating lower biomass levels if compared to the NDVI which gained very high absolute values even soon at lower biomass levels. Our results confirmed the greater saturation behavior of the NDVI, as can be seen in figure 5, where the saturating values of the NDVI and of the NDRE are compared.

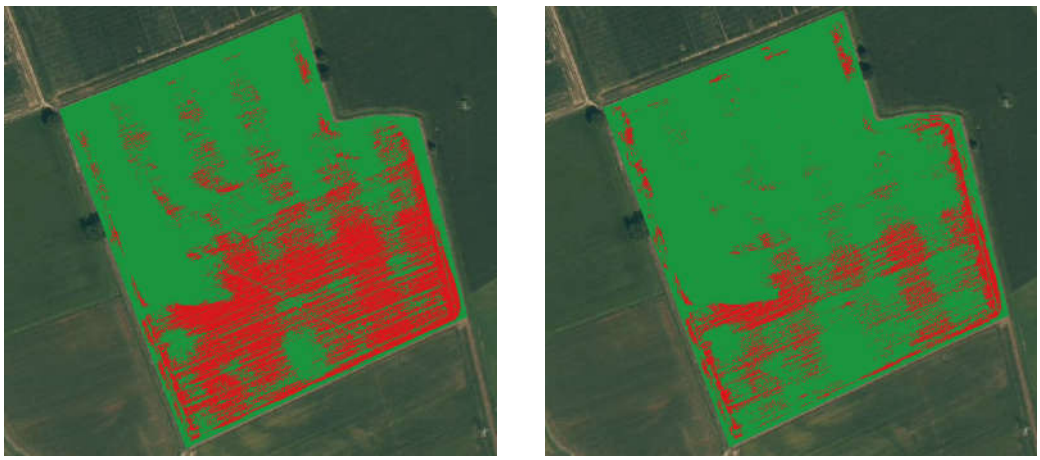

Figure 5. – NDVI (left) and NDRE (right) values at GS 31. Red pixels represent index values above the 90th percentile of the maximum index value recorded in the year 2016.

Taking into account the results, it can be concluded that the best time to do a field survey with an optical sensor to map in-field variability for nitrogen management purposes resulted the GS 31. In fact, the crop monitoring at this phenological stage guaranteed a satisfactory estimation of the above ground biomass (R^2 of cross-validation= 0.82 and RMSECV= 0.28 t ha^{-1}) which was also found to be closely related to the grain yield (r=0.86) whereas the monitoring carried out at GS 25 was found to be unable to distinguish nitrogen effects. Furthermore, the above biomass measured at GS 25 is less correlated to grain yield (r=0.58). The definition of the homogenous zones for site-specific nitrogen management was carried out for the GS 31, the results are showed in figure 6.

Figure 6. – Map of the wheat field at GS 31 divided into three homogeneous zones, based on NDRE, at 5m (left) and 15 m (right) of spatial resolution: the most productive area is in green, the area characterized by medium production in yellow and the lower productive area in red.

The proper number of homogeneous zones, according to the RMSECV, was found to be three. Then, the homogeneous field areas were classified on the basis of the NDRE values by inverting the regression equation. In this way, it was possible to identify NDRE values

which separated the homogenous areas: NDRE values less of 0.49 characterized the less productive areas, NDRE values ranging between 0.49 and 0.59 represented the area with medium biomass production whereas the index values higher than 0.59 identified the most productive area. The value of 0.59 represented also the point at which NDRE saturated. Furthermore, the resulting zones are comparable to the areas identified by different levels of grain yield production (figure 7), due to high correlation between the above ground biomass measured at this phenological stage and the yield.

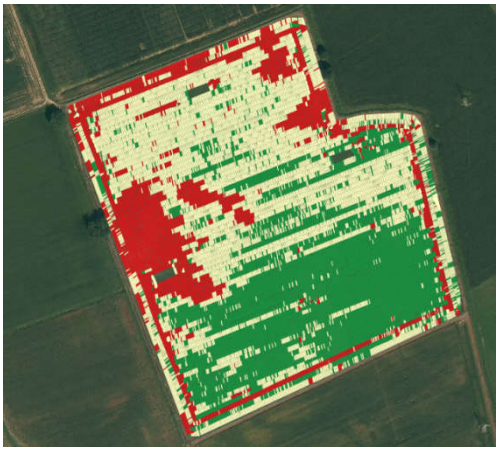

Figure 7. – Grain yield map divided in three levels of grain yield, from high (green) to low (red).

Thanks to the high correlation found between the above ground production and the nitrogen uptake was also possible to estimate on stochastic basis the average biomass production and the corresponding nitrogen uptake (table 4).

Table 4. – The estimated average above ground biomass production and nitrogen uptake of each homogeneous zone at GS 31.

	Estimated above ground biomass ($t\ ha^{-1}$)	Estimated nitrogen uptake ($kg\ N\ ha^{-1}$)
ZONE 1 (low biomass level)	1.4	28.9
ZONE 2 (medium biomass level)	2.3	65.0
ZONE 3 (high biomass level)	2.5	73.0

Finally, it must be considered that the identified variability depended not only on nitrogen levels but also on the effects that lower water availability had on nitrogen availability. This is showed by the behavior of the NDRE values of the area 3 (figure 8), characterized by sandy soil, which clustered together showing the ability of the index to see, indirectly, the effect of more stressors.

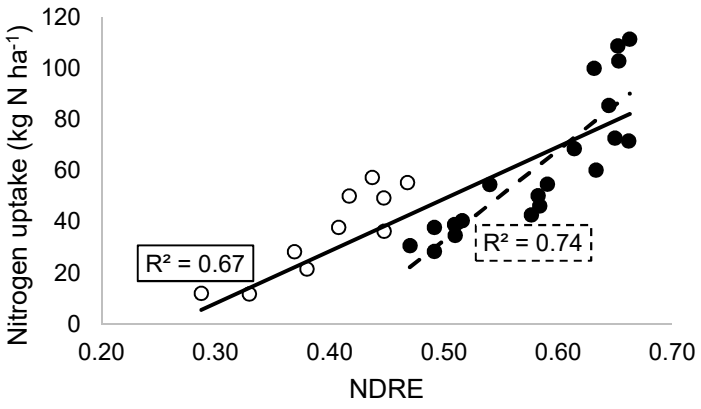

Figure 8. – NDRE *vs* nitrogen uptake at GS 31. White dots represent the clustered samples of the area 3 whereas black dots are samples coming from the areas 1 and 2. Estimation performances were reported for the dataset with and without the samples of area 3.

3.3 Grain yield estimation

Since the year 2016 was characterized by good weather conditions, it could be considered as a standard growing season thus, a representative estimation of the grain yield was

performed. An OLS regression model for each studied phenological stage was built between the values of the tested vegetation indices and the grain yield. Table 5 shows the results in terms of the calibration determination coefficients, taking into account also the different spatial resolution at which the data were extracted.

Table 5. – Determination coefficients of the OLS regression models built between NDVI, GNDVI, NDRE and the grain yield at different phenological stages and following different methods of data extraction (Voronoi polygons, regular grid at 5m and regular grid at 15 m).

DATA EXTRACTION	Vegetation Index	GS 25	GS 31	GS 45
Voronoi polygons	*NDVI*	0.40	0.52	0.61
	GNDVI	0.45	0.55	0.67
	NDRE	0.53	0.57	0.68
Regular grid 5 m	*NDVI*	0.51	0.61	0.73
	GNDVI	0.55	0.67	0.79
	NDRE	0.63	0.69	0.80
Regular grid 15 m	*NDVI*	0.65	0.74	0.83
	GNDVI	0.68	0.79	0.89
	NDRE	0.76	0.80	0.91

As expected, the data extraction method that led to the best results was the regular grid of 15 m. The records of the yield maps, in fact, are not taken at the exact coordinates points of the harvested plants but when the machine is moving. This fact decreases the accuracy of the joining of the camera spectral information with the yield data. Decreasing the spatial resolution of the grain yield data allowed a more robust correspondence with the spectral data leading to better estimation performances. This result is already visible comparing the map of Voronoi polygons with the map of 5 m regular grid which guaranteed better estimation performances of all the vegetation indices. Another step of de-resolution (from 5 to 15 m) produced even better estimation results without substantial loss of technical usefulness.

The vegetation index that led to the best performance in grain yield estimation was the NDRE, based on the red-edge band. Finally, independent validation was applied and the results of the performance in prediction were produced for grain yield estimation using NDRE extracted from the 15 m regular grid (Figure 9). The RMSEP of the built regression models were 0.71, 0.70, 0.82 t ha^{-1} for the GS 25, 31 and 45, respectively. Very similar, but slightly worse results, were also gained by using GNDVI as predictor.

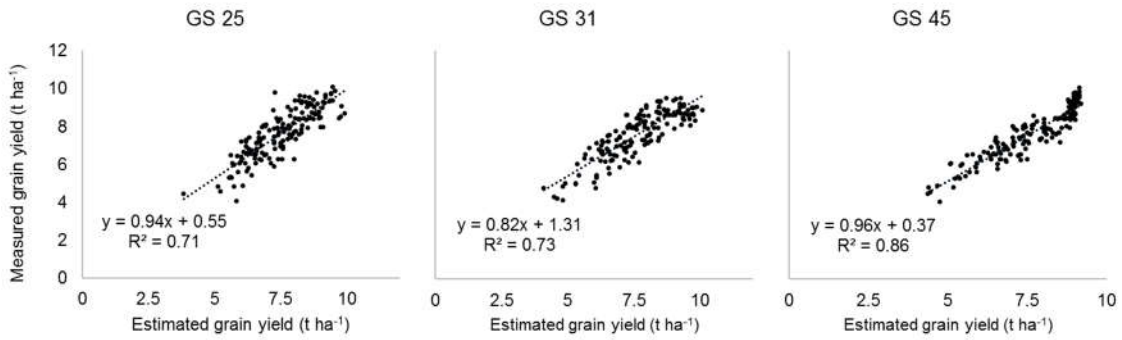

Figure 9. – Estimated *vs* measured grain yield at different growth stages (GS). The estimation was based on NDRE values extracted with a 15 m regular grid.

The reliability of the estimation performances was confirmed by the determination coefficients of the regression models built using the dataset composed by the hand-harvested samples of the experimental plots: the NDRE was the best estimator of wheat grain yield with R^2 of 0.85, 0.89 and 0.95 for the GS 25, 31 and 45, respectively. The NDVI resulted in less satisfactory performances. These findings represent very good results, according to the literature that found out linear relationships with R^2 0.42-0.90 between the grain yield and normalized difference vegetation indices measured in similar phenological stages from both tractor- and UAV-mounted multispectral sensors (Geipel et al., 2016; Schmidhalter et al., 2003).

The suitable window to do the field survey for nitrogen management purposes was confirmed to be at 31 BBCH by the difference in grain yield prediction performances (assuming that nitrogen availability is the most effective limiting factor. In fact, figure 10 shows that the best moment for a field survey capable to identify most of the variability in crop yield would be at GS 45, irrespective of the method of data extraction. Nevertheless, the response of the crop to nitrogen fertilization would be minimal at this stage, considering that wheat shows the highest nitrogen demand at the stem elongation growth stage (GS 30-40).

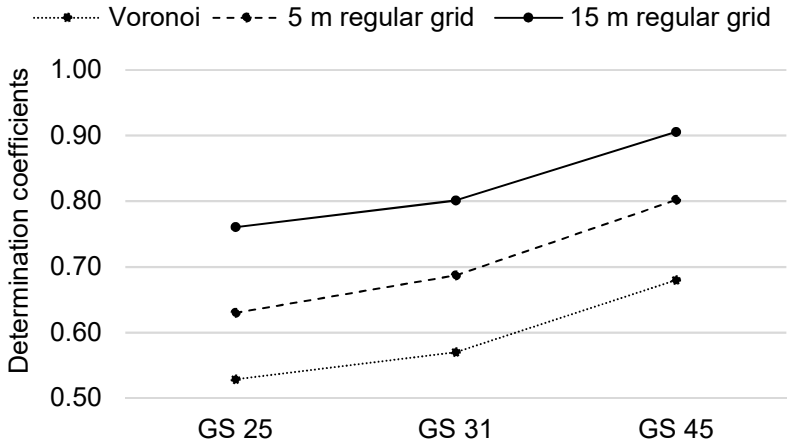

Figure 10. – Determination coefficients of the linear regression models for the estimation of grain yield from NDRE measured at different growth stages (GS) following three different methods of data extraction.

The performances in grain yield estimation carried out at GS 25 and 31 were satisfactory and similar thus, the time window from GS 25 to 31 was confirmed to be the most suitable to monitor crop variability for nitrogen management aims because the vegetation indices showed a powerful ability in discriminating difference in yield production also at early stages.

In particular, the good grain yield estimation performances at GS 25 prove (together with the effect of soil properties on nitrogen uptake showed in figure 8) that the index response to a limiting factor might not be univocal. In fact, at this phenological stage grain yield was successfully predicted whereas changes in above ground biomass of the plants at same time of the field survey were not identified. The index was able to see differences linked to both soil and crop factors. In this framework, the UAV-based crop monitoring could play a role in the context of precision agriculture when more information is available about soil variability, weather conditions and the variability of the potential grain yield production in order to translate the identified within-field variability in prescription maps, carrying the information of accurate crop nitrogen demands. Other methods could involve more mechanistic approaches such as the integration of remote optical sensing and crop growth models at farm level. In this way the UAV monitoring could be used to force and spatialize a simplify model to fit it to the observed in-field variability.

4 CONCLUSION

A UAV mounting a professional digital camera recording five visible and near-infrared channels was used to survey a winter wheat field during the 2016 growing season. The ability of this system to map the within-field variability was tested by identifying the best moment to do the aerial survey and then classifying the field in homogenous zones for nitrogen management purposes.

The proposed method gave promising results, stressing the importance of crop monitoring carried out with an imaging sensor capable of recording reflectance in the red-edge region of the spectrum. In fact, the red-edge based index (NDRE), among the tested vegetation indices (NDVI and GNDVI), was found to be the best predictor, along the growing season, of the above ground biomass present at the moment of the flight and of the grain yield. In particular, the NDRE was found to be highly correlated to the grain yield, reaching R^2 ranging from 0.76 (GS 25) to 0.91 (GS 45). Although at GS 45 the index had the best result in grain yield estimation, the best time to survey the field for crop monitoring was found to be at GS 31, which would be more suited to fertilization purposes since it represents a time of high crop nitrogen demand. Furthermore, an estimation of the above ground biomass at GS 31 was carried out in order to identify a reliable number of homogenous areas of the field characterized by different target yields and nitrogen demands. The NDRE gained satisfactory results in cross-validation: R^2=0.82 and RMSECV=0.28t ha^{-1}. Then, relying on the RMSECV basis, the minimum number of management zones that best represented the variability of crop biomass was found to be three. Moreover, the NDRE threshold values of the identified classes were set at 0.49 (if NDRE were lower, the corresponding biomass production was classified as the poorest) and 0.59 (if NDRE were higher, the corresponding biomass production was classified as the highest). For each zone we were able to identify

the average biomass production and its nitrogen uptake, as the basis for an accurate prescription map for fertilizer applications. Since the observed within-field variability was not only attributable to the nitrogen levels but also to soil properties, the last step (from the map of biomass variability to the prescription map for nitrogen fertilization) could be done integrating more levels of information, coming from the soil, from the atmosphere and from grain yield history. Nonetheless, the proposed procedure is promising. Further studies should be carried out firstly to understand the reliability of this method with respect to more complex approaches (geostatistics or clustering for zones definition), and then to create an integrated system to support nitrogen fertilization decisions.

5 AKNOWLEDGEMENTS

This research was funded by DiSAA (Linea 2, Azione A, Piano di sostegno alla ricerca 2015-2017), University of Milan.

6 REFERENCES

Basnyat, P., McConkey, B. G., Noble, G., & Meinert, L. B., 2001. Agriculture field characterization using GIS software and scanned color infrared aerial photographs. http://www.usask.ca/soilsncrops/conference-proceedings/previous_years/Files/2001/2001docs/ 253.pdf.

Bazzi, C.L., Souza, E.G., Schenatto, K., Carnieletto, J., Matte, M.T., 2015. Software for Managing, Analysis and Definition of Management Zones in Precision Agriculture. Presented at the First Conference on Proximal Sensing Supporting Precision Agriculture. doi:10.3997/2214-4609.201413858

Benítez, F.L., Anderson, L.O., Formaggio, A.R., Benítez, F.L., Anderson, L.O., Formaggio, A.R., 2016. Evaluation of geostatistical techniques to estimate the spatial distribution of aboveground biomass in the Amazon rainforest using high-resolution remote sensing data. Acta Amazonica 46, 151–160. doi:10.1590/1809-4392201501254

Buttafuoco, G., Castrignanò, A., Cucci, G., Lacolla, G., Lucà, F., 2016. Geostatistical modelling of within-field soil and yield variability for management zones delineation: a case study in a durum wheat field. Precision Agriculture 1–22.

Cao, Q., Miao, Y., Feng, G., Gao, X., Li, F., Liu, B., Yue, S., Cheng, S., Ustin, S.L., Khosla, R., 2015. Active canopy sensing of winter wheat nitrogen status: An evaluation of two sensor systems. Computers and Electronics in Agriculture, Precision Agriculture 112, 54–67. doi:10.1016/j.compag.2014.08.012

Eitel, J.U.H., Long, D.S., Gessler, P.E., Smith, A.M.S., 2007. Using in-situ measurements to evaluate the new RapidEye™ satellite series for prediction of wheat nitrogen status. International Journal of Remote Sensing 28, 4183–4190.

Erdle, K., Mistele, B., Schmidhalter, U., 2011. Comparison of active and passive spectral sensors in discriminating biomass parameters and nitrogen status in wheat cultivars. Field Crops Research 124, 74–84.

Geipel, J., Link, J., Wirwahn, J.A., Claupein, W., 2016. A Programmable Aerial Multispectral Camera System for In-Season Crop Biomass and Nitrogen Content Estimation. Agriculture 6, 4. doi:10.3390/agriculture6010004 http://www.bae.ksu.edu/precag/Remote%20Sensing/Other%20Ways%20to%20Obtain%20NDVI%20data%20greenseeker%20etc.doc.

Hunt, E.R., Hively, W.D., Fujikawa, S.J., Linden, D.S., Daughtry, C.S., McCarty, G.W., 2010. Acquisition of NIR-green-blue digital photographs from unmanned aircraft for crop monitoring. Remote Sensing 2, 290–305.

Jannoura, R., Brinkmann, K., Uteau, D., Bruns, C., Joergensen, R.G., 2015. Monitoring of crop biomass using true colour aerial photographs taken from a remote controlled hexacopter. Biosystems Engineering 129, 341–351. doi:10.1016/j.biosystemseng.2014.11.007

Lancashire, P.D.; H. Bleiholder; P. Langeluddecke; R. Stauss; T. van den Boom; E. Weber; A. Witzen-Berger, 1991. A uniform decimal code for growth stages of crops and weeds. Ann. Appl. Biol., 119 (3), 561–601. doi:10.1111/j.1744-7348.1991.tb04895.x.

Li, F., Miao, Y., Zhang, F., Cui, Z., Li, R., Chen, X., Zhang, H., Schroder, J., Raun, W.R., Jia, L., 2009. In-season optical sensing improves nitrogen-use efficiency for winter wheat. Soil Science Society of America Journal 73, 1566–1574.

Moges, S.M., Raun, W.R., Mullen, R.W., Freeman, K.W., Johnson, G.V., Solie, J.B., 2005. Evaluation of green, red, and near infrared bands for predicting winter wheat

biomass, nitrogen uptake, and final grain yield. Journal of Plant Nutrition 27, 1431–1441.

Price R. R. Other Ways to Obtain NDVI data using Field Sensors - Greenseeker, Crop Circle, Yara, etc. K-State Extension and Research.

Raun, W.R., Solie, J.B., Stone, M.L., Martin, K.L., Freeman, K.W., Mullen, R.W., Zhang, H., Schepers, J.S., Johnson, G.V., 2005. Optical Sensor-Based Algorithm for Crop Nitrogen Fertilization. Communications in Soil Science and Plant Analysis 36, 2759–2781.

Reyniers, M., Vrindts, E., 2006. Measuring wheat nitrogen status from space and ground-based platform. International Journal of Remote Sensing 27, 549–567. doi:10.1080/01431160500117907

Rodriguez, D., Fitzgerald, G.J., Belford, R., Christensen, L.K., 2006. Detection of nitrogen deficiency in wheat from spectral reflectance indices and basic crop eco-physiological concepts. Crop and Pasture Science 57, 781–789.

Schenatto, K., Souza, E.G., Bazzi, C.L., Beneduzzi, H.M., 2015. Management Zones with NDVI Data through Corn and Soybean Yield, in: First Conference on Proximal Sensing Supporting Precision Agriculture.

Schenatto, K., Souza, E.G., Bazzi, C.L., Bier, V.A., Betzek, N.M., Gavioli, A., 2016. Data interpolation in the definition of management zones. Acta Scientiarum. Technology 38, 31–40.

Schmidhalter, U., Jungert, S., Bredemeier, C., Gutser, R., Manhart, R., Mistele, B., Gerl, G., 2003. Field-scale validation of a tractor based multispectral crop scanner to determine biomass and nitrogen uptake of winter wheat, in: Precision Agriculture:

Papers from the 4th European Conference on Precision Agriculture, Berlin. pp. 615–619.

Sona, G., Passonia, D., Pintoa, L., Pagliaria, D., Masseroni, D., Ortuanib, B., Facchib, A., 2016. Uav Multispectral Survey to Map Soil and Crop for Precision Farming Applications. ISPRS-International Archives of the Photogrammetry, Remote Sensing and Spatial Information Sciences 1023–1029.

Stewart, C.M., McBratney, A.B., Skerritt, J.H., 2002. Site-specific durum wheat quality and its relationship to soil properties in a single field in northern New South Wales. Precision Agriculture 3, 155–168.

Taylor, James, and Brett Whelan. "A general introduction to precision agriculture." Australian Center for Precision Agriculture (2005).

Witzenberger, A.; H. Hack; T. van den Boom (1989). Erläuterungen zum BBCH-Dezimal-Code für die Entwicklungsstadien des Getreides - mit Abbildungen. Gesunde Pflanzen, 41, 384–388.

Zhang, H., Lan, Y., Lacey, R., Hoffmann, W.C., Westbrook, J.K., 2011. Spatial analysis of NDVI readings with different sampling densities. Transactions of the ASABE 54, 349–354.

Zhu, Y., Li, Y., Feng, W., Tian, Y., Yao, X., Cao, W., 2006. Monitoring leaf nitrogen in wheat using canopy reflectance spectra. Canadian Journal of Plant Science 86, 1037–1046.

GENERAL CONCLUSION

Remote sensing of vegetation, involving the use of optical sensors, to map the crop within-field variability was evaluated in this work.

The literature survey, reported in chapter one, was carried out to evaluate the feasibility of optical remote sensing to estimate nitrogen management variables in maize. This summary evaluation was done because, while many experiments were conducted to test the feasibility of optical sensing for supporting nitrogen management decisions, a lack of a summarised knowledge on this topic was observed. In general, the studied literature showed that by using various platforms and sensors, optical sensing of crop canopy has good potential to estimate nitrogen-related variables although it is based on empiric regressions relying on local condition, cultivar, year *etc*. Furthermore, in conclusion, three main scientific gaps were identified:

1) Most of the works carried out focused the attention on the use of multispectral sensors. On the one hand, multispectral sensors require less post-processing thus, are the most suited for in-field applications. On the other hand, hyperspectral sensors have also been developed and they allow the study crop reflectance using hundreds of narrow bands. However, some of the experiments that exploited hyperspectral sensors failed to conduct multivariate data analyses preferring the simplified approach of index calculation. This limited the ability to determine if the use of the information coming from the all the recorded wavebands would have improved crop variable estimation.

2) Most of the studied works on the use of optical sensors to estimate nitrogen related variables were conducted with experiments in which nitrogen was the unique limiting factor, making it impossible to verify the effects of other factors on sensor response to nitrogen. However, the study of the interaction between nitrogen and water availability is very

interesting in our environments. It must be considered that water stress effects on canopy reflectance are similar to those of nitrogen stress. Moreover, water stress causes changings in canopy geometry that could limit the ability of the optical sensors to retrieve correct information on nitrogen status. Finally, the rare studies attempted to verify simultaneous effects of nitrogen and water stress on the response of optical sensors gave contrasting results in terms of wavebands and indices able to discriminate the effects of the stressors. More attempts to manage the simultaneous presence of the two stressors using optical sensing have to be done.

3) Two important issues in the use of optical sensing concerned the spatial and temporal resolution of the optical sensors. The former, if too low, is not effective to map in-field crop variability. The latter has a key role in identifying the best moment of fertilizers application which affects crop nitrogen use efficiency.

In order to contribute to filling the knowledge gaps identified in point 1 and 2 a pot greenhouse experiment has been presented in chapter two. The aim was to assess the capability of hyperspectral line scan imaging to estimate crop variables under combined water and nitrogen stress using multivariate data analysis and two data compression methods: canopy average spectra and hyperspectrogram extraction. This work represented the first successful attempt in the application of hyperspectragram-based estimations of plant variables for vegetation monitoring purposes proving that it is a reliable technique which could be suitable for in-field crop monitoring purposes. The image hyperspectral data extraction proved successful to discriminate water and nitrogen supply effects. This is particularly true for the determination of water content that was the most successful even because the water stress had the strongest effect on canopy geometry that affected, in turn,

the canopy spectral response. The determination of nitrogen concentration suffered by the effects of water stress on crop canopy, gaining worse performance. Instead, satisfactory results were obtained by the multivariate regression model built on the dataset of nitrogen stressed canopy alone, without water limitations. These findings suggested that even if imaging spectroscopy has great potential in crop stress diagnosis, the combined effects of more stressors on crop canopy reflectance have to be fully investigated.

The field experiments of the chapter 3 aimed to test the potentialities and limitations of two type of multispectral imaging sensors mounted on an unmanned aerial vehicle (UAV) in order to map the within-field crop variability for nitrogen management purposes. The first sensor tested was a commercial digital camera modified to acquire reflectance in visible and near-infrared channels. We found out that this low cost imaging system on board the UAV, even with the limitations due to channels overlap and saturation, led to very good performance in the estimation of the above ground biomass of maize at V9 in two years of experimentation. This was possible thanks to the very high spatial resolution of the imaging sensor that allowed a reliable estimation of the canopy fraction cover. The second sensor tested in a case of study on winter wheat was a professional multispectral camera in five channels. It was able to estimate grain yield also at early growth stages. Moreover, three homogeneous zones were identified for differences in above ground biomass that could be used for site-specific fertilization because we were able to estimate the average above ground biomass and crop nitrogen uptake for each zone. However, crop variability was not only attributable to the nitrogen levels but also to soil properties (which affected water availability) so, the prescription map for nitrogen fertilization should be done integrating

more levels of information in order to guarantee an accurate and robust prediction of plant demand.

All the experiments carried out highlighted the importance of the red-edge region of the spectrum for the estimation of above ground biomass and nitrogen concentration, where the sensor allowed it. This finding confirmed the results reported by the literature which linked changes in red-edge region with difference in nitrogen nutrition levels. However, the soil water level affects nitrogen availability and these effects were visible in the field experiment on winter wheat. In fact, the calculated red-edge-based vegetation index identified the wheat variability as the sum of the effects of both nitrogen and water availability. In general, this could be considered a limitation of the vegetation monitoring with optical sensors for nitrogen management purposes because the spectral response of canopy reflectance to a limiting factor was not found to be univocal. It could be concluded that the UAV-based crop monitoring could play a role in the context of precision agriculture if intended as a part of an integrated monitoring system able to retrieve more complex information about soil variability, weather conditions and crop variability.

Further research has to be carried out to implement a decision support system that would join information coming from all the factors affecting the agroecosystem. This could be possible studying i) the application of techniques of data fusion coming from different sensors; ii) the implementation of complex dynamic simulation models of the soil-crop system which are guided by remote sensed optical information of the crop status.

REFERENCES OF "GENERAL INTRODUCTION" SECTION

Barnes, E.M., Moran, M.S., Pinter, P.J., Clarke, T.R., 1996. Multispectral remote sensing and site-specific agriculture: examples of current technology and future possibilities. Precision Agriculture 845–854.

Eitel, J.U.H., Long, D.S., Gessler, P.E., Hunt, E.R., 2008. Combined Spectral Index to Improve Ground-Based Estimates of Nitrogen Status in Dryland Wheat. Agronomy Journal 100, 1694. doi:10.2134/agronj2007.0362

Joseph, George. Remote Sensors – An overview, in: "Fundamentals of Remote Sensing – Second Edition". Universities Press, 2005.

Lan, Y., Thomson, S.J., Huang, Y., Hoffmann, W.C., Zhang, H., 2010. Current status and future directions of precision aerial application for site-specific crop management in the USA. Computers and electronics in agriculture 74, 34–38.

Lemaire, G., Jeuffroy, M.-H., Gastal, F., 2008. Diagnosis tool for plant and crop N status in vegetative stage: Theory and practices for crop N management. European Journal of agronomy 28, 614–624.

Olfs, H.-W., Blankenau, K., Brentrup, F., Jasper, J., Link, A., Lammel, J., 2005. Soil- and plant-based nitrogen-fertilizer recommendations in arable farming. Journal of Plant Nutrition and Soil Science 168, 414–431. doi:10.1002/jpln.200520526

Pattey, E., Strachan, I.B., Boisvert, J.B., Desjardins, R.L., McLaughlin, N.B., 2001. Detecting effects of nitrogen rate and weather on corn growth using micrometeorological and hyperspectral reflectance measurements. Agricultural and forest meteorology 108, 85–99.

Rodriguez, D., Fitzgerald, G.J., Belford, R., Christensen, L.K., 2006. Detection of nitrogen deficiency in wheat from spectral reflectance indices and basic crop eco-physiological concepts. Crop and Pasture Science 57, 781–789.

Schlemmer, M.R., Francis, D.D., Shanahan, J.F., Schepers, J.S., 2005. Remotely measuring chlorophyll content in corn leaves with differing nitrogen levels and relative water content. Agronomy Journal 97, 106–112.

Tempfli, G.C. Huurneman, W.H. Bakker, L.L.F. Janssen, W.F. Feringa, A.S.M. Gieske, K.A. Grabmaier, C.A. Hecker, J.A. Horn, N. Kerle, F.D. van der Meer, G.N. Parodi, C. Pohl, C.V. Reeves, F.J.A. van Ruitenbeek, E.M. Schetselaar, M.J.C. Weir, E. Westinga, E. and T. Woldai. "Principles of Remote Sensing: An Introductory Textbook." ITC Educational Textbook Series, 2009.

Wang, T.-C., Ma, B.L., Xiong, Y.-C., Saleem, M.F., Li, F.-M., 2011. Optical sensing estimation of leaf nitrogen concentration in maize across a range of water-stress levels. Crop and Pasture Science 62, 474–480.

Zillmann, E., Graeff, S., Link, J., Batchelor, W.D., Claupein, W., 2006. Assessment of Cereal Nitrogen Requirements Derived by Optical On-the-Go Sensors on Heterogeneous Soils. Agronomy Journal 98, 682–690. doi:10.2134/agronj2005.025